OPTICAL AND INTERFEROMETRIC STUDIES

OF

GROWTH PHENOMENA ON CARBORUNDUM CRYSTALS

BY

AJIT RAM VERMA

THESIS

PRESENTED FOR THE DEGREE OF

DOCTOR OF PHILOSOPHY

IN THE UNIVERSITY OF LONDON

ProQuest Number: 10096577

All rights reserved

INFORMATION TO ALL USERS
The quality of this reproduction is dependent upon the quality of the copy submitted.

In the unlikely event that the author did not send a complete manuscript
and there are missing pages, these will be noted. Also, if material had to be removed,
a note will indicate the deletion.

ProQuest 10096577

Published by ProQuest LLC(2016). Copyright of the Dissertation is held by the Author.

ABSTRACT.

The theory of the growth of a perfect crystal
is outlined and a brief description is given of the
development of this theory, taking into account the
presence of imperfections, especially dislocations,
in the crystal. The molecular 'growth spirals' and
other features predicted by this theory put forward
by Burton, Cabrera and Frank require improved exper-
imental techniques for their study, which are described.
The experimental study of the growth features divides
itself into two parts:-

> (1) Microscopic studies
>
> (2) Interferometric studies.

The different growth features observed on the
faces of silicon-carbide (Si-C) crystals are illustrated
and explained. The observed 'growth spirals' can be
divided into three types:

> (1) Elementary spirals with step heights equal
>   to the size of the X-ray unit cell
>
> (2) Spirals originating from dislocations of
>   multiple strength, the step heights being
>   a multiple of the X-ray unit cell
>
> (3) Interlaced spirals in which the step heights
>   are a fraction of the unit cell.

The microscopic studies illustrate the information about the shape of the spirals, the behaviour and interaction of growth fronts with one another, originating from different sources, the growth pattern for a number of screw dislocations emerging on the crystal face, fault surfaces, and their statistical properties such as density of dislocations etc. From these studies the type of information obtainable about the conditions of growth is the size of the critical nucleus and the supersaturation.

The interferometric techniques utilized for the measurement of step heights are discussed. A study of the measured step heights leads to an understanding of the interesting property of 'polytypism' as observed in silicon-carbide crystals which occur in different types as shown by X-ray diffraction data. The 'growth spirals' demonstrate the X-ray predictions and confirm them.

CONTENTS

For convenience in comparing the
Text and the Figures, the Thesis
has been bound in two   separate
Volumes.

Vol. 1.   The Text.

Vol. 2.   The Figures and Diagrams.

CONTENTS

Vol. I   Part I

THEORIES OF CRYSTAL GROWTH

Part II

SILICON-CARBIDE, ITS FORMATION, CRYSTAL
STRUCTURE AND POLTYPISM

Part III

EXPERIMENTAL METHODS USED IN THE PRESENT STUDY

Chapter V   MICROSCOPIC TECHNIQUES

Chapter XI   CONCLUSIONS

PRESENT POSITION OF EXPERIMENTAL OBSERVATIONS

Encl: Reprints (1) Verma, A.R.,   1951, Nature 167, 939.

(2)   "   " "   1951, Phil.Mag. 42, 1005.

PART I.

THEORIES OF CRYSTAL GROWTH.

CHAPTER I.

THEORY OF THE GROWTH OF A PERFECT CRYSTAL.

1.1.   INTRODUCTION.

The history of the theory of crystal growth
divides itself into two parts. Firstly, the theory of the
growth of an ideally perfect crystal and secondly the
growth of real crystals which are imperfect. The essential
ideas of the growth of perfect crystals were first
formulated by Gibbs (1878). This theory has been developed
during the last thirty years by Volmer (1920 onwards),
Kossel (1927), Stranski (1928), Becker and Döring (1935)
and Frenkel (1945,1946). Burton, Cabrera and Frank (1949,
1951) who have reexamined some aspects of the earlier
theory, have developed a theory of crystal growth which
takes into account the presence of imperfections, especially
dislocations. The experimental observations of the present
investigation are connected with the latter theory, and
have not only confirmed many of its predictions but have
also supplemented them with new facts. However, for the
sake of continuity, a brief account of the theory of the
growth of a perfect crystal will be given, no attempt
being made to discuss this extensive and well-developed
quantitative theory. Instead the subject will be presented
more from a geometrical and pictorial point of view,

emphasizing those results which have a bearing on the later theory in which the dislocations play such an important role.

1.2. GROWTH OF A PERFECT CRYSTAL.

A crystal of any shape may be considered as being bound by close-packed planes of atoms containing steps. The surfaces which coincide with close-packed planes are the only ones which are planar in the sense that all the surface atoms lie on a plane. The vicinal faces may be regarded as close-packed planes separated by steps. For the purpose of illustrating the growth of a perfect crystal, the simple Kossel model may be considered, the molecules being taken as cubes which/stacked face to face. Each cube is attracted equally by all its six neighbours and only the nearest neighbours attract one another.

The structure of any low-index face of a perfect crystal at the absolute zero of temperature at which there are no thermal vibrations may be shown as fig. ($1 \, \delta \, 1a$), which represents the profile of a completely flat surface partially covered by another molecular layer. The boundary line where there is a difference of level equal to an intermolecular spacing between the two sides of the line is called a step on the crystal surface. In general this step will also be incomplete, giving a "kink" of the type marked 'A' in fig. ($1a$), in the step. As shown below, these

2.

"kinks" play an important part, by acting as "exchange sites" in the positioning of new molecules in the building up of the crystal in order to complete a new layer.

As the temperature is raised from absolute zero, the component molecules will start vibrating relative to one another, the vibrations becoming progressively stronger as the temperature is increased. Soon molecules will be shaken from the crystal and will fly about in the space surrounding it. These free molecules constitute the vapour. Thus there will be a certain vapour concentration (average number of vapour molecules per unit volume) in contact with the crystal surface. Those molecules which are at the "kink" positions are more likely to leave the crystal and vapourize, though this will also happen for some molecules at other positions. This can be pictured in the above model, since the molecules at the "kinks" are bound only by three molecules, whilst those on the straight portions of the step are bound by four and those on the flat portions of the surface by five. The energy needed for a molecule to leave the "kink" position such as A is equal to the evaporation energy W . Two processes will occur simultaneously; while some molecules will be leaving the crystal, others will be arriving at the crystal from the vapour. An equilibrium state is reached when the rates of these two processes are equal. The surface will now look

more like fig. (2), having changed from fig. (1a) in two ways. Firstly the step has acquired a number of kinks such as A. Secondly a small number of molecules have been adsorbed on the crystal surface and on the step, shown in fig. (2) as B, and also a similar number of surface vacancies C, a smaller number of pairs of adsorbed molecules D or pairs of vacancies have been created. Aggregates of larger numbers of molecules may also be formed but their propojtion will be progressively smaller, as the number of molecules in the aggregate increases.

(i) Frenkel (1945), Burton and Cabrera (1949, 1951) have studied the structure of a monomolecular step and have calculated the number of kinks per unit length. These kinks will be of two kinds, one may be called a positive and the other a negative kink. Suppose the step is along the x-axis, following it along the direction of increasing x, points where y increases or decreases by a unit spacing 'a', the intermolecular distances, are called positive and negative kinks respectively. They have shown that if n_+ and n_- is the number of kinks of opposite sign per atomic spacing measured along the nearest principal direction, then in equilibrium

$$n_+ n_- = \exp(-2w/kT) \quad - - - - - - - (1)$$

where w is the energy necessary to form a kink, T is

4.

the absolute temperature, k is the Boltzman's constant.
They estimate w to be of the order of $\dfrac{W}{12}$, where W
is the evaporation energy.

The mean distance x_0 between the kinks is given
in terms of 'a', the interatomic distance by

$$x_0 = \tfrac{1}{2} a \left\{ \exp. \left(w/kT \right) + 2 \right\} \quad \cdots\cdots\cdots\cdots\cdots\cdots \quad (2)$$

$$\sim \tfrac{1}{2} a \, \exp. \left(w/kT \right) \quad \cdots\cdots\cdots\cdots\cdots \quad (3)$$

Introducing ϕ, the nearest neighbour interaction,
which is related to the evaporation energy W by the
equation

$$\phi = \tfrac{1}{6} W \quad \cdots\cdots\cdots\cdots\cdots\cdots\cdots \quad (4)$$

Equation (3) may be written as

$$x_0 = \tfrac{1}{2} a \, \exp \left(\phi/2kT \right) \quad \cdots\cdots\cdots\cdots \quad (5)$$

For growth under typical conditions, which may be taken
as such that the temperature lies between 0.5 and 0.8
times T_b, the boiling point in degrees K, $\phi/kT \sim 4$
and equation (5) gives

$$x_0 \sim 4a \quad \cdots\cdots\cdots\cdots\cdots\cdots \quad (6)$$

This concentration of kinks in the steps will remain

practically unchanged even if the vapour is super-
saturated.

(ii) The proportion n_s of the surface sites
covered by adsorbed molecules has been given by Burton,
Cabrera and Frank (1951) as approximately

$$n_s = exp\left(-W_s/kT\right) \quad\text{...............} (7)$$

where W_s is the energy required to transfer a molecule
from a site A to the plane surface. They have
estimated W_s to be about $\frac{1}{2}W$.

It was first realized by Volmer that adsorbed
molecules diffuse with considerable ease over the crystal
surface. Therefore, the process of growth of a crystal
surface with steps will be the result of three processes.
Firstly, a transport of molecules from the vapour to the
adsorbed layer. Secondly, the diffusion of adsorbed
molecules towards the steps. Thirdly, the diffusion of
adsorbed molecules along the edge of the steps towards a
kink. These processes are shown pictorially in fig.(1).
The mean displacement x_s of adsorbed molecules, which
is the average distance a molecule wanders on the crystal
surface between the time it hits the surface and the time
it evaporates again is given according to Burton, Cabrera

and Frank (1951) by the equation

$$x_s = a \, \exp\left\{ (W_s' - U_s) / 2kT \right\} \quad \text{---------} (8)$$

where U_s is the activation energy for surface diffusion
i.e. for migration from one surface site to another, and
this has been estimated to be of the order of $\frac{1}{20} W$;
W_s' is the evaporation energy from the surface to the
vapour and is given by $W_s' = 3\phi$ i.e. half the total
evaporation energy W . From this, neglecting U_s, we
can estimate that

$$x_s \sim a \, \exp\left(3\phi / 2kT \right) \quad \text{-------} (9)$$

which is

$$\sim 4 \times 10^2 \, a \quad \text{------} (10)$$

for typical values of $\phi / kT \sim 4$.

This shows that $x_s \gg a$ from which it follows
that in growth from the vapour, the rate of direct arrival
of molecules from vapour at any particular point on a
crystal surface is generally small as compared with the
rate of indirect arrival by way of surface migration.

The points where growth actually occurs are the
kinks in the steps. This can be pictured again in the
above model, for, when an atom meets a step, it is held

at the step where it is more tightly bound to the crystal, being in contact on two of its six sides. However, it continues to diffuse along the step until it hits a kink or re-entrant angle, where it makes three bonds with the crystal. When the crystal is in equilibrium with the vapour, molecules join and leave these points with equal frequency. The rate of departure depends only on the temperature while the rate of arrival is proportional to the vapour concentration. Hence when the vapour pressure is increased above the equilibrium value, more molecules join kinks than leave them and so the step advances. The velocity v_∞ of a 'straight step' is given by Burton, Cabrera and Frank (1951) as

$$v_\infty = 2 \sigma x_s Z \beta \qquad --------- (11)$$

Where Z is the frequency with which the molecules from the equilibrium vapour strike a lattice site in the surface; β is a factor which is unity in simple cases, and σ is the supersaturation defined by

$$\sigma = \alpha - 1, \qquad \alpha = \frac{p}{p_0} \qquad ------- (12)$$

in which p is the actual vapour pressure and p_0 the saturation value, α being called the saturation ratio. Qualitatively this means that all molecules which hit the surface in the "diffusion zone" of width $2 x_s$ will reach the advancing step and since there is a large

8.

concentration of kinks (i.e. exchange sites) in the step
they will be adsorbed.

A curved step with a radius of curvature ρ
advances with a velocity v_ρ given by

$$v_\rho = v_\infty \left(1 - \frac{\rho_c}{\rho} \right) \qquad \text{------- (13)}$$

where ρ_c, ~~is~~ the radius of critical nucleus defined by
equation (16) is given by

$$\rho_c = a\phi \big/ 2kT \ln \alpha \qquad \text{------(16)}$$

Thus all the steps initially present on the surface
of the crystal, during the process of growth will travel
towards the edge of the crystal and disappear forming a
completed surface, which will contain a few adsorbed
molecules and perhaps a few vacancies. Any further growth
will be possible only if new steps can be formed.

1.3. SURFACE NUCLEATION.

Frenkel (1945) extended the idea of the formation
of kinks in a step to the formation of steps on a perfect
crystal face, in a similar way. Detailed calculation by
Burton and Cabrera (1949,1951) shows that steps will not
be created by thermodynamic fluctuations on a low-index
face unless the temperature is close to the melting point,

when the surface rapidly becomes rough. Therefore, for
the growth to continue, steps must be formed, gradually,
if at all, at ordinary temperatures.

Gibbs (1878) first appreciated that this requires
the initiation of a new layer which is a nucleation process.
Before a new layer can grow, a nucleus or an island
monolayer of the type shown in figs. (1 & 3) must be
formed on the surface. The problem of nucleating an island
monolayer on a close-packed crystal surface is similar to
the familiar problem of nucleating a water droplet. For
a given supersaturation, there is a critical radius ρ_c of
the nucleus (assuming it to be circular), such that a
nucleus of radius greater than ρ_c will grow and if less,
it will evaporate. This arises because the line energy of
the step of the island monolayer causes a local equilibrium
vapour pressure which is inversely proportional to its
radius of curvature. Thus a nucleus with a small radius
of curvature has a high equilibrium vapour pressure.
Hence, the supersaturation which is the excess of ambient
vapour pressure over the equilibrium pressure is less, and
for a sufficiently small nucleus, the supersaturation may
actually be negative so tha t the nucleus evaporates. The
formation of a new layer thus depends upon improbable
fluctuations among aggregates of adsorbed molecules
ultimately producing a critical nucleus. The probability

10.

of this occurrence was first calculated by Becker and
Döring (1935) on the assumption of a rectangular nucleus
and is of the form

$$Z \, (S/s_0) \, \exp \, (-A_0 / kT) \quad \text{------- (14)}$$

where Z is essentially the rate of arrival of fresh
molecules at single surface lattice sites; S is the
surface area of the crystal face under examination; s_0 is
the area per molecule in the layer; and A_0 is half the
total edge free energy of the critical nucleus and is
given by

$$A_0 = \frac{2 \, \rho_c \, \phi}{a} \quad \text{------ (15)}$$

In the simple case of a circular nucleus ρ_c , the radius
of the critical nucleus is given by

$$\rho_c = a \phi \, / \, 2 \, kT \ln \alpha \quad \text{------ (16)}$$

and therefore $\quad A_0 = \phi^2 \, / \, kT \ln \alpha . \quad \text{-------- (17)}$

Recently Burton, Cabrera and Frank (1951) have
re-examined the theoretical basis of this equation with a
more detailed consideration of the shape of the nucleus in
various stages of growth, and the influence of molecular
diffusion on the surface of the crystal. They concluded

that apart from an unimportant numerical factor, the
formula (14) is a correct deduction in view of the
assumption made.

To make an estimate of this probability typical
numerical values can be substituted in formula (14).
Z cannot exceed 10^{13} sec^{-1} even in a dense
environment, therefore, for a crystal of millimetric
dimensions, the whole factor outside the exponential
must be less than 10^{27} ; generally it is about 10^{22}.
For any observable growth rate on the time scale of a
laboratory experiment (say 10^{-3} layers per sec. i.e.
1 micron per month), it follows that $\ln \alpha$ must be at
least $\left(\frac{\phi^2}{kT} \right) / 90$ which with typical value of ϕ / kT
signifies a supersaturation of at least 25% to 50%.
Thus the nucleation rate is an extremely sensitive function
of supersaturation. Above this critical supersaturation,
the growth rate would increase rapidly with supersaturation,
the process not being limited by nucleation. Below this
critical supersaturation, the probability of nuclei
formation would become rapidly negligible.

These theoretical conclusions are however, not in
agreement with experimental observations. Volmer and
Schultze (1931) trying to verify this result studied the
growth rate of individual iodine crystals in slightly
supersaturated vapour at $0^{\circ}C$.

They found the growth rate proportional to the super-saturation down to a value of 1%. Only below this degree of supersaturation did it fall below proportionality and then not abruptly.

On the other hand, the observations of Haward (1939) are in agreement with the theory of surface nucleation. He studied the deposition of several sublimable solids like $Hg I_2$ on a metal surface, coated with a previous deposit of the same substance. This coated metal target was subjected to a vapour 'beam' of controlled intensity at a fixed temperature. Using a weighing technique to measure the mean overall rate of deposition, the theory of surface nucleation was verified.

There are, however, no other known experiments of this kind. In general for those crystals which grow, the growth rate is proportional to supersaturation down to values much lower than the theoretical supersaturation of surface nucleation theory.

1.4. SUMMARY.

To summarize then, the position is as follows. Any crystal face with a step will continue to grow because of the high concentration of kinks in it created by Thermal fluctuations. During the process of growth

13.

this step will travel to the edge of the crystal and thus disappear leaving a complete crystal surface. When all the steps have been eliminated by advancing and forming complete layers, further growth will continue only if new steps can be formed. Now on a low-index face, steps cannot be created by thermodynamic fluctuations in the same way as the creation of kinks in a step, below a certain critical temperature which is close to the melting point. Therefore, for further growth on low-index faces, steps must be formed gradually at ordinary temperatures by some mechanism. This can happen by the formation of a two-dimensional nucleus or island of molecules, the edges of which will provide the necessary steps. It has been shown that the probability of the formation of nuclei is a very sensitive function of supersaturation and is quite negligible below a certain critical value which for typical values of the constants involved is of the order of 25% to 50%. However, real crystals grow at observable rates at supersaturations of 1% or lower — infact the most regular and well developed crystals are obtained at low supersaturations. At these low supersaturations the probability of the formation of nuclei is negligible.

This, therefore, leads us to the conclusion that the growth of crystals at low supersaturations can only be explained by recognizing that real crystals are not perfect.

This idea first introduced by Frank (1949; Burton et al. 1949, 1951) for the growth of a crystal, provides us with another mechanism by which a surface remains stepped no matter how far the steps advance. Therefore, the growth of the crystal face will continue. In the following chapter a description of the development of this theory will be given.

CHAPTER II.

GROWTH OF AN IMPERFECT CRYSTAL

2.1. DISLOCATIONS

Smekal first pointed out that an important difference in the properties of crystals is related to the distinction between ideal and real crystals. Certain properties of crystals which are essentially independent of crystal defects were designated by him as structure-insensitive, whilst those depending upon the presence of defects were called structure-sensitive properties. Among the structure-insensitive properties, may be named the specific heat, elasticity, thermal expansion and compressibility, the energy of formation, the principal features of optical absorption (colour) and dispersion, and finally dia - and para magnetism. The important structure sensitive properties are, diffusion phenomena, the ionic and electronic conductivity in insulating crystals and semi-conductors, the internal photo-effect, plasticity, and crystal strength.

The imperfections introduced to explain these structure sensitive properties of a real crystal, are of three different types. The first type of crystal defect consists of lattice flaw where foreign atoms have taken up the normal positions of the atoms in the crystal lattice, a vacant site may be said to be a special case of this. The second type is known as interstitial atoms. These consist

16.

of either foreign atoms or atoms of the crystal material, outside the regular geometrical positions *in* the crystal lattice. The third type which is called dislocations, consists of purely geometrical faults in the crystal lattice. Of these, only the last type has any effect on the lattice at distances greater than a few inter-atomic spacings.

The concept of a dislocation arises naturally as a result of the crystallographic nature of plastic flow. It is observed in strained metals that slip lines mark important crystal planes and the plastic strains can be resolved into simple shears along these planes, the plastic flow being determined by the shear stress. Furthermore, gliding occurs in the direction of closest atomic packing in the glide plane and not in the direction of maximum resolved shear stress. Therefore, this shows that the plastic flow occurs by the sliding of certain atomic planes called slip planes, the structure of which remains crystalline during flow.

Now, if we consider a plane of atoms A , sliding in a certain crystallographic direction across a neighbouring plane B , different portions of A will, in general, slip over B by different amounts. This will be so, because the atoms in a crystal are not rigidly bound to each other but are elastically coupled so that thermal vibrations and local irregularities will make the forces acting over the glide

17.

planes non-uniform. A boundary may be pictured such that
on either side of this, the two planes A and B have
slipped by different amounts. The type of line discontinuity
marking this boundary is called a dislocation. There are
two standard types of dislocations, the 'edge' and the 'screw'
dislocation, with a series of intermediate cases which can
be regarded as composed of these two standard types. An
excellent account of the theory of dislocations has been
given by Cottrell (1949). These dislocations will be briefly
illustrated by simple models.

2.2. EDGE DISLOCATIONS

The type of dislocation which was first introduced
by Taylor (1934) Polanyi (1934) and Orowan (1934) is called
the 'edge' dislocation. This may be pictured as follows.
Consider a block of crystal (fig. (4)) in which the lower
half of the crystal is pulled with respect to the upper half
in the direction shown by arrows. The result is shown in
fig. (4). We see that the part A B E F has slipped in the
direction A'F' and the part E F D C has remained unslipped.
E F marks the boundary between the two regions which have
slipped by different amounts and is the dislocation line.
The atomic structure in the side plane perpendicular to E F
is shown in fig. (5). It will be seen in fig. (5) that atoms
in the upper half crystal P are compressed along the slip
direction and those in the lower half Q are extended. The

18.

situation is analogous to the insertion of an extra half plane of atoms from above. The dislocation line lies at the edge of this plane and hence its name. It will be observed that the dislocation line E F is perpendicular to the slip direction A'F'.

Dislocations can also exist which are the inverse of that shown in figs. (4) and (5), and will be created when the extra half plane of atoms is inserted from below instead of from above. These two types are called the positive and negative dislocations. Since, by inverting the diagram, or crystal, a positive dislocation can always be turned into a negative one or vice versa, this distinction would be trivial. The real distinction between the positive and negative dislocations is given by the forces exerted between the dislocations, since dislocations which are of the same sign repel each other while those of unlike sign attract one another.

2.3. SCREW DISLOCATIONS

The second type of dislocation was first introduced by Burgers (1939) and is called a screw dislocation. This may again be illustrated by a crystal model. A cut A B E F is made in the crystal (fig. (6)) and the crystal material to the right of the cut is pushed down by one molecular diameter. The result is shown in fig. (7). A step had now

been created, on the surface of the crystal such that on
the left hand side, the plane of the crystal surface is
higher and on the right hand side it is lower. The step
does not extend throughout the surface of the crystal but
extends only from the point F to the edge of the crystal.
The line E F is the boundary line between the right and
left parts of the crystal which have slipped by unequal
amounts and hence is the dislocation line. The model of
fig. (8) illustrates the arrangement of molecules for a
dislocation line meeting the surface of the crystal at right
angles. The molecules in the crystal no longer lie on planes
as in the ideal lattice but are continuously displaced. At
distances larger than a few intermolecular distances from
the dislocation line, the crystal deviates very little from
perfection: only very near the dislocation line some
irregularity seems to appear. In fig. (9) showing arrange-
ment of molecules in the slip plane A B C D, a part A B E F
of this plane has slipped in the direction E F, while the
remainder F E C D has not slipped. In fig. (9) the dotted
lines and circles, represent the molecules to the *left* of
the slip plane whereas the molecules to the *right* of the
slip plane are represented by full lines and circles. It
may be pointed out that the dislocation line E F is parallel
to the slip direction.

A route may be considered on any lattice plane of
the crystal, along a line drawn through nearest neighbouring

20.

atoms in such a way that it forms a closed plane loop. Such a line is called a Burgers circuit. If by tracing the line in the real lattice, corresponding to the circuit in the perfect lattice, this line does not form a closed loop, then a geometrical fault of the dislocation type is present. The vector required to complete the Burgers circuit is called the resultant Burgers vector of the dislocations encircled.

This may be pictured in the above model of figs. (7 & 8) by considering a route taken from the top of the step, going round the dislocation point F back to the bottom of the step. We have followed a path on the surface of the crystal which was flat before the creation of the dislocation, and instead of finishing at the starting point we finish one molecule beneath it. In order to complete the Burgers circuit i.e. to reach the starting point, a vector equal to the height of the step is needed. Burgers gave the name "dislocation strength" to the modulus of this vector.

The crystal containing one screw dislocation is not built of molecular layers stacked on top of each other as in ideal case, but instead consists of a single molecular plane in the form of a helicoid of a spiral staircase and hence the name screw dislocation; the dislocation line being called its axis.

The Burgers vector is independent of the distance of

the Burgers circuit from the dislocation, giving evidence
only of the total effect of the dislocations encircled. Pairs
of dislocations of equal but opposed Burgers vector may escape
detection unless the Burgers circuit is taken as small as
possible. A more detailed description of the general behaviour
of the Burgers circuit has been given by Frank (1951). Since
the Burgers circuit can be continuously displaced along the
dislocation line without change in its Burgers vector, a
dislocation cannot terminate within the crystal.

The screw dislocation may be either of the right-
handed or the left-handed type. In the right-handed type,
moving along the Burgers circuit from a higher to a lower
level, the route will be clockwise, whereas in the left-
handed type it will be anticlockwise. The right-handed dis-
location will be obtained when the crystal material to the
right of the cut A B E F (fig. 7) has been pushed down with
respect to the other, the inverse operation will create a
left-handed screw dislocation. Since these dislocations may
be turned into one another by turning the crystal, this dis-
tinction would again be trivial, but as before it is the
forces exerted between the dislocations that distinguish
them - like dislocations repel and those unlike attract each
other. As is shown in the next section right-handed and left-
handed screw - dislocations give rise to 'growth spirals'
which are clockwise and anticlockwise respectively. This

22.

distinction is of importance when growth fronts originating
from different sources interact with one another.

2.4. GROWTH SPIRAL

The dislocations that take part in the growth of a
crystal are of the screw type. As seen in the last section,
a screw dislocation emerging on the face of a crystal provides
it with a step. This step is self perpetuating in the sense
that when one, two or any number of layers of atoms have been
laid down on the crystal surface, the step remains. Hence
the steps needed for the growth of a crystal are provided by
the screw dislocations and the need of two dimensional
nucleation never arises. This offers an explanation to the
observed growth of crystals at low supersaturations.

The process of growth under these circumstances in
the presence of screw dislocations will be similar to that
outlined for a perfect crystal with a step. The step provided
by the screw dislocation will have kinks as before and when
the atoms are adsorbed on the crystal surface, they diffuse
to the step and finally to the kinks where they are adsorbed
for the building up of the crystal and the step will advance.
In the case of a perfect crystal the step extended all the
way across the crystal surface so that it could advance
parallel to itself, thereby completing a new layer. However,
the step provided by the emergence of a screw dislocation,
terminates at the dislocation point, where it remains fixed.

Hence, when growth takes place, the step can advance only by rotating round the dislocation point somewhat like the hand of a clock. At a particular supersaturation each point on a straight step will advance with the same speed, therefore, the section of step near the dislocation will have a higher angular velocity for the same linear velocity and consequently make a larger number of revolutions in a given time than the sections further out. Thus the step will wind itself into a spiral. Actually, for the section of the step near the centre because of the higher curvature there will be a higher equilibrium vapour pressure and therefore a lower local super-saturation, so that its rate of advance is slower and its curvature is everywhere less than ρ_c^{-1} , as seen from equation (13). When the steady state has been reached, the whole spiral will rotate uniformly about the dislocation. Several stages of the development of a growth-spiral are shown in fig. (10) which shows the top of the crystal in fig. (8) looking from above. In fig. (10) the spiral has been drawn as a smooth curve. The exact shape of the spiral and the more complex shapes arising from a number of dislocations is left to a later section.

These considerations, which were first put forward by Frank (1949), predict that on the surfaces of the crystals which have grown by this mechanism, flat molecular pyramids should be observed. An ideally long anneal would get rid of these dislocations but in practice some may always be expected

to remain. The available experimental evidence in support
of this theory will now be given.

3.1. DIFFICULTIES OF OBSERVATION

The elementary, molecular growth features (as distinct
from gross growth features) are the ideally simple features
which are easily interpreted by theory and are therefore
likely to reveal considerable information about the mechanism
of crystal growth. Therefore, it is only these molecular
growth features, which have not been influenced by any
accidental disturbances of growth, that have been studied in
the present investigation.

Before the discovery of electron-microscope only
optical instruments, such as a light microscope, were available
to study these growth phenomena, for which purpose two
resolutions of the instruments are required viz. the lateral
resolution perpendicular to the direction of observation, and
the resolution of depth. The depth resolution needed is of
the order of a few Angstrom units and is characteristic of the
crystal under examination, whereas the lateral resolution in
an optical microscope is limited by the wave-length of light.
Consequently the growth features had to be sufficiently far
apart, to be resolved. This necessitates making observations
on almost perfect crystals, molecularly flat over wide areas;
such crystals are rare. After obtaining such a crystal, the
problem still remains to make visible those features only a
few Angstrom units high. It is only recently that the optical

CHAPTER III
PAST OBSERVATIONS

3.1. DIFFICULTIES OF OBSERVATION

The elementary, molecular growth features (as distinct from gross growth features) are the ideally simple features which are easily interpreted by theory and are therefore likely to reveal considerable information about the mechanism of crystal growth. Therefore, it is only these molecular growth features, which have not been influenced by any accidental disturbances of growth, that have been studied in the present investigation.

Before the discovery of electron-microscope only optical instruments, such as a light microscope, were available to study these growth phenomena, for which purpose two resolutions of the instruments are required viz. the lateral resolution perpendicular to the direction of observation, and the resolution of depth. The depth resolution needed is of the order of a few Angstrom units and is characteristic of the crystal under examination, whereas the lateral resolution in an optical microscope is limited by the wave-length of light. Consequently the growth features had to be sufficiently far apart, to be resolved. This necessitates making observations on almost perfect crystals, molecularly flat over wide areas; such crystals are rare. After obtaining such a crystal, the problem still remains to make visible these features only a few Angstrom units high. It is only recently that the optical

26.

techniques of multiple-beam interferometry and phase-contrast microscopy have developed sufficiently to make possible the study of such features.

The technique of electron microscopy is very superior for lateral resolutions but has only a limited resolution in depth probably of the order of 50 A e.g. the observation by Dawson and Vand (1951) of growth spirals of long-chain paraffins with step height equal to 47 A. This limitation will make it impossible to observe most of the growth features of step heights less than this. Naturally experimental observations of such growth features will be necessarily limited.

3.2. EARLIER OBSERVATIONS

Several workers have studied the surfaces of growing crystals. Marcelin (1918) and Kowarski (1935) studied the growth of m-toluidine from alcoholic solutions, which gows in extremely thin plates, thin enough to give interference colours. Discontinuities in the shade of interference colours, which meant discontinuities in thicknesses were observed to move across the surface of the crystal. It was calculated that some of these layers formed were only a few molecules in thickness. Volmer (1923) observed similar thin layers on thin crystals of $Pb\,I_2$ formed by mixing $Pb(NO_3)_2$ and KI solutions.

Bunn and Emmett (1949) studied a number of crystals

using dark ground illumination under high resolution and
found that on fairly thick crystals of some substances layers
several hundred Angstrom units high could be seen spreading
across the *face*. On some crystals the layers were so thick
that they could be seen by ordinary transmitted light or in
birefringent crystals by using crossed nicols. Non-polar
crystals were not observed to show layer formation and hence
the studies were confined to ionic or polar crystals. As a
result of their observations they found that layers often
start from the centre of the faces spreading outwards, the
thicknesses of the layers increasing as they approach the
edges. At rapid growth the boundaries of these layers are
irregular, but at slow growth these take regular shapes
conforming to the symmetry of the crystal face. Dissolved im-
purities were observed to influence strongly the thickness and
shape of the layers.

Evidence of the formation of surface nuclei was
concluded from these observations and they thought that this
process of layer formation observed for layers of thicknesses
of several hundred Angstrom units would give the correct
impression of what happens for molecular layers.

Instead of observing a crystal while it is growing,
another approach for their study is to observe the surface of
a crystal on which growth has been arrested. The observation
of such a crystal will reveal its history. In this latter

case of observation much better techniques can be employed and is therefore likely to yield more information. The present investigation comes under this category.

Growth pyramids of vicinal faces have long been observed and were recognized as a normal feature of slow growth (Miers (1903-4). Growth pyramids of this type can be seen on major rhombohedral faces of quartz crystals, but only limited information can be obtained from them since their structures cannot be resolved and bunching of steps is very frequent.

At the start of the present investigation, the only reported experimental data which demonstrated the growth of the crystals by spiral mechanism was that of Griffin (1950). He was the first to observe, using ordinary microscopy, line markings on the $(10\bar{1}0)$ faces of beryl crystals, which there is reason to believe are the edges of growth layers. Calibration by multiple-beam interference fringes has shown that the step-height at these lines is less than 34 A i.e. less than four unit-cells - of the crystal. The behaviour of these steps around obstacles, where they neither split nor form multiple steps, suggests that each is like a unit step. Further these lines take the form expected from the edges of "monomolecular" growth terraces and in particular regions of the crystal face terminate in a manner which would be expected from the examination of a growth terrace terminating at a screw dis-

locations. In addition, the observed patterns originating from a single and double screw dislocations correspond with the theoretically predicted shapes. From these facts, it was concluded that the observed steps are a unit cell high and thus the observed spiral was interpreted as a "growth spiral" in accordance with Burton, Cabrera and Frank's theory (1951).

Spiral markings on silicon-carbide crystals have been observed for some time past. Menzies and Sloat (1929) reported such observations and more recently Padurow (1949) and Kalb and Wittborg (1951). But none of these workers has tried to offer any explanation as to the spiral formation, nor has any measurement of step height been made.

Thus the experimental position at the start of the present work was that the observations were meagre and qualitative. No exact measurement of the step height had been reported. In the interim period several other experimental observations have become available, and these are described in Chapter (XI) where the present position of the experimental observations is surveyed.

PART II

SILICON - CARBIDE, ITS FORMATION, CRYSTAL - STRUCTURE AND POLYTYPISM

CHAPTER (IV)

FORMATION OF SILICON-CARBIDE CRYSTALS, POLYTPISM AND NOTATIONS.

4.1. FORMATION OF SILICON-CARBIDE CRYSTALS.

In 1890 Acheson tried to crystallise carbon by dissolving it in aluminium silicate in an electric arc, as a result blue crystals were obtained which were called carborundum. Analyses showed it to be Si-C. Later these crystals were made by reducing silica with carbon in an electric furnace. Naturally occurring Si-C crystals have been found as small hexagonal plates in a meteorite in Arizona, this mineral being called moissanite.

Best commercial grades of carborundum are pale green but various green and blue shades as well as black samples are common. Carborundum free from traces of iron is without colour. The cubic modification of silicon-carbide often occurs as yellow crystals, whereas the crystals of the rhombohedral and the hexagonal modifications occur in different colours and this colouring seems to be independent of the crystal modification (polytypism, see 4.2). It may be thought that the colouring is due to impurites. The considerable differences observed in the relatively low metallic conductivity of different specimen's have also been attributed to impurities (Weigel 1915). The crystals studied in the present investigation were pale green, dark green, blue and black in colour.

The exact mode of the growth of silicon-carbide (Si-C) crystals is not known. The melting point of silicon-carbide has been estimated to be near 2230° C (Weigel 1915) and it will probably dissociate at that temperature, so that

silicon-carbide crystals do not grow from their own vapour.
Carbon and silica present inside the furnace, react at that
temperature, generating more volatile gases SiO and CO
which supply C and Si needed for the growth of silicon-carbide
crystals. It is thought that these gases will be adsorbed
on the surface of the growing crystal and will undergo surface
diffusion reacting with one another to form Si-C, the excess
oxygen being removed as CO_2 (or perhaps O_2) which generates
C O on the hot carbon while C O also reduces SiO_2 to the
relatively more volatile SiO . The surface of the growing
crystal may have a layer of combined oxygen; the state of
the surface would vary with temperature and the $CO-CO_2$
balance in the atmosphere and would be quite complex. (Frank
1951a).

4.2. DIFFERENT TYPES OF SILICON-CARBIDE CRYSTALS
AND 'POLYTYPISM'

Silicon-carbide, which is strongly homopolar, occurs
in over 12 known and possibly some more types. Among these,
only one cubic form has been observed and there is no
likelihood of anymore. This cubic form has a structure
corresponding to $\beta-ZnS$ (sphalerite) and hence it is suit-
ably called $\beta-SiC$. All the remaining types are called
$\alpha-SiC$ and are based either on hexagonal or rhombohedral
unit cells. The basal pinacoid is predominantly developed
and the crystals usually occur as hexagonal plates. The

opposite faces of the hexagonal plates differ in appearance
in all modifications. One face is planar, the other often
stepped, and it is on these plane faces that growth spirals
have been observed. The various forms are so closely related
to each other that a special term "polytypism" has to be used
to distinguish it from the normal "polymorphism" (Baumhauer
1911, 1915; Thibault 1944); the various modifications being
called the "polytypes" of silicon-carbide.

4.3. DESCRIPTION OF THE TYPES : RAMSDELL'S NOTATION

The different polytypes of silicon-carbide were called
type I, II, III etc., in the order of discovery, without
referring to their crystal structure. As the number of the
known types grew larger, it was soon realised that some
designation, which will describe the type appropriately, had
to be found out. Such a designation should be simple and accur-
ate, and should describe the structure as fully as possible.

X-ray studies revealed that all types are composed of
identical layers and differ only in their arrangement of these.
Each type is uniquely distinguished by the number of layers
necessary for the arrangement to repeat itself. Thus the
total number of layers within the length of c — axis for the
types with the hexagonal unit - cell or the rhombohedral types
referred to the hexagonal unit may be taken to represent the
type and Ramsdell (1947) added to this number the letter "H"
or "R" depending upon whether the unit cell is hexagonal or

33.

rhombohedral respectively. The different types are given in
the table (I) and the unit cell constants as determined by
X-ray methods are given in table II.

Table I

Ramsdell's Notation of Different Modifications.

β-Si C	α - Si C				
CUBIC	HEXAGONAL			RHOMBOHEDRAL	
Notation	Old Notation	Ramsdell's notation		Old Notation	Ramsdell's Notation
β -Si C	II	6 H		I	15 R
	III	4 H		IV	21 R
				VI	33 R
				V	51 R

This notation uniquely distinguishes the different
types and will be used for brevity in future. However, this
notation does not reveal the geometry of the regular arrange-
ment of the different layers in the unit cell. The different
notations described below reveal this regularity in a simple
manner.

34.

Table II

Unit Cell Dimensions.

Type	Hexagonal Cell		Rhombohedral Cell	
	a_0	c_0	a_{rh}	α
4 H	3.073A	10.053A	-	-
6 H	3.073A	15.079A	-	-
15 R	3.073A	37.70 A	12.69A	13° $54\frac{1}{2}'$
21 R	3.073A	52.78 A	17.683A	9° $58'$
33 R	3.073A	82.94 A	27.704A	6° $21\frac{1}{2}'$
51 R	3.073A	128.178A	42.763A	4° $07'$

β -Si C Cubic a_0 = 4.349 A.

4.4. INTERVAL SEQUENCE

Ott (1925) in his report of the type I, 15 layered rhombohedral crystal, described the structure in terms of the sequence of silicon (or carbon) atoms along the symmetry axes. In a given axis there are five atoms which are separated by layer intervals of 2, 4, 3, 4, 2. Thus the sequence (24342) was used to describe the structure. For the 33 and 51 layered rhombohedral types the interval sequences are (242433342242) and (2424243333342424242) respectively. Not only does this interval sequence become

more and more unwieldy with the increasing number of layers in the unit cell, this method is not equally applicable to the hexagonal structures since for them the symmetry axes, are not all alike, the sequence along the 6-fold axis being different from that along the 3-fold axis. Therefore, this notation gave place to more superior methods of describing the types.

4.5. CLASSICAL ABC NOTATION

The structure of silicon-carbide crystals may be described in terms of the close-packed layers of spheres. As is well known, equal spheres close-packed in a plane will lie with their centres at the corners of equilateral triangles each sphere touching six others in its own plane. All three-dimensional close-packed structures may be regarded to be built up of layers of this sort. These layers when projected normally on a plane parallel to one of them fall into three possible positions, and may be labelled. A, B and C. The possible close-packings correspond to any sequence of these letters with no successive letters alike. The simplest form of close-packing is AB AB AB .... etc., and is the hexagonal close-packing. The arrangement ABC ABC ABC .... etc., gives the cubic close-packing.

In each of the known structures of silicon-carbide crystals we have a silicon-lattice and an identical inter-penetrating carbon lattice, which is displaced relative to the

other parallel to the c-axis, both structures being infinitely extended. Each carbon is tetrahedrally bonded to four silicon atoms and vice versa. The lattice of three modifications viz: 15R, 6H & 4H is shown in fig.(11). The c-axis is parallel to the vertical direction.

All silicon and carbon atoms lie on the symmetry axes, and all symmetry axes lie in the ($11\bar{2}0$) planes. Therefore, the structure is most conveniently represented in a projection in the plane perpendicular to the c-axis. Since the carbon and silicon lattices are identical and displaced only along the c-axis, they will coincide in this projection; therefore, each corner of the net-work of equilateral triangles represents both C and Si atoms.

All silicon-carbide types being built of layers of close-packed spheres will have trigonal symmetry by simple rotation about the c-axis. Each layer has 2-3 and 6 fold symmetry axes normal to its plane. When two or more layers are put over one another, the 2-fold axes do not coincide with one another and, therefore, vanish. The 6-fold axes coincides with the 3-fold axes, so that the resultant structure has only 3-fold symmetry. The symmetry elements are shown in fig. (12a).

Now if in these close-packed layers we represent the silicon atoms by Roman letters and carbon atoms by corresponding Greek letters, the layers may be called $A\alpha$, $B\beta$, $C\gamma$ layers.

The different carborundum types will be built of such layers

$A\alpha$, $B\beta$, $C\gamma$ of which no two successive layers are

identical. In future for brevity these may be called A, B and

C layers, remembering that the corresponding Greek letter is

implied in the case of silicon-carbide crystals.

4.6. REPRESENTATION OF THE POLYTYPES IN THE CLASSICAL ABC NOTATION

It is possible to represent the different polytypes

by specifying the successive layers comprising the unit cell,

in terms of the A, B, C notation. The representation of

some of the different polytypes is given in table(III).

Table III

Crystal modification		CLASSICAL ABC notation
Old notation	Ramsdell's notation	
I	15R	ABCACBCABACABCB
II	6H	ABCACB
III	4H	ABCB
VI	33R	ABCACBABCACBCABACBCABACABCBACABCB

In a similar way all the different polytypes consist-

ing of larger number of layers can also be represented. It

will be noted that this representation becomes more and more

unwieldy with the increasing number of layers and also does

38.

not directly reveal the relationship between successive layers.

4.7. STACKING OPERATORS, ZHDANOV SYMBOL AND FRANK'S NOTATION

The arrangement of the successive layers is best represented in terms of the relationship between two layers or in terms of the "stacking operators". Though all the layers are equivalent to each other, they are displaced or rotated through 60° with respect to each other. The pairs AB and BA are to be differentiated from one another. In the case of silicon-carbide crystals these layers are $A\alpha$ $B\beta$ and $B\beta$ $A\alpha$, but as mentioned before for brevity only Roman letters may be used, the Greek letter being implied. The difference between AB and BA is best seen from figure (12b). If the layer B is on top of A, each atom of B (represented by x) lies at the centre of an equilateral triangle formed of the three atoms of A (represented by o), such that with the suitable rotation of the figure, as in the figure drawn, these triangles are oriented as $\triangle$ i.e. the centre of the three spheres that provide a dimple, into which the sphere of layer B fits, form an equilatral triangle which is oriented as $\triangle$. If, on the other hand, the layer A lies on top of B, the atoms of A lie at the centres of the equilateral triangles formed of the atoms of the layer B, such that these equilateral triangles are oriented as $\triangledown$. Thus the relationship itself

between the layers may be represented as $\triangle$ and $\triangledown$ respectively. It can at once be seen that when C follows B and A follows C, the relationship is again $\triangle$ i.e. if A, B and C layers follow each other in this cyclic order, the relationship between the layers is always $\triangle$. However, the other three alternative arrangements i.e. A following B; B following C; C following A, will be represented by $\triangledown$. This representation has mnemonic value also since a rotation through 60° converts the operation $\triangle$ into $\triangledown$.

This notation used by Frank (1951a) will represent the various polytypes of silicon-carbide crystal as given in the table IV, and will, hereafter, be referred as Frank's notation.

Table IV

Crystal Modification in Ramsdell's notation	Frank's Notation
15R	$(\triangle\triangle\triangle\triangledown\triangledown) \triangle\triangle\triangle\triangledown\triangledown\triangle\triangle\triangledown\triangledown$
6H	$(\triangle\triangle\triangle\triangledown\triangledown\triangledown) \triangle\triangle\triangle\triangledown\triangledown\triangledown - - - $
4H	$(\triangle\triangle\triangledown\triangledown) \triangle\triangle\triangledown\triangledown - - - - $
33R	$(\triangle\triangle\triangle\triangledown\triangledown\triangledown\triangle\triangle\triangle\triangledown\triangledown) \triangle\triangle\triangle\triangledown\triangledown\triangledown\triangle\triangle\triangle\triangledown\triangledown - - - - $
51R	$(\triangle\triangle\triangle\triangledown\triangledown\triangledown\triangle\triangle\triangle\triangledown\triangledown\triangledown\triangle\triangle\triangle\triangledown\triangledown) \triangle\triangle\triangle\triangledown\triangledown\triangledown - - - -$

Thus it will be seen that, for the hexagonal types, the number of $\triangle$ and $\triangledown$ necessary to repeat itself is the

same as the number of layers in the unit cell. In the rhombohedral types referred to the hexagonal unit, the number of layers within the unit cell is 3 times the number of $\triangle$ and ∇ operators. The $\triangle$ and ∇ repeat unit is enclosed within round brackets. This fact will be further brought out by the interferometric study (see Chapter 10).

This notation can be further contracted in the Zhdanov symbol (Zhdanov 1945) which consists of pairs of numbers in which the first is the number of consecutive $\triangle$s and the second the number of consecutive ∇s following the $\triangle$s . Thus silicon-carbide of type 15R would be represented by the symbol (32) and the commonest variety of silicon-carbide type 6 H by the symbol (33). The various polytypes of silicon-carbide are represented in Zhdanov's symbol in the table V.

Table V

Crystal Modification in Ramsdell's notation.	Zhdanov's Symbol
15 R	(32)
6 H	(33)
4 H	(22)
33 R	(3332)
51 R	(33 33 32)
69 R	(33 33 33 32)
87 R	(33 33 33 33 32)

Ramsdell (1947) in his notation has given these numbers a slightly different significance and calls it the

"zig-zag sequence", which represents the sequence of succeeding atoms in the $(11\bar{2}0)$ section. Fig. (13) shows one such section. If a Si (or C) atom lies on A in one layer, in the next layer the atom may lie either to the right on B or to the left on C. Say it lies to the right. Then the third layer may have its atom continued to the right or it may change direction and lie to the left. Thus the positions of atoms in the succeeding planes when joined together will give a zig-zag pattern in the $(11\bar{2}0)$ section. Such an arrangement can be described in terms of the number of layers added in each direction in succession and is called by Ramsdell "zig-zag sequence". Thus silicon-carbide crystals of types 15R, 6H etc., will be represented by (32 32 32) and (33) etc., respectively. It may again be pointed out that in rhombohedral types, the symbol is always repeated three times. This is done to complete the unit cell such that the last layer lies directly above the initial layer. In the table II which gives the unit cell constants of the different polytypes, it may be noted that this correlates with $a_{rh} = \frac{1}{3}$ of the lattice parameter c.

Ramsdell pointed out that the various polytypes belong to the (3....2) series and predicted the type 69R, with the zig-zag sequence $(33\ 33\ 33\ 32)_3$ and also other hexagonal structures like 10H, 16H etc. He also noted that the numbers in the zig-zag sequence are either 2, 3, or 4, and that the

number 1 does not occur in these structures. He further made
an important generalization that not only is the (33) structure
of type 6H the commonest of all modifications, it also occurs
within most of other structures.

4.8. NOTATION USED BY JAGODZINSKI

Some other workers notably Jagodzinski (1949) have
used a slightly different notation. In this notation consider-
ation is taken not only of pairs of layers but of one layer
on either side of a single layer. Any layer which is preceded
and succeeded by the same type of layer is denoted by 'h' but
if the two are different, the layer is denoted by 'k'. Thus
the layer B in the arrangement ABA or CBC will be denoted by
'h' and in the arrangement CBA or ABC, it will be denoted by
'k'. Identical 'h' and 'k' notations can be used for A and C
layers. According to this notation silicon-carbide crystal
of type 15R will be (h k k h k) and type 6H will be (h k k).
Jagodzinski, further developed the general equations for the
interaction between neighbouring layers in the arrangement
and showed that the most probable layer type consisting of
more than six layers of close-packed atoms is the silicon-
carbide type with 15 layers. This is the second commonest
variety of silicon-carbide crystals.

Part 111

EXPERIMENTAL METHODS USED IN THE

PRESENT STUDY

CHAPTER V

MICROSCOPIC TECHNIQUES

In the present investigation the experimental work
may be divided into two parts. Firstly the observation of
growth spirals and other molecular features and secondly the
measurement of step-heights. Therefore, two distinctly
different techniques were employed for their study. Various
microscopic techniques were utilized for the observation of
these features; and for the measurement of step heights multiple
beam interferometric techniques were used.

In both the microscopic and interferometric studies
the silvering technique is needed; both the crystal surface
and the optical flat used for interferometric studies have to
be coated with a highly reflecting layer of silver. The
silvering of the crystal surface is necessary for two purposes.
Firstly for the microscopic observation and secondly for the
interferometric study when it forms the second (or the back)
surface of the interferometer. The silvered optical flat forms
the front or the first surface of the interferometer in the
reflected system, and, therefore, it is essential, in order
to secure good visibility of the fringes that it should have
a low absorption. To achieve this, a silvering technique was
used, as described below (see Strong (1940) and Tolansky (1946,
1948)).

5.1. THE SILVERING TECHNIQUE

A commercial evaporating unit, built by Edwards and Co., of type E_3 was used for this purpose. This consists of a large vacuum chamber in the form of a glass bell jar 60 cm high and 40 cm. in diameter. This can be evacuated by a three stage silicon-oil diffusion pump backed by a rotary oil pump. The backing vacuum and final vacuum can both be read directly by the Pirani gauge and Phillips ionisation gauge supplied in the unit.

The surfaces of specimens must be thoroughly cleaned before silvering. The glass optical flat after being cleaned with soap water is cleaned with hydrogen peroxide ($H_2 O_2$) and distilled water, and then rubbed with clean dry cotton wool until no breath figures are obtained by lightly breathing on it. For the cleaning of silicon-carbide crystals, which are very resistant to chemical action, it was possible to use acids and other reagents e.g. nitric acid. Before the evaporation of silver, a final cleaning of the surfaces is performed inside the evaporation chamber by ionic bombardment from a high voltage discharge passed at a pressure of 1 mm. of mercury and lower. After this discharge cleaning spectroscopically pure silver is thermally evaporated from a molybdenum strip on to the specimens at as low a pressure as possible (usually $1 \times 10^{-5} cm.$ of Ag), so that a highly reflecting layer of silver with a low absorption is obtained.

Under these conditions the silver layer contours the

surface very closely without imposing any structure of its own. Electron-microscopic studies show that the distance of migration of silver atoms on the substrate, when deposited under these conditions is not more than 500 A (Picard and Duffendack 1943) and for high rates of evaporation, the mean distance of migration may be considerably reduced and it may be assumed that this will result in better contouring of the surface. (Levinstein 1949). The usual rate of evaporation was such tha t 90% reflectivity could be achieved in less than 10 seconds. In this evaporating unit the filament and specimen distance is quite large (nearly 50 cm), so that any variation in density over the optical flat (diameter 2.5 cm) or over crystal specimens (usually less than 5 mm. in size) is negligible; in fact it can be calculated to be less than 1% over a circle of 10cm. diameter.

5.2. TECHNIQUES OF OBSERVATION

The elementary growth features on silicon-carbide crystals are only faintly visible because of the small step heights (e.g. for type 6 H, the step height is 15 A). Various optical techniques were tried for the observation of these features.

(a) Off-Focus Bright-Field Narrow Pencil Illumination

Since the crystals are opaque, they had to be studied in reflection. This has the additional advantage that for a step of height t, this increases the path difference

46.

between the rays to 2t.

The clean surface of the crystal, when examined by a metallurgical microscope, using bright-field illumination, does not show up any of the molecular growth features, the surface appearing smooth. Therefore, the technique which was utilized by Griffin (1950) for the observation of growth features on beryl crystals was next tried. This consists first in depositing a thin, highly reflecting layer of silver, by the technique described in the previous section. The surface is then examined in reflection with a metallurgical microscope using bright field illumination, with the field iris stopped down to give a narrow illuminating beam. By slightly going off-focus, a phase difference is introduced between the diffracted wavefronts, which produces an intensity distribution, revealing much detail on the crystal surface. Even this method was not successful for the observation of the very elementary growth spirals.

(b) By Smearing Impurity on the Crystal Surface

It was soon discovered that a small amount of impurity can make these features visible. Fig (30) is an example where by suitably wiping the impurity on to the crystal surface (without silvering it) the faint spiral features have been made quite visible. This behaviour is easily understood since particles of impurity will pile up at the edges thereby increasing the visibility. This method, though it was often

47.

found helpful is not very satisfactory.

(c) Breathing Technique

This method consists in observing the clean surface of the crystal by a metallurgical type of microscope and focussing it sharply on the crystal surface. Breathing lightly on the crystal surface while it is under observation increases the visibility and the "lines" flash out because of condensation of water vapour but soon disappear when water evaporates. The 'lines' so observed have a dotted and diffuse appearance, but the visibility achieved is quite high. This method though very convenient and handy for **visual observations is not quite suitable for photography. However, the utility of this technique for a preliminary survey** of a large number of crystals in the search for the suitable crystals to be studied, is to be emphasized.

(d) Phase-Contrast Microscopy

The technique found most satisfactory for the observation of the growth spirals consisted first in depositing a highly reflecting (about 90%) layer of silver on the crystal and examining it in reflection using phase-contrast illumination.

The principles of phase-contrast microscopy were first given by Zernicke (1934, 1935) and it is now a well established technique. No attempt will be made to give a detailed mathematical account of the theory. The theory *and* practice

48.

of phase-contrast microscopy has been discussed by several workers. (Burch and Stock 1942; Kohler and Loos 1941; Payne 1947; Taylor 1947, 1949). An excellent account of the principles and applications of this technique with an exhaustive bibliography is given by Bennett, Jupnik, Osterburg and Richards (1951). An elementary qualitative explanation of this technique is given below.

For the sake of simplicity, the object specimen will be considered as a single particle. This elementary theory can be extended to object fields of more than one particle, when the particles are far enough apart with relation to the resolving power of the objective so that the images of the various particles are formed independently of one another. It will be assumed that the microscope is adjusted for Kohler illumination i.e. the source of light is focussed upon the iris diaphragm of the substage condenser so that the opening of the condenser diaphragm may be regarded as a source of illumination. Further in discussing the image formation by the objective of the microscope, we shall consider the light wave radiated by a single point of the condenser diaphragm, and it may be assumed that to a first order of approximation the main effect of including the light from the remaining parts is simply to produce a brighter image of the specimen.

If, the condenser diaphragm is placed near the first focal plane of the substage condenser, the light wave radiated from a point in the opening of the iris (in fig. (14a) it is

49.

shown to be on the axis of the condenser lens for the sake
of simplification), emerges from the substage condenser as
a substantially plane wave and, therefore, parallel rays
pass through the object specimen. If the object specimen
is an ideally simple one for phase contrast microscopy it may
be taken as a single transparent particle embedded in a
homogeneous medium of nearly the same index of refraction.
Consider a light wave incident upon the specimen and its
surrounding medium. The light transmitted by the surrounding
medium and the particle will have the same amplitude because
of equal absorption but will differ in the optical paths
traversed i.e. there will be a slight difference in phase.
Therefore, the light transmitted by the surrounding medium
and the particle may be represented by the two equal vectors
S and P respectively (fig. 14 b), such that P is rotated
with respect to S by a small angle ϕ corresponding to the
path difference. The vector P can be resolved into a
component parallel and equal to S, and a small component D
which will be nearly at $\pi/2$ to the vector S if ϕ is small
Therefore, the incident wave does not pass without inter-
ruption through the object plane but may be resolved into
two parts (1) the S part which is the undeviated wave by the
presence of the object and (2) the remaining part D, which
may be regarded as the deviated wave created by the light
S in its passage through the object. The deviated wave D
is zero at all points of the object plane except where there

50.

is the object detail and will be diffracted as a set of
roughly spherical waves expanding from the individual detail
etc. These are drawn diagr ammatically in fig. (14 a) where
the undeviated part is drawn by the solid line and the
deviated part by the broken line. The undeviated wave con-
tinues on its original course as a set of parallel rays and
is focussed in the second focal pla ne of the objective where
the geometrical image of the source of light is formed and
is subsequently spread uniformly over the image plane. The
deviated wave originating from the object details is spread
over the second focal plane of the objective and is sub-
sequently focussed in the focal plane of the eyepiece. This
important distinction between the deviated and the undeviated
wave is the basis of phase-contrast microscopy.

The above analysis shows that the image of the
surrounding medium is illuminated by the undeviated wave and
therefore the amplitude and phase of light illuminating this
region will be determined by the vector S whereas the image
of the particle is formed by both the undeviated and deviated
waves and since these two waves overlap upon the geometrical
image of the particle, they interfere with one another to
give the resultant vector P which will determine the phase
and amplitude of the light which forms the image of the
particle. This conclusion is true irrespective of the path
difference between the particle and the surrounding medium.

Here it has been assumed that no light is diffracted outside

51.

the objective.

Since the amplitudes of both S and P waves are the
same, their vectors differing only in phase, the eye will
not detect the specimen, since it does not detect any changes
in phase, being sensitive only to intensity and colour changes.
Therefore, an ordinary microscope will fail to reveal the
presence of the specimen. If, however, the phase of either
the undeviated wave S or the deviated wave D is changed by
$\pi/2$, the S and D waves will be either in phase or out of
phase by π and therefore the image of the particle will then
be illuminated by light of amplitude $|S| \pm |D|$ and will be
either brighter or darker than the background, the intensity
of which is determined only by the vector $|S|$. This is
exactly what the phase contrast microscope does. When regions
of greater retardation are imaged darker than the background
it is called the positive phase contrast and when brighter
than the background it is called a negative phase contrast.
At the back focal plane of the objective, where the geometrical
image of the condenser diaphragm is formed, a 'phase-plate'
is placed which consists of a dielectric layer of optical
thickness $\lambda/4$. The undeviated wave is focussed at the back
focal plane forming the image of the condenser diaphragm,
and if the phase plate exactly covers this area, the undeviated
wave on passing through it will be changed in phase by $\pi/2$.

Generally the deviated wave D is much weaker than the

direct light S, in order to obtain optimum contrast the
amplitudes of the two should be made nearly equal. Since
we cannot increase D without also increasing S proportionate-
ly, we have the only alternative of decreasing the intensity
of the direct light S. This decrease is accomplished by
placing on the phase plate in the path of light S, some
absorbing material, so that the amplitudes of the undeviated
and deviated waves are arranged to give maximum contrast.
It may be mentioned in passing that if the phase plate is
opaque, the S wave is completely obstructed, then the particle
will appear with maximum contrast, but in practice the image
is not suitable for the usual purposes of microscopy on
account of the loss of definition in the image. This may be
accounted for, since it is the deviated wave alone that forms
the image and it will reveal the edges rather than the
surface details. This, in principle, is the working of dark
ground illumination.

Description of the Apparatus Used

The apparatus used was the Cooke Troughton & Simms
phase contrast equipment for incident illumination. This
equipment can be fitted on the Vicker's projection microscope.

A diagrammatic scheme of the arrangement is shown in
fig. (14 c). An annular diaphragm D serves as the entrance
pupil of the optical system consisting of a field lens, the
microscope objective, and the reflecting surface of the

specimen (Si-C crystal). The light source is imaged on the
diaphragm D by the condenser lens. The field lens and the
objective form an image D_1 of the field stop on the specularly
reflecting surface of the object specimen. The light is
reflected from the surface of the specimen and passed through
the objective again to form a real image D_2 of the diaphragm
D. Image D_2 becomes the exit pupil and therefore the
location of the phase plate.

In this equipment, the optical assembly, the micros-
copic objective lenses, the beam splitter and the phase plate
are mounted on the objective. The phase plate is located
between the beam splitter and the eyepiece (shown by solid
lines in fig. 14c) since in this position both the amount of
stray light and losses of illumination are minimized.
It is a positive phase contrast, with a single phase plate
having 80% absorption with a phase retardation of $\pi/2$ and it
is found that this single phase plate serves moderately well
for the entire practical range of small optical path differ-
ences.

The surface of the crystal specimen must be adjusted
perpendicular to the optical axis of the microscope so that
the image of the diaphragm is centred upon the optical axis
when the condenser diaphragm has been centred. An auxiliary
microscope is provided, which can be inserted in place of the
normal eyepiece. This enables the examination of the back

focal plane of the objectives so that the image of the diaphragm can be made to coincide exactly with the phase plate.

The ring form of the substage annulus together with an annular phase plate has a considerable advantage. Since this form has complete axial symmetry, it introduces practically no undesirable lack of symmetry in the image, and the resolution is improved and depth of focus diminished due to the use of a larger objective aperture by direct light. Furthermore, less diffracted light is wasted owing to overlapping between the higher order spectra and the retarding annulus of the phase plate.

(e) On the Visibility

. Phase-contrast microscopy depends upon altering phase changes into amplitude changes, conversely it changes real opacity into apparent changes of phase and for such features this technique is not suitable. Again, phase contrast microscopy is based on the physical possibility of complete or partial separation of the deviated and undeviated spectral orders at the phase plate. For coarser detail it may not be possible to isolate the diffraction effects from the direct light on account of small separation between the zero and higher order spectral images. Further the surface of the specimen should be in one plane and specularly reflecting in order to form a sharp image of the annular condenser diaphragm on the phase plate. If the different parts of the surface of

55.

the specimen form different images of the diaphragm, as
happens when small areas of the specimen though highly reflect-
ing are inclined to each other, the advantage of the phase
contrast technique is lost. In the limiting case, when the
surface of the specimen diffuses light completely, no image
of the annular diaphragm can be formed after the light passes
through the objective the second time and the phase contrast
can not be used at all.

Silicon-carbide crystals are ideal for this purpose.
The faces are molecularly flat, the step-heights between the
successive arms of the spiral being only a few angstrom units.
The light from the surface is specularly and coherently
reflected. There are no prominences or protuberances on the
surface to scatter light to give unwanted background intensity:
it is only the diffraction at the edges of the spiral steps
that is solely responsible for the deviated wave and since all
the steps in a particular growth spiral are of the same height
and often with equal spacing between the successive steps,
the diffraction effect will be occurring in an ideally
symmetrical way. Further, by silvering the crystal so that
the surface has a high reflection coefficient, phase plates
with quite a high absorption can be employed to give a
correspondingly high contrast in the image, and the time of
exposure is considerably shortened, thereby cutting down the
stray background intensity. Even then it is rather surprising

that such small steps as 15 A, which will correspond to a change in path of 30 A in reflection, have been revealed. However, with the equipment used these features are often still faint and only just visible. In order to make these features reproduceable, photographic methods for increasing the contrast have been employed. (See next section).

In phase-contrast microscopy the best contrast is obtained when the specimen is exactly in focus. This is in contrast to bright-field microscopy where defocussing is used to see specimens of low contrast (Linfoot 1945). If the inhomogeneties on the surface of the specimen are not confined approximately to a thin lamina, in putting the specimen out of focus to see these details, the image will bear no simple correspondence to the object itself. On the other hand, in phase contrast microscopy the maximum contrast is obtained when the specimen is accurately in focus so that the image bears a closer resemblance to the object; the phase contrast image is symmetrically diffused above and below the focus. Furthermore, the phase contrast microscope is operated at full aperture and it is unnecessary to close the condenser diaphragm partially as in the case of the bright-field microscope, in order to obtain enough edge diffraction to see such a specimen. Therefore, in phase contrast microscopy there is practically no decrease in resolution and spurious images are less likely to occur.

In fig. (82) it is seen that the visibility and contrast is much greater than that of fig. (81) which shows

the photograph, using phase contrast equipment, of the same part of the crystal after silvering. In fig. (82) the surface of the crystal was not very clean when it was silvered. The silver deposit was not uniform, the surface appearing mottled. Examination with the same phase-contrast equipment gave this surprisingly high visibility. This suggests that impurity can make the steps more visible.

(f) Photographic Processing

The photographic processing consists of the following series of operations. Firstly, very contrasty photographic plates such as Kodak B-20 Process plates were used, the exposure time being critically controlled to bring out the edges of the spiral steps prominently. These plates were then developed in a contrasty developer such as Kodak D-8 caustic developer. In some cases, especially if the step height was comparatively large, this photographic processing provided a negative of sufficient contrast, and further contrast was obtained in printing, by using extra-hard photographic paper. In some cases these negatives did not have sufficient contrast and by printing them against another contrasty photographic plate and again adjusting the time of exposure critically, the contrast was considerably increased - indeed any amount of contrast can be achieved by working at the heel portion of the exposure - density curve of the photographic plate, the only disadvantage being that contrast at unwanted places of

the negative also increases. Unless otherwise stated, all the pictures have been taken by the use of the above phase-contrast microscope.

6.1. GENERAL

For the measurement of step height, multiple-beam interferometric techniques were used. Since multiple-beam interferometry is quite a well established technique, no attempt will be made to give a general treatment of the theory, a full account of which has been given by Tolansky (1948). Only those points which have a special bearing on the present investigation, and some new modifications introduced for these studies will be indicated.

The crystals of silicon-carbide are opaque, therefore, interference fringes in the reflected system were always utilized. The theory of the reflected system has been discussed by Hamy (1906) and Holden (1949). The fringes are produced by matching the crystal surface on which a thin layer of silver (about 500 A thick and 90% reflectivity) has been deposited, against a similarly silvered optically polished glass flat. The optical flat used was supplied by Adam Hilger and was true to $\lambda/40$ ($\lambda 5461$) over the central area of nearly 1 cm. diameter, but was certainly flat to a much smaller fraction of this over small areas.

In an interferometer of which the two component surfaces are parallel to each other separated by a distance t, are

CHAPTER VI

INTERFEROMETRIC TECHNIQUES FOR THE MEASUREMENT OF STEP
HEIGHT

6.1. GENERAL

For the measurement of step height, multiple-beam
interferometric techniques were used. Since multiple-beam
interferometry is quite a well established technique, no
attempt will be made to give a general treatment of the theory,
a full account of which has been given by Tolansky (1948).
Only those points which have a special bearing on the present
investigation, and some new modifications introduced for these
studies will be indicated.

The crystals of silicon-carbide are opaque, therefore,
interference fringes in the reflected system were always
utilized. The theory of the reflected system has been dis-
cussed by Hamy (1906) and Holden (1949). The fringes are
produced by matching the crystal surface on which a thin layer
of silver (about 300 A thick and 90% reflectivity) has been
deposited, against a similarly silvered optically polished
glass flat. The optical flat used was supplied by Adam Hilger
and was true to $\lambda/40$ ($\lambda 5461$) over the central area of
nearly 1 cm. diameter, but was certainly flat to a much smaller
fraction of this over small areas.

In an interferometer of which the two component sur-
faces are parallel to each other separated by a distance t and are
λ

60.

silvered such that the transmission and reflection coefficients
of amplitude are $T^{\frac{1}{2}}$ and $R^{\frac{1}{2}}$ respectively, the transmitted series
of multiple reflected beams when summed up gives the well
known Airy intensity distribution

$$I = \frac{T^2}{(1-R)^2} \cdot \frac{1}{1 + \frac{4R}{(1-R)^2} \sin^2 \delta/2} \quad \text{---------} (18)$$

where $\delta = \frac{2\pi}{\lambda} \cdot 2\mu t \cos\phi$, is the constant phase lag between
the successive beams, ϕ being the angle formed by the normal
and the ray between the silvered surfaces.

The properties of the reflected system in multiple
beam interference are much more complicated. The peculiar
properties of the reflected system are due to the fact tha t
the first reflected beam has a phase change compared w⁻ith
the second beam altogether different from that between any
other two successive beams. It is found that for highly
reflecting silver films (R > 80%), the intensity distribution
in the reflected interference system is very nearly comple-
mentary to that in the transmitted system forming narrow
symmetrical minima.

In order that sharp interference fringes should be
produced for two highly reflecting surfaces inclined at a
small angle, Airy summation should apply. But in this case
the path difference between the successive reflected beams

is not constant but alters progressively with the order of reflection so that the beams gradually get out of step ultimately, the retardation becoming $\lambda/2$ tending to destroy the condition for the formation of sharp fringes. The path difference between the first and the nth beam is $2nt - \frac{4}{3}n^3\theta^2 t$ where θ is the wedge angle. Hence the second term $\frac{4}{3}n^3\theta^2 t$ should be restricted to a maximum value of $\lambda/2$. Therefore, t should be as small as possible and must in any case be less than the critical value.

For the study of the topography of the crystal surface it was always found advantageous to utilize high dispersion fringes which are produced by having a very small wedge angle between the crystal surface and the optical flat. Further, in accordance with the previous result the separation between the two surfaces was reduced to as small a value as possible — normally only 2 or 3 wave lengths of light. This could be achieved because the small portions of the surfaces of silicon-carbide crystals studied, are exceptionally flat without any ridges or protuberances, so that the two surfaces could be brought in very close contact. The experimental technique for achieving this is simple. A brass jig was used in which the optical flat fits in a groove at the base and the crystal specimen fixed on to another brass plate can be brought close to it at any inclination by adjusting the three nuts which press against three springs separating the two brass plates.

Under these conditions extremely sharp multiple-beam interference fringes were obtained, actually a fringe width $\sim \frac{1}{50}$ of an order separation were easily achieved. It may be emphasized that since the interference gap was adjusted to be very small the multiply reflected beams effectively scan the same part of the crystal surface and thereby reveal the true topography.

In the present study the two types of interference fringes used are, firstly Fizeau fringes of equal optical path formed by illuminating the interferometer with a parallel beam of monochromatic light (λ 5461). The experimental arrangement for the production of Fizeau fringes in the reflected system is shown diagrammatically in fig. (15). Secondly the fringes of equal chromatic order formed with white light using a spectrograph, were utilized. These fringes were obtained by placing the spectrograph such that its slit occupies the position previously occupied by the photographic plate in the arrangement for Fizeau fringes.

6.2. USE OF FIZEAU FRINGES

When the step height is comparatively large ($\sim$ 100 A) it was found possible to determine the individual step heights by the shift of Fizeau fringes at these steps. The shift of the Fizeau fringe at a step, as a fraction of the order separation (i.e. the distance between successive fringes), gives

63.

the height of the step as a fraction of $\lambda/2$. An example of this method of the determination of step height is shown in fig. (16a) which shows Fizeau fringes passing over the spiral steps of fig. (16b). It is seen in fig. (16a) that the dispersion is not constant and therefore for the evaluation of the step height an average value was taken.

However, in most of the features the individual steps are rather close to each other and the step heights too small to be detected by the individual shift of Fizeau fringes at these steps. The two simple cases of growth spirals in which the average step height can be determined are (a) circular spirals and (b) polygonal spirals with straight edges, having a regular spacing between the successive arms of the spiral. The relevant formulae for the determination of the average step height of these simple cases are developed below.

(a) Rounded Spirals

A rounded spiral is effectively a spiral conical hill. In the simple cases as illustrated in figs. (21) and (35) etc., it may be considered to be a conical hill made of a series of concentric steps with a constant spacing d and a step height h (fig. 17a). A Fizeau fringe in the direction AB will be shifted by an amount s = EP when it climbs each step, and will be broken into small parallel portions CD, EF, GH .... The apparent direction of the fringe will be CEG....O, since these

64.

portions are small. For the special case when the fringe

passes over the peak, the apparent direction of the fringe

will be radial and hence perpendicular to the steps. A

symmetrical shift will occur in the opposite direction down

the hill from O in the direction OL. If θ is the angle be-

tween the true and apparent direction of the fringe, the

fringe will bend through an angle 2θ at the peak. From the

figure

$$s = d.\sin\theta \quad\text{------------}\quad (19)$$

By knowing the dispersion X, the distance between successive

fringes which corresponds to a difference of $\lambda/2$ in the

width of the interference gap, the step height h corresponding

to fringe shift s is given by:

$$h = \frac{s}{X}\cdot\frac{\lambda}{2}$$

$$= \frac{d.\sin\theta}{X}\cdot\frac{\lambda}{2} \quad\text{------------}\quad (20)$$

The optical flat is adjusted such that high dispersion

fringes are obtained with one of the finges passing over the

peak where it will be observed to bend. This adjustment is

very delicate especially using high dispersion fringes.

From this Fizeau picture θ is measured, and knowing d from a microphotograph at the same magnification, h is found.

Here the spiral conical hill has been regarded as a circular conical hill which is very nearly true. Fig. (18a) illustrates an example of this method which shows a Fizeau fringe (λ 5461) passing over the spiral of fig. (18b).

Since the step height is obtained from the mean of all those contributing to form the peak, irregularities of the optical flat and the lack in faithfulness of silver contouring are averaged out. This method is, therefore, capable of considerable accuracy.

(b) Polygonal Spirals with Straight Edges

In this analogous case the pyramidal hill may be regarded to be composed of series of parallel steps on each side of the vertex. For a series of parallel steps of step - height h and separation d the Fizeau fringes will have an apparent direction at an angle θ to the real direction. In the particular case when the Fizeau fringe has been adjusted to run perpendicular to the series of steps on one side of the vertex, the apparent direction of the Fizeau fringe will be inclined at an angle θ_1 on one side of the vertex and θ_2 on the other side, to the true direction of the fringe. θ_1 and θ_2 from fig. (17b) are given by the relations

66.

$$\sin \theta_1 = \frac{s}{d} \qquad \text{-----------(21)}$$

$$\sin \theta_2 = \frac{s}{d} \cdot \cos(\theta_1 + \theta_2) \qquad \text{----------(22)}$$

and putting $\theta_1 + \theta_2 = 2\theta$ -----------(23)

From these three equations θ_1 and θ_2 may be eliminated in terms of θ, s and d, giving

$$\frac{s}{d} = \frac{\sin 2\theta}{\sqrt{1 + 3\cos^2 2\theta}} \qquad \text{-----------(24)}$$

Using the relation

$$h = \frac{s}{X} \cdot \frac{\lambda}{2} \qquad \text{------------(25)}$$

the step height h is given by

$$h = \frac{d.\sin 2\theta}{\sqrt{1 + 3\cos^2 2\theta}} \cdot \frac{1}{X} \cdot \frac{\lambda}{2} \qquad \text{-----------(26)}$$

Here 2θ is the total angle through which the fringe appears to bend at the vertex. When 2θ is small, as is usually the case for small step heights equation (26) reduces to

$$h = \frac{d. \sin 2\theta}{2} \cdot \frac{1}{X} \cdot \frac{\lambda}{2} \qquad \text{----------(27)}$$

$$\doteqdot \frac{d \sin \theta}{X} \cdot \frac{\lambda}{2} \qquad \text{----------(28)}$$

which is identical with the equation (20) used for circular

67.

spirals. Fig. (19b) illustrates an example of this which shows the Fizeau fringes passing over the spiral of fig. (19a).

6.3. USE OF FRINGES OF EQUAL CHROMATIC ORDER

Application of fringes of equal chromatic order to the evaluation of step height is very much simplified in the special case of a Fizeau fringe passing over the centre of the spiral. The interferometer is adjusted so that the middle point of the length of the slit of the spectrograph passes over the peak of the conical hill, and is parallel to one arm of the Fizeau fringe. Then over one half of its length along the slit the interferometer will have a constant thickness till it reaches the peak after which the gap will increase depending upon the number of steps crossed by the slit. This will, therefore, lead to a system of fringes of equal chromatic order parallel to the spectrum lines in one half and sloping towards the red in the other. The increase in gap δt is given by the relation

$$2 \delta t = n \delta \lambda \ \text{--------- (29)}$$

where $\delta \lambda$ is the corresponding change in wavelength in a particular fringe of order $n = \dfrac{\lambda'}{\lambda - \lambda'}$ where λ' is the wavelength of the neighbouring order ($n + 1$). From fig. (20)

$$\delta t = 2 N h \ \text{-------- (30)}$$

where N is the total number of steps crossed by the slit,

and h is the step height. Fig. (18c) illustrates an example
of this method which shows the fringes of equal chromatic
order corresponding to fig. (18a). The spectrograph used
in this figure was a Hilger constant deviation spectrograph
with a dispersion of approximately 50A per m.m. near λ 5461.

6.4. BY COUNTING THE NUMBER OF STEPS ON EITHER SIDE OF A BOUNDARY LINE

In one case another determination of the step height
has been possible. In fig. (18b) starting from the centre
of the spiral we can reach any point A on the line of dis-
continuity (running from left to right to the centre of the
figure) either by going round the 'fish-like' obstruction in
a clockwise or an anti-clockwise direction. In the former
case, we encounter say N_1 steps. Therefore, the point A is
N_1 steps lower with respect to the centre of the spiral. In
the latter case we go down say N_2 steps from the peak of the
hill in order to arrive at A. Thus at A the difference in
level on the two sides of this line of discontinuity is that
corresponding to $(N_2 - N_1)$ step heights. This difference is
quite large (over 50 steps) and is, therefore, capable of
being measured accurately and easily, either by Fizeau fringes
as shown in fig. (18d), or by fringes of equal chromatic
order. Knowing this, the step height has been evaluated but
it is subject to uncertainty due to the possible presence of
hidden dislocations in the obstacle and in the line of dis-
continuity.

6.5. SUPER POSITION OF FIZEAU OVER THE MICROPHOTOGRAPH

In this method the microscopic picture and the corresponding Fizeau fringes passing over this feature are photographed separately as usual, and are then superimposed over one another photographically, at the same magnification. In this way the exact position of the Fizeau fringe, the corresponding separation between steps etc., are all known with certainty. This method is of particular use when the separation between the successive steps is not constant, in which case the Fizeau fringes will appear curved. For the evaluation of step heights in such cases, two straight portions of the Fizeau fringes pa ssing over the vertex of the growth hill can be chosen, one on either side of the vertex and the corresponding step separation 'd' can be substituted in equation (28). This will, consequently, lead to higher accuracy in the determination of step height. Fig. (19c) illustrates an example in which the Fizeau fringes fig. (19b) passing over the spiral of fig. (19a) have been superimposed on it.

6.6. EFFECT OF DIFFRACTION

In all these figures, the effect of diffraction at the steps can be observed and this becomes more noticeable for molecular steps with high dispersion fringes formed in a small interferometric gap. As seen in fig. (16a), a portion of the fringe runs along the edge of the step in both

directions on either side of the fringe and is of minimum extension when the fringe is perpendicular to the step. Fig. (18e) is an illustration of the effect for the spiral of fig. (18b) under very high dispersion. This diffraction has been of considerable assistance since it makes the topographical features visible simultaneously with the interference fringe, so that it becomes possible to adjust the fringe direction and position exactly over a certain feature, e.g. the fringe can be made to pass exactly over the peak of the hill or it can be adjusted perpendicular to the edges of steps, or the exact number of steps crossed by the slit of the spectrograph in the case of fringes of equal chromatic order can be determined accurately.

Part IV

OBSERVATIONS ON SILICON-CARBIDE CRYSTALS

(A)   MICROSCOPIC STUDIES

(B)   INTERFEROMETRIC STUDIES

(A) MICROSCOPIC STUDIES

INTRODUCTION AND CLASSIFICATION OF SPIRALS

Silicon-carbide crystals often have very well de-
veloped and molecularly flat surfaces over wide areas and
hence are most suitable for the observation of the molecular
growth features of the type predicted by Burton, Cabrera and
Frank's theory. Previous observations on Si-C crystals have
already been quoted.

Simultaneously with the author (Verma 1951), Amelinckx
(1951) also observed spirals on silicon-carbide crystals.
Amelinckx could show that the step heights of some spirals
was up to 35A and thought that some were probably unimolecular,
but no exact measurements were reported. By comparison with
Griffin's work on beryl, these spirals were inferred to be
growth spirals. However, by the application of improved
experimental techniques discussed in Part III, it was possible
in the present investigation to study these features in
greater detail, the results of which not only confirm many
of the theoretical predictions but also provide new facts and
data.

As has been seen in Part III, the experimental
observation may be divided into two parts viz. the microscopic,
which will be presented first and the interferometric.

On the (0001) faces or the basal planes of silicon-

carbide crystals numerous growth spirals have been observed.

The different types of growth spirals observed can be divided

into three types.

(1) The elementary type of spirals originating from a simple
     dislocation in which the step height is <u>equal</u> to the size
     of the X-ray unit cell.

(2) Spirals originating from dislocations of multiple strength
     in which the step height is a <u>multiple</u> of the size of the
     X-ray unit cell.

(3) Interlaced spirals in which the step height is a <u>fraction</u>

     of the size of the X-ray unit cell.

ELEMENTARY SPIRALS

This first class of spirals are those in which the step height between the successive arms of the spiral is equal to the size of the X-ray unit cell. These spirals are usually faint to observe because of the small step-heights (e.g. for type 6 H, the step height is 15 A) and are, therefore, seldom seen with the ordinary microscope. It is therefore unlikely if this type of spiral had been seen by previous workers.

7.1. SHAPE OF THE SPIRALS

(a) Circular Spirals

Taking the simplest case, when a single screw dislocation emerges on the face of the crystal, a molecular ledge will run from this point of emergence on the crystal surface to one of its boundaries. If now the supersaturation of the vapour in contact with the crystal is raised, growth will start when the supersaturation has been raised to such a value that the critical nucleus as defined by equation (16) can pass between the dislocation point and the crystal boundary. As seen in Chapter (II) the ledge will curl up and form a spiral. The exact shape of the spiral will depend upon the rate of advance of a growth front in different crystallographic directions. The simplest case will be that in which the rate of growth is independent of the crystallographic orientations.

Such conditions are likely to occur in growth from vapour when the factor β does not vary with orientation in the crystal face in the following equation (equation (11)) which gives the rate of advance of a 'straight' step

$$v_\infty = 2(\alpha - 1) x_s Z\beta \quad -------- \quad (11)$$

As seen from equations (2) & (9) viz.

$$x_o = \frac{1}{2} a \exp(\phi/2kT) \quad ----- \quad (2)$$

$$x_s = a \exp(3\phi/2kT) \quad ----- \quad (9)$$

under which circumstances the estimates of surface diffusion distance x_s and mean distance x_o between the kinks on the steps are such that $x_s \gg x_o$ even for orientations of closest-packed directions. Thus when the distance between the "Frenkel-kinks" or exchange sites is small and the mean displacement of the adsorbed molecule is large, the molecules will have a high probability of adhering to the step if adsorbed near it, irrespective of the orientation of the step. Therefore, the rate of ledge advance will be independent of the crystallographic orientation and a rounded spiral will result, the shape of which can be calculated under these assumptions, as given by Burton, Cabrera and Frank (1951).

We know that a ledge which forms a portion of the spiral and has a radius of curvature ρ , will advance with

a velocity v_ρ given by

$$v_\rho = v_\infty (1 - \rho_c/\rho) \qquad - - - - - - - - (13)$$

provided the supersaturation is not too high. ρ_c is given by equation (16) viz.

$$\rho_c = a\phi / 2kT \ln \alpha \qquad - - - - - - - (16)$$

Let $\theta(r)$ represent the rotating spiral in (rotating) polar co-ordinates (r, θ). The radius of curvature at a point r will be

$$\rho = \frac{(1 + r^2 \theta'^2)^{3/2}}{2\theta' + r^2 \theta'^3 + r\theta''} \qquad - - - - - - - - (31)$$

where θ' and θ'' are the derivatives of $\theta(r)$. If the angular velocity of the whole spiral is ω, the normal velocity at the point r is

$$v(r) = \omega r (1 + r^2 \theta'^2)^{-\frac{1}{2}} \qquad - - - - - - - (32)$$

These three equations give $\theta(r)$ and ω. A good approximation is obtained by taking an Archimedean spiral

$$r = 2\rho_c \theta > 0 \qquad - - - - - - - (33)$$

which has the proper central curvature. ω is then given by

$$\omega = \frac{v_\infty}{2\rho_c} \qquad - - - - - - - - (34)$$

76.

A better approximation as calculated by Burton, Cabrera and Frank is

$$\theta = \frac{3^{\frac{1}{2}}}{2(1+3^{\frac{1}{2}})} \left[r/\rho_c + \ln(1+r/3^{\frac{1}{2}}\rho_c) \right];$$

$$\omega = 3^{\frac{1}{2}} v_\infty / 2\rho_c (1+3^{\frac{1}{2}})$$

$$= 0.63\, v_\infty / 2\rho_c$$

$$\left. \begin{array}{c} \\ \\ \\ \end{array} \right\} \quad ------(35)$$

The value of ω obtained by equation (35) differs from equation (34) only by a factor close to 1, showing that ω is insensitive to the actual law of dependence of v on ρ in the range in which $\rho \sim \rho_c$.

The spacing between the successive arms of the spiral will be constant and will be given by

$$\delta r = 4\pi \rho_c \qquad --------(36)$$

Such circular spirals are illustrated in figs. (21) (33) (35) (36) etc. The spacing between the successive arms of the spiral is not constant and in nearly every case the spacing is close at the centre, increases gradually, finally becoming constant. This may be attributed to increasing supersaturation in the last phase of growth.

(b) Polygonal Spirals

Any dependence of the rate of advance of a growth
front on its orientation would impose a distortion of the
growth spirals. This will happen when the factor β in the
above quoted equation (11) varies with orientation in the
crystal face. An obvious source of variation is that in which
the step is parallel to certain close-packed directions. The
step will, then, have relatively few 'kinks', the kink energy
being high. Thus the condition $x_s \gg x_0$ will no longer be
true, so that when the kinks are few and far between and the
distance moved by the adsorbed molecule is small, polygonal
spirals will result, the edges of the steps becoming straight
in directions at right angles to the directions of minimum
growth. Between these two extreme cases, there will be a
series of intermediate ones.

Thus for growth taking place under these conditions,
when the growth spirals become polygonal, they will exhibit
the symmetry of the crystal faces. When viewing spirals on
the (0001) planes, the edges of the stacks of monolayers are
being observed along the c-axis and will therefore exhibit
symmetries corresponding to these monolayers. Each monolayer
of C or Si (and the following Si or C) by itself has hexagonal
symmetry, but the two layers put together have only trigonal
symmetry since the hexagonal axes of one coincide with the
threefold axes of the other. A hexagonal symmetry can arise
by virtue of a 6_3 screw axis.

Fig. (22) shows the extreme case of a hexagonal spiral observed on a crystal identified to be of type 6 H. This is a regular hexagonal spiral, showing clearly the dependence of the growth rate on the crystallographic orientation. The edges very near the centre show a curvature, which in accordance with the theory, decreases with the distance from the centre. Soon the straight step-lines start rounding off at the corners and become gradually curved on moving away from the centre. These step lines do not meet the line of discontinuity sharply, but tend to curve away from it, as shown in fig. (22), for the outer five or six step lines.

Fig. (16b) shows a further example of a spiral with straight edges. This spiral has a high visibility under phase-contrast illumination. Calibration by multiple-beam interference fringes has shown the step height to be nearly 130A. Here the central 1 or 2 turns are nearly circular before it becomes hexagonal. In one corner four edges are displaced from the regular shape and the straight edges are observed to have 'kinks' at several places.

Figs. (25), (26) and (29) are further examples. In fig. (25) some 10 turns at the centre stand out from the remaining turns. They are very closely spaced as compared to the rest of the figure and have an almost constant spacing, their shape being nearly circular. It may be noted that the step lines have a dotted appearance which may be due to the

deposition of impurity or some local etching at the edges of steps. Figs. (26) and (29) are being commented upon later in Sec. (7.2).

Fig. (18b) shows a spiral observed on a silicon-carbide crystal of type 6 H. It is nearly circular at the centre and gradually takes on the hexagonal symmetry of the crystal face. This exemplifies the intermediate case where the conditions of growth are not preponderantly either in favour of a circular or a polygonal spiral. Figs. (23) and (24) are further examples of such a case.

The central part is circular in many of the polygonal spirals. Fig. (34) shows further example of this behaviour. This indicates that the growth of the central part, which represents the last phase of growth, took place under conditions such that circular spirals could be formed. It may be assumed that in the last phase of growth when the furnace was switched off, the supersaturation increased as the temperature decreased. The shape may be attributed to these two controlling factors. Thus in fig. (25), the supersaturation was high in the last phase of growth and it remained fairly constant over such a period that some 10 spiral turns closely spaced could be developed.

The reverse case of a circular spiral having a centre with straight edges forming a polygonal spiral, has not been observed.

7.2. PROPERTIES OF GROWTH FRONTS AND THE INTERACTION
OF GROWTH SPIRALS

In order to understand the more complex growth patterns observed on crystal faces where two or more screw dislocations emerge, a description of some of the general properties of growth fronts will be given.

The regular circular spiral shape produced by growth controlled by a single screw dislocation will, under constant conditions, rotate without changing its shape, which at least for fast rotation will appear as if circles are being emitted from the centre, travelling outwards at a constant speed. For polygonal spirals the straight portions are actually advancing radially and so a similarity to wave emitted from a point source does present itself.

The analogy, however, useful in many cases, cannot be extended to interference between growth fronts from two sources, but the terminology will be adopted to a certain extent.

When the advancing growth fronts meet an obstruction, they can propagate round corners as shown at the upper end of the 'fish' like obstruction in fig. (18b). It might be said that this point behaves like a secondary source of growth fronts.

The growth fronts emitted by two sources do not inter-fere like ordinary wave fronts. Where the two edges meet,

they fuse and annihilate each other over the common portion.
Numerous examples of this can be seen in figs. (24), (33), (35),
(46), (47) etc.

When there are several screw dislocations actively
emitting growth fronts, a point on the crystal face will be
in the dominant field of only one of these and this alone deter-
mines the number of growth fronts passing over it. This is
illustrated in figs. (33), (35), (44) etc. By choosing the
point of observation on the crystal face of fig. (44) which
shows the growth fronts emitted by five screw dislocations and
fixing it, say, near the bottom screw dislocation, the number
of growth fronts passing over it is solely determined as if
this alone were active.

Sometimes amongst the dislocations emerging on a
crystal face, one may dominate the rest. This will happen if
the supersaturation at one centre is slightly greater than
that at other centres. The growth pattern originating from
these weaker sources will continually shrink and if conditions
remain constant ultimately only one growth pyramid will be seen.
This is illustrated in fig. (26) where the central screw dis-
location is dominant and determines the rate of crystal growth
of the face. The weaker screw dislocations play little part
in growth, and merely pass on the growth fronts received from
the dominant screw dislocation with a slight delay and in
slightly modified form. This is clearly seen in fig. (26). Here

82.

the central screw dislocation has developed some four turns before reaching the point where the second small screw dislocation emerges. They quickly accomodate each other and the growth fronts issuing from the central screw dislocation, as they travel past this dominated screw dislocation, are only slightly distorted from their regular shapes. However, in the last phase of growth, when the furnace is switched off, the growth fronts would stop arriving from the dominant centre, and the growth steps attached to the weaker screw dislocations would be able to develop one or two turns of their own, as seen in fig. (26). Near the edge of fig. (26), some more screw dislocations emerge on the face of the crystal. Fig. (27) shows this portion of fig. (26), and fig. (28) is an enlargement of this area. These new screw dislocations also yield within a short while to the domination of the central one and quickly fall in line; their behaviour also being the same as outlined before. A further example of such a behaviour is shown in fig. (29).

7.3. GROWTH PATTERN FOR TWO SCREW DISLOCATIONS

(a)   Two Screw Dislocations of the Same Sign:
            Phenomenon of Co-operation

The growth pattern when two or more screw dislocations emerge on the face of the crystal can now be explained. Taking the next simplest case of two screw dislocations of the same hand closer together than $2\pi \rho_c$ they will generate a pair of

83.

non-intersecting growth spirals. In the lower half of fig. (30) this unique example is illustrated where the spiral is doubled with the members strictly "parallel". These two dislocations may be said to co-operate with one another and will behave like one dislocation of double strength.

With the increase of distance between the two dislocations, the ledges originating from one will intersect with the ledges starting from the other. In fig. (31) the growth pattern for two screw dislocations A and B of the same hand is drawn schematically for the simple case of circular spirals. The step-height and structure of the step wall originating from these two dislocations is assumed to be identical. (The more general case, where fault surfaces will be produced is discussed in Sec. 7.8). The ledge starting from A goes on rotating and generating the spiral until it meets at p_1 the ledge originating from B, where it terminates. According to the properties of growth fronts, the two ledges will fuse with one another at p_1. As the spirals unfold themselves the ledges meet at p_1, p_3, p_5, ---- in the upper half, and at p_2, p_4, p_6, ---- in the lower half of the figure. (The loci of points of intersection are treated in Sec. 7.6). Over the common portion, between p_1 and p_2 (p_3 and p_4) etc., the two ledges annihilate themselves and the missing parts of the two spirals are shown by the dotted line. The resultant figure is the solid line curve. Starting at the dislocation point A and going round the spiral we descend by one step in

each complete turn until we come to the point p_1 . From p_1 we go round the spiral B, to the point p_4 , and then again on the spiral A to the point p_5 . Thus in going round the resultant curve once, we descend by two steps from p_1 to p_5 to p_9 and so on. Similarly starting from the dislocation point B and going round we descend by two steps from p_2 to p_6 etc. As the curves gradually smooth out at the points of contact, the figure will appear to be two spirals alternately spaced.

Fig. (31) has been drawn for circular spirals, and the case for spirals with straight edges can similarly be drawn where the behaviour will be the same. Furthermore in fig. (31) the spiral attached to A has been shown to have developed two turns and that attached to B only half a turn before the two meet each other. It is quite possible for either of them to make any number of turns (including less than one turn) before meeting. The following figures illustrate the different cases. Fig. (32) shows the case of two screw dislocations of the same sign where both spirals are circular and the separation between the two dislocation points is such that each spiral has developed nearly one turn before meeting the other. The compound growth pattern in accordance with the method outlined, has developed in this figure for some two or three turns after which the ledges from the neighbouring dislocations interact with one another.

With the increase of separation between the two

dislocation points the growth pattern will have a shape similar to that drawn in fig. (31) and illustrated by figs. (33) and (35).

It has been seen that a spiral may not be circular or polygonal throughout. The central turns of several polygonal spirals have been observed to be circular. The resultant growth pattern will be built up by a mechanism similar to that drawn in fig. (31), with the difference that after the central circular portions, the ledges of the spirals change into straight edges. This transition may be gradual or sudden. Fig. (34) shows the case of two similar screw dislocations close to one another so that growth starts from both of them. The spirals are circular at the centre for one or two turns after which they settle down as spirals with straight edges. The meeting of the growth fronts from the two dislocations results in small kinks in the innermost straight edges. As in the case of circular spirals, by going round the resultant figure, we descend by two steps in each turn and the figure has the appearance of two spirals alternately spaced. The step-height between successive lines in any particular direction remains one unit. The spiral of fig. (34) has been observed on a crystal of type 15R, the full spiral being shown in fig. (19a).

(b) Two Screw Dislocations of Opposite Sign

When two screw dislocations of opposite sign emerge on the face of the crystal a ledge will run between them

86.

(fig. (37)). Growth will start if the supersaturation is raised to such a value that the diameter of the critical nucleus ($2\rho_c$) is less than the distance between them. In the more general case when the critical nucleus is not circular, this will be equivalent to a correctly oriented critical nucleus passing between the two dislocation points. As long as the supersaturation is kept above this value, the adsorbed atoms will join the step and therefore the step tends to spiral around both dislocations. This is shown in fig. (38) looking down from above. However, as the step doubles back on itself (fourth stage shown in fig. 38a), the two points A and B which are at the same level can join up by atoms filling in the lower level C to form a bridge. This stage is shown in fig. (38b). The parts D and E of the step grow very rapidly since the curvature is negative; that is the length of the step decreases as the step advances. Thus a closed loop has been generated and in the final stage, the step has returned to its original position and is ready to start again to go through the above cycle again. Therefore, as successive loops are developed the surface of the crystal becomes a pyramid, which will be composed of sheets or molecular layers. This development of the growth step is illustrated in three dimensions in fig. (39).

Fig. (35) shows this behaviour for circular spirals. In the left half of the figure, one right handed and the other

left handed screw dislocation emerge on the crystal surface.
The spiral attached to the left handed screw dislocation is
developed for about three turns when it meets the ledges
originating from the right handed screw dislocation. There-
after, in accordance with theory, successive closed loops
are generated. These loops are circular for the most part
with only a slight distortion over a small portion. The
step height of these circular spirals has been measured to be
15A, the crystal being of type 6 H.

Fig. (40) shows a unique case of two screw dislocations
of opposite sign close to each other and equally developed.
Here the spirals have straight edges. The resultant growth
pattern consists of closed sheets except at the centre where
the layer is incomplete and shows its formation from two
screw dislocations of opposite sign. The closed loops are
triangular at the centre, but on going away from the centre,
become hexagonal, with three alternate edges longer. The step-
height i.e., the thickness of each layer has been measured to
be nearly 120A, see fig. (107) and this indicates that these
features occur on a polytype with a large unit cell (see
Sec. 10.2).

Fig. (41) which is a bright-field photograph of an
unsilvered crystal, shows two dislocations of opposite sign
each giving rise to a hexagonal spiral. When the successive

arms of the two spirals meet each other, they generate closed loops. At the points of intersection, an edge can be observed, indicating that the levels of the two steps joining together are not the same.

Another rare case is shown in Fig. (42) which consists of closed hexagonal sheets with no trace of dislocations at the centre. The closed hexagonal figures might have originated from two dislocations of opposite sign, alternatively there may be some other mechanism.

7.4. DISCUSSION OF THE OBSERVATIONS ON PAIRS OF SCREW DISLOCATIONS

When two dislocations of opposite sign emerge on the crystal face, they interact with each other. The forces exerted between them have been calculated by Taylor (1934) for two edge dislocations. The radial force F_R and the tangential force F_a are given by the relations:

$$F_R = -\frac{G\lambda^2}{2\pi(1-\nu)}\frac{1}{R} \quad -------(37)$$

$$F_a = -\frac{G\lambda^2}{2\pi(1-\nu)}\frac{\sin 2\alpha}{R} \quad -----(38)$$

Where G is the shear modulus of the material; ν is the Poisson's ratio, and λ is the dislocation strength; R is the distance between the two dislocations, and α is the

angle which the line joining the two dislocations makes with the x-axis. Hence dislocations of opposite sign attract each other with a force that varies as the reciprocal of the distance between them. For dislocations of the same sign, the above expressions are reversed in sign and therefore the dislocations repel each other.

There is however a constraining force anchoring these dislocations to their equilibrium positions between the lattice rows. Peierls (1940) first calculated this force, which was later on extended by Nabarro (1947). They find that this force depends upon the elastic constants of the medium. According to Nabarro's calculation, the stress required to move the dislocation by overcoming the constraining force is:

$$\sigma_t \cdot \frac{4\pi}{1-\nu} e^{-2\pi/(1-\nu)} \quad - - - - - - - - - (39)$$

where σ_t is the theoretical shear stress for a perfect lattice ($\simeq G/10$), and ν and G are as previously defined.

This, does not take into account the strength of the dislocation, on which, this force should depend in some way.

At a certain distance of separation between the two dislocations, these forces viz: the attractive and the anchoring forces will balance each other. During the process

90.

of growth of silicon-carbide crystals, when the temperature is high, the two dislocations of opposite sign will draw towards one another and will finally coalesce, joining to form a common centre (which is a hollow core), unless the distance of separation is more than the above equilibrium value.

Experimentally, pairs of dislocations of opposite sign are seldom observed. Amongst all such pairs observed so far on silicon-carbide, a pair of dislocation of opposite sign close to each other such that the two spirals are equally developed (i.e. the first, second, etc., arms of the spiral from one dislocation meet the corresponding arms from the other) has not yet been observed for the dislocations of the elementary Burgers vector of small step height (e.g. 15 A for type 6 H). However, for a comparatively larger Burgers vector one such pair of close dislocations equally developed has been observed. This rare case is the one shown in fig. (40). Since its step height is nearly 120A, this is possibly due to the constraining force depending upon the strength of the dislocation i.e. the Burgers vector.

The closed sheets of fig. (42) have a very faint visibility and consequently the step height is small. In this case, the two dislocations of opposite sign can be drawn sufficiently close to each other. When they are separated by a distance such that the critical nucleus cannot pass

between the two, the growth will cease and no new closed
loops will be generated.

7.5. GROWTH PATTERN FOR THREE AND LARGER NUMBER OF DISLOCATIONS

(a) Growth Pattern for Three Screw Dislocations

The growth pattern for three or a larger number of
screw dislocations can now be explained. The growth pattern
for three screw dislocations of the same hand observed on a
crystal of type 6 H is illustrated in fig. (43). Once more
the spirals are circular at the centre and become hexagonal
after a few turns. In the central part the three dislocations
are at a distance such that the ledges from them intersect
and fuse with one another so that the growth pyramids inter-
leave. When the spirals finally become hexagonal, they co-
operate with one another, so that by following any one of the
edges, the resultant curve descends by three units in each
turn. However, it should again be emphasized that the step
height between successive edges in any orientation will be
only one unit.

At the centre the ledges are more closely spaced
and once they have settled down, the ledges are more widely
spaced. This may be attributed to the high supersaturation
of the final stage of growth. This will also explain the
non-co-operation of the three dislocations separated by these
distances, since with the increase of the supersaturation the

92.

radius of the critical nucleus will decrease and for the same distance of separation between the dislocations, they may be separated by distances larger than ρ_c . In the earlier phase, when the spirals have wider spacing, the two spirals on the right co-operate and dominate the one on the left. This can be seen from the shape of the first widely separated spiral turns.

(b) Five Separated Screw Dislocations

Fig. (44) illustrates the interaction of five screw dislocations. Starting with the double screw dislocation at the extreme right and calling it A, the lower of the two may be called A_1 and the upper one A_2. The screw dislocation points at the top, left, and bottom of the figure are called respectively B, C, and D. At a point which is slightly to the right of the centre of the figure, a crowding of growth fronts occurs. This point which is at the end of a line of discontinuity running to the centre of the figure from left to right, may be called O. Between O and B there are five growth fronts as arcs of circles emitted by the dislocation point A_1'. The 6th. growth front meets the growth front advancing from B, and at the middle part for nearly over 1 cm. they fuse with one another, and over the common portion annihilation occurs. The compound growth front assumes a characteristic shape of Ω . This behaviour continues for the 7th. and the following growth fronts until we come to the

13th. growth front. The 13th. growth front meets the growth fronts advancing from C where again over a small portion of it, annihilation occurs. Now the compound growth front assumes another characteristic shape ⎯⌒⌒⎯ . The portion of the 13th. growth front on the lower side of the annihilated part is not wholly an arc of a circle with A_1 as centre. It has a point of inflexion and the lower portion bends to the left when it meets the boundary or the line of discontinuity, coming diametrically from the left of the figure. This kink to the left can be seen in the 12th., 11th., 10th., 9th., and possibly 8th., and 7th., growth fronts. Beyond the 13th., growth front towards the point C, growth is dominated by C. In the lower portion of the 13th., growth front a small shaded area is visible near the line of discontinuity, the left edge of which is an arc of circle with C as centre. This shading can faintly be seen in the lowest part of the 12th., and possibly the 11th., growth fronts.

At O due to the interaction of different growth fronts a crowding occurs. Here the compound growth fronts are not arcs of circles with the different dislocation points as centres, but instead there is a gradual change in curvature.

Fig. (45) shows the growth pattern due to the emergence of six screw dislocations, all of the right-handed type. Here again the step lines are nearly circular at the centre, finally becoming straight. Since the group of

dislocations is near the edge of the crystal, the resultant growth pattern is not fully developed on all sides.

7.6. RESULTANT GROWTH PATTERNS FOR A VERY LARGE NUMBER
OF DISLOCATIONS

Interaction of Growth fronts and Curves of Intersection

(i) General Case

When a large number of dislocations emerge on the surface of the crystal, the resultant growth patterns are quite complicated. Figs. (46), (47) and (48) illustrate some examples. In fig. (46) the step lines are all circular, whereas they are polygonal with rounded corners in figs. (47) and (48). These complicated growth patterns arise by the inter-action of the growth fronts spreading from the various sources. Some of the properties of the growth fronts have been outlined in section (7.2). Some further general principles that govern their interaction, and the shape of the locus of points of intersection will now be given.

The successive arms of the spirals originating from any two dislocations can join with each other only if the two dislocations are of the same strength i.e. the two step heights are equal. Conversely if successive steps from two dislocations join and fuse together, it can be concluded that the step heights of the two spirals are equal. Since this joining

95.

together of steps is observed in figs. (47) and (48) for
the successive steps from all the interacting dislocations,
the step height must be a fixed unit and its measurement on
any one of them will give the value of all the rest. There-
fore it ma y be concluded tha t in any one region of the
crystal, the dislocations have the same strength.

If then the nth step from one source O_1 meets the mth
step from the other sources O_2, they will join together if
they are at the same level. Thereafter pairs of steps that
can join together are $(n+1)^{th}$ with $(m+1)^{th}$; $(n+2)^{th}$ with
$(m+2)^{th}$ etc., such tha t the order difference between these
steps fusing wi th one another is always constant and equal to
$(n-m)$. Microscopically speaking, on either side of the locus
of points of intersection, the portions of the two pyramids
should slope in the same direction, i.e. on travelling along
this locus of points of intersection we will be moving from
a higher to a lower level, or vice versa, for both the
pyramids. Examples of this can be seen in figs. (47) and (48).

Further, if the spacing between the nth and the
$(n+1)^{th}$ arms of one spiral is d_1 and between the mth and the
$(m+1)^{th}$ arms of the other is d_2, the two pairs of steps will
meet the locus of points of intersection at angles θ_1 and θ_2
respectively, such that

$$\sin \theta_1 / \sin \theta_2 = d_1/d_2 \quad \text{------------------}(40)$$

The value of $(\theta_1 + \theta_2)$ at a particular point of intersection is fixed by the initial conditions of the distance of this point from the two sources, the distance between the two sources and the shapes of the two spirals.

In the more general case d_1 and d_2 are the lengths of perpendiculars dropped from the point where the $(n+1)^{th}$ and $(m+1)^{th}$ arms meet each other, upon the tangents drawn to the nth and m^{th} arms of the two spirals at the point where they meet. The tangents to the nth and $(n+1)^{th}$ arms of one spiral may not be parallel to each other, so that not only the spacing between the successive arms changes, but also their directions may change, in which case the locus of points of intersection will have to turn suitably in order to satisfy the above sine condition. This is illustrated in fig. (49) where with the change of direction by the steps through an angle about 60°, the locus of points of inter- sections also turns through a simila r angle. Other examples of the interaction of growth fronts and the loci of their points of intersection in accordance with the above conditions are seen in figs. (47) and (48), where a large number of polygonal spirals with varying spacings are interacting with one another. Another example of the interaction is seen in fig. (50) where as a result of the meeting of the growth fronts from three dislocations at the centre of the figure closed triangular loops are formed. (The figure includes only two

97.

out of these three interacting dislocation centres. The third one will be towards the bottom of the figure).

If the two series of steps originating from two dislocations, on reaching the same region of the crystal, are unable to satisfy any of the above conditions, e.g. sine condition, they will not join with one another. These steps will then terminate in such a region. The points where the steps terminate will be ends of screw dislocations. Such a behaviour is seen in fig. (48) along a dotted line (running from nearly left to right in the middle of the figure) with a small gap in the centre, over which region four steps of the two spirals are seen to join together. We can reach any one of these four steps (say the second from the left) from a point A in a number of ways. In going from A to the chosen step we have to go down 30 steps, this number being independent of the path taken. A direct path can be traversed or one involving the crossing of different hexagonal spirals by going round the right hand end of the line of discontinuity. This is to be expected since the different spirals are of the same strength.

Fig. (51) illustrates another example where the spiral edges, though having the same step height, are unable to fuse with one another. These two series of step lines with their spacing nearly in the ratio 1:2 happen to meet each other at right angles. They cannot satisfy the sine condition and

98.

therefore the steps have to terminate. Thus they create a
barrier of dislocations between them, shown as a dotted line
of discontinuity running nearly vertically across the middle of
figure. Figs. (53) and (54) are further examples of the
termination of the step lines. In fig. (54) at every point
of termination of the step lines a dot can be seen. This may
be due to the deposition of impurity at these points.

(ii) Special Case : Circular Spirals

The exact shape of the curves of intersection can
be calculated in the simple case of rounded spirals. By
introducing the approximation used for the interferometric
measurements of step heights, according to which these spirals
may be regarded as composed of circles of constant spacing

$\delta r = 4\pi \rho_c$, the condition $(n-m)$ = constant, directly gives
the locus of the point of intersection P of the two rounded
spirals originating from the two source centres O_1 and O_2.
Thus $(n-m). \delta r$ will be a constant from which we have $O_1 P -$
$O_2 P$ = constant. This gives the locus of the point of inter-
section, a hyperbola which for $(n-m)$ = 0 reduces to a straight
line perpendicular to $O_1 O_2$ and passes through its middle
point (Burton, Cabrera and Frank, 1951).

A locus of points of intersection, which is hyperbolic,
is illustrated in fig. (33) for two circular spirals unequally
developed. The condition $(n-m)$ = 0 corresponds to the
symmetrical case of two spirals equally developed and is

99.

illustrated in the upper half of fig. (52) where the locus of points of intersection for two spirals equally developed is seen to be nearly a straight line, perpendicular to the line joining the two dislocation points and passing through their middle point. Here the two series of steps with equal spacing (i.e. $d_1 = d_2$) meet the locus of points of intersection at equal angles ($\theta_1 = \theta_2 \neq 0$). In fig. (33) as the spacings of the two spirals become equal (i.e. $d_1 = d_2$), in accordance with the sine condition θ_1 will become equal to θ_2, and in this case the steps tend to be parallel to each other at the points of intersection (i.e. $\theta_1 = \theta_2 = 0$).

As shown by Burton, Cabrera and Frank (1951) a small influence is transmitted along each step from the points where the two spirals meet, into the respective centres. This will tend to increase the rate of rotation of the spiral whose centre is nearer the points of contact (the upper one in fig. (33)) trying to synchronize the two in phase. This will smooth out the corners formed by the meeting of the two series of steps. This is observed in all the interacting spirals.

7.7. STATISTICAL PROPERTIES : DENSITY OF DISLOCATIONS

For a very large number of dislocations emerging on the surface of the crystal, in addition to the study of the individual behaviour of the dislocations, certain statistical properties of the whole population can be studied, the chief

amongst them being the density of dislocations, their type and strength.

The density of dislocations varies widely on different specimens of silicon-carbide (Si-C) crystals. In figs. (16b) (22), (25) etc., there is only one dislocation, the growth fronts from which fill the whole surface. In figs. (21), (24), (33), (34), (36) there are several. The largest density of dislocations observed, for circular spirals is shown in fig. (46), and for polygonal spirals in figs. (47) and (48). In fig. (46) the density of dislocations is $\sim 10^4$ screw dislocations per sq.cm. of the crystal surface whereas in figs. (47) and (48) it is $\sim 10^5/cm^2$.

A note worthy point is that in fig. (46) there are nearly 20 screw dislocations all of which are of the right-ha nded type. Similarly all the polygonal spirals shown in figs. (47) and (48) a re of the left-handed type. Thus, it is characteristic that in any one region of the crystal, there is a large predominance either of right-handed or left-handed screw dislocations.

Further, as discussed in Section (7.6) the series of successive steps from any two screw dislocations in figs (47) and (48) are observed to fuse with one another. This can only be explained if the step-heights of the two series of steps, originating from the two dislocations are the same i.e. the two dislocations are of the same strength. Since

101.

this is true for all the dislocations in figs. (47) and (48), it may be concluded that in any one region of the crystal the dislocations have the same strength.

Thus it is characteristic that in any one region of the crystal, the dislocations are not only predominantly of the same sign but also have the same strength.

7.8. FAULT SURFACES

The interaction of two dislocations of unequal strength may be considered now. When two steps advancing on the same level towards one another, from two sources, meet each other, the result is dependent upon the nature of the step wall. Three cases will arise.

(i) If the two step walls are identical i.e. are composed of the same number of molecular layers their relative arrangements being the same, they will fuse together forming an unbroken crystal surface. Thus in fig. (31) where the simple case of the interaction of two identical dislocations is represented, between the points p_1 and p_2 where the two steps have fused with one another, the surface of the crystal is flat and unbroken. In the case of silicon-carbide, which is a polytypic crystal, there are several possibilities of forming identical steps, attached to the two dislocations e.g. both of them may be of a type with Zhdanov symbol (33) or (32) or (33 32) etc., the step heights being the simple

102.

units for these types. Figs. (36), (44), (46), (47) etc., come under this category.

(ii)   The second case will a_rise when the two step walls consist of the same repeat unit but have different step heights e.g. both may be of a type with Zhdanov symbol (33) but they may be different multiples of this structure, say, n (33) and m (33),(see Chapter 8). In this case, since the structure of step walls is identical, they will fuse with one another but since their step heights are unequal, they will leave a step of height equal to the excess of the repeat unit of one over the other - equal to (n - m) (33) in the above example.

Fig. (55) illustrates this case. Here, over the part where the steps from the two hexagonal spirals meet and fuse with one another, a faint step can be seen running between the two points of contact. Since the two dislocations are of opposite hand and the faint step line follows the step lines of the spiral on the left hand side, it may be concluded that the dislocation on the left hand side is the stronger.

Fig. (41) was another example where two dislocations of opposite sign each give rise to a hexagonal spiral. At the points of intersection an edge can be observed, indicating that the levels of the two steps joining together are not the same. Further examples are shown in figs. (56), (57) and (58). Figs. (57) and (58) are the enlargements of upper and lower

103.

portions respectively of fig. (56). In fig. (58) the faint step line which gives the excess of one step height over the other can be seen clearly.

(iii)   In the third case, the two dislocations may be of different strength and also may have different structure. The two step walls will now consist of different numbers of layers and will also be differently arranged. Thus for example, one dislocation may be of a type with Zhdanov symbol (33) and the other with (32). In this case the two steps cannot fuse with one another in a perfect way crystallographically. They will leave a line of discontinuity which will mark out a fault surface.

Examples of fault surfaces are shown in the following figures (59 to 63). Consider fig. (63). As the growth steps on the right hand side of the figure originating from a screw dislocation not included in the figure, advance into the loop formed by the line of misfit, it shows that the crystal material inside the loop is crystallographically perfect and may be termed a "good crystal". (For definition see Frank 1951)   ⚹ ⚹. Therefore, misfit in the crystal lattice is confined to the boundary line. The step lines are observed to meet the boundary line at sharp angles creating re-entrant corners, which shows that the step marking out the fault surface does not advance appreciably, and may act as a barrier to the progress of growth layers. It is possible that the lines of

discontinuity seen in different figs. e.g. (36), (44), (46)
etc., may be of this nature.

Furthermore, the different dislocations in any one
region of the crystal may have originated from one dislocation
with a large Burgers vector. As the step associated with the
large Burgers vector will not terminate abruptly, but macro-
scopically speaking taper away, it will actually break into
discrete dislocations and most likely into dislocations of
unit Burgers vector. However, amongst the group of dislo-
cations, those which are different in structure from the
majority group, will give rise to the misfit surfaces and
will be locked at the barriers, leaving only those dislocations,
the step lines from which fuse with each other perfectly.
The dislocation with a large Burgers vector will naturally
break into component dislocations which are of the same sign.
Since like dislocations repel each other, they will tend to
spread apart as growth proceeds.

This may offer an explanation to the significant
observation that in any one region of the crystal, the dis-
locations are of the same sign and have also the same strength.

7.9. GROUPS OF DISLOCATIONS : SOME GEOMETRICAL PATTERNS

Quite often groups of dislocations arranged in
different ways emerge to the surface of the crystal and the
growth patterns take complex geometrical shapes. A group of

some 50 dislocations of the same sign arranged along a line
of length L is seen in fig. (64) to generate a spiral system
of s branches. The resultant activity of the group will be

$$\frac{1 + s}{1 + L/2\pi \rho_c} \qquad \text{------------} (41)$$

times that of a single dislocation (Burton, Cabrera and
Frank 1951), where ρ_c is the radius of critical nucleus
defined by equation (16). Fig. (65) illustrates another
such group where steps are seen to group together giving a
repeat pattern.

Some further examples of these geometrical patterns
are given in the following figures (66 to 69). In all these
figures, a bunching together of steps has taken place.
Fig. (67) shows the interaction of two groups of dislocations.
At the points where the series of steps from these two
sources meet each other, the step lines are observed to fuse
with one another. This will be possible only when the step
walls originating from the two dislocations have the same
structure. Further, since the steps originating from the
two dislocations are not elementary, the two series of steps
on either side of the locus of points of intersection, can
fuse with one another if they can bunch or dissociate into
smaller steps so as to bring the crystal level on both sides
the same. That this is so, is seen in fig. (67) where on

106.

either side of the locus of intersection, there is a continuity in the arrangement of step lines.

7.10. SOME RESULTS ABOUT THE CONDITIONS OF GROWTH

The different informations which can be derived, from the microscopic observations, about the conditions at which the growth of silicon-carbide crystals took place are, the radius of critical nucleus and the supersaturation. From figs. (36) and (44), the spacing between the successive arms of the circular spiral, when it is nearly constant is, approximately, 2.5 m.m. at a linear magnification of 90. From equation (36)

$$\delta r = 4\pi \rho_c \quad , \text{ we have}$$

$$\rho_c = \frac{2.5}{90 \times 4\pi} \, mm \approx 2\mu \quad --------(42)$$

This gives the size of the critical nucleus to be about 4μ. The supersaturation can be calculated from equation (16) viz.

$$\rho_c = a\phi \Big/ 2kT \ln \alpha$$

provided ϕ/kT can be estimated. For this estimation Trouton's rule may be used according to which

$$\frac{\phi}{kT} = 3.5 \, \frac{Tb}{T} \quad -------------------(43)$$

107.

and at an absolute temperature of 0.6 of the boiling point of the material $\frac{\phi}{kT} \sim 6$. Substituting, the supersaturation α is given by

$$\alpha \approx 0.2 \% \quad \text{-------------------------(44)}$$

This shows that the crystals grew at fairly low value of supersaturation.

CHAPTER VIII

SPIRALS ORIGINATING FROM DISLOCATIONS OF MULTIPLE

STRENGTH AND MULTIPLE DISLOCATIONS

8.1. LARGE STEP HEIGHTS AND DISLOCATIONS OF MULTIPLE STRENGTH

The step formed by the emergence of a screw dislocation
on to the crystal surface will have a step height corresponding
to the differences in the amounts of slip between neighbouring
regions of the crystal. Because of the existence of discrete
atomic structure in the glide plane, this will be limited
to the value of the X-ray unit cell of the crystal or in
some lattices a small multiple or fraction of this. The
spirals discussed in Chapter (VII) are of the simple type in
which the step heights are equal to the heights of the X-ray
unit cell e.g. in type $6 H = 15A$ (See Chapter X). Because
of the small step heights the visibility of these spirals was
low.

The spirals described below, have a much higher
visibility and interferometric measurement shows that they
have relatively large step heights; indeed, they can often be
seen simply with a microscope using bright-field illumination
without silvering the crystal. However, the following figures
have been taken using the silvering technique and observing
them with phase contrast illumination.

As silicon-carbide (Si-C) is a polytypic crystal, a

large step height may be due to its being equal to (I) the
height of a large X-ray unit cell (2) a multiple of a smaller
X-ray unit cell. The latter type of spiral results from a
dislocation of multiple strength, the Burgers vector being
a multiple of the X-ray unit cell.

8.2. DISSOCIATION OF STEPS

Fig. (70), which is a bright-field photograph of an
unsilvered crystal face, illustrates a spiral originating
from a dislocation of multiple strength, observed on a crystal
of type 6 H, as determined goniometrically (see Sec. (10.2)).
The central part of the spiral of fig. (70) is shown in fig.
(104), using phase contrast illumination. From the shift of
the Fizeau fringes (fig. (105)) over these spiral steps, the
step height between the successive arms of the spiral has
been determined to be nearly 620 A.

The rate of advance of a multiple step will be
controlled by the deposition rate at the bottom of the step
(Frank 1951 ^{a}) and as long as the bottom of the step is not
privileged with respect to the diffusion of the molecules
from the gas, the multiple step will not dissociate into its
component steps. In fig. (71), showing the right half of the
spiral in fig. (70) using phase contrast illumination, the
edges do not remain straight after three or four turns from
the centre and become irregular. This behaviour continues for
a few more turns after which the steps dissociate into five

110.

visible components (see fig. 72). The edges of these
multiple steps will not be close packed. The Fizeau fringes
(fig. (105)) passing over these steps are seen to be contin-
uous over the edges of the steps while climbing them. This
indicates that the edges are not steep. Furthermore the
crystal face between the successive edges is not close packed.
This is illustrated by fig. (72), which is an enlargement of
the right hand portion of fig. (71), where some faint step
lines can be seen between successive edges. Figs. (73) and
(73a) show the behaviour of the steps on the left part of
fig. (70).

The dissociation of a step into its components takes
place preferentially in certain orientations. In figs. (71)
and (72), the dissociation has taken place preferentially in
one orientation, and at 60° to this direction, this dissociation
is much less marked. Fig. (74) is a better example showing
the dissociation on the three alternate sides of the hexagonal
spiral. This is easily comprehensible since in Si-C, a growth
layer which is fastest in any one orientation becomes slowest
in orientations at 60° to it; the faster moving steps will
overtake it and pile up behind.

Fig. (75) shows the spiral growth pattern observed on
a crystal of type 33R. Here two spiral step lines start from
a common hollow. They stay as two separate steps for about
half a turn, after which the step lines come closer together
finally touching each other along an edge, after which they

111.

separate out and remain as two for the rest of the turns. This behaviour is in contrast to that observed in fig. (74).

A spiral showing trigonal symmetry with three corners rounded, is illustrated in fig. (76). The step-lines reach the edge of the crystal after it has developed for nearly two turns. However, the spiral continues to unfold itself, and as seen at the lower right hand corner of the figure, the steps separate out into two components giving each step line the appearance of a broad line.

8.3. MULTIPLE DISLOCATIONS

Dissociation is seen to take place quite near the origin in the example shown in fig. (78). Here amongst the dissociated steps, in three orientations, the outermost edges (which correspond to the bottom layers of the group) are straight and parallel to each other in the successive arms of the spiral, whereas at the inner edges, the usual irregularity is observed. Fig. (77) shows separately the third and the fourth arms of the spiral of fig. (78).

Figs. (79) and (80) illustrate further examples of multiple dislocations. In fig. (79), in contrast to fig. (78), the growth is faster at the six corners, the rate increasing towards the outer (or bottom) layer in the group. At some of these corners crosslacing of the step lines (See Chapter IX) is observed and may be responsible for the faster growth (c.f. figs. (92) and (93)).

CHAPTER (IX)

INTERLACED SPIRALS

9.1. SIMPLE INTERLACED SPIRALS

Observation

This is a new type of spiral which was not predicted
by theory. The following figures (81 to 99) illustrate
'spirals' belonging to this type. As seen in fig. (81) and
other subsequent figures the appearance of these spirals is
similar to that of a spider's web. This appearance arises
because in each of these hexagonal spirals at the six corners
the edges fork out and meet the neighbouring two edges, and
since this happens at the six corners for all the steps, a
criss-cross appearance results. These interlaced spirals
may be divided into two classes, firstly simple interlaced
spirals and secondly banded interlaced spirals in which a
certain number of steps group together.

Fig. (81) illustrates simple interlaced hexagonal
spirals, showing interlinking of four such interlaced spirals.
Fig. (81) is the usual phase-contrast micro-photograph. The
much higher visibility of fig. (82) shewing the same part of
the crystal has already been commented upon in Sec. (5.2 e).

Fig (83) shows the interlinking of two interlaced
spirals at a higher magnification (x1200). In the middle of
fig. (84) a single interlaced spiral is shown, whose central

few turns are very closely spaced, after which, the spacing suddenly increases. Here the step lines follow a pattern which resembles fig. (88). From the first widely spaced step lines, on moving towards the left, in the middle of the 8th., step line the emergence of another small interlaced spiral can be observed. This interlaced spiral remains under the domination of the central one, its behaviour being very much similar to the behaviour of domination as outlined for simple spirals in section (7.2); it merely passes on, the growth fronts received from the central dominant screw dislocation and slightly alters the shape of growth fronts as they pass near it. This is a unique example showing the phenomenon of domination in the case of interlaced spirals. Some further examples of these interlaced spirals are shown in figs. (85) and (86).

Explanation

An explanation of this has been given by Frank (1951α) and depends upon the dependence of growth rate on crystallographic directions and the change of the growth rate of the monolayers in different orientations of the crystal. Considering say the silicon-carbide of type 6 H, its Zhdanov symbol is (33). Using Frank's notation it may be written as

$$(\triangle \ \triangle \ \triangle \ \triangledown \ \triangledown \ \triangledown)$$

These six monolayers together, form the X-ray unit cell, and will form a step of height 15 A. In this sequence of six

114.

monolayers, the force field for each monolayer is slightly
different, and therefore one of these monolayers will have
the slowest rate of growth. The other, faster moving, mono-
layers will overtake it and pile up behind it, forming a
step of height corresponding to the whole repetition period.
Thus the slowest growing monolayer will be at the bottom of
the stack of monolayers and would determine the rate of growth
of the stack as a whole. As long as the conditions of growth
are such that the monolayers in the stack are not separated
from one another, this pile will advance as a single unit and
will constitute a single step line, so that in any one orient-
ation of the crystal, step lines 15A high corresponding to each
stack of monolayers will be observed. But it is not certain
that the slowest growing monolayer in one orientation say (o$\bar{1}$1)
will also remain the slowest growing in orientations 60° to
it i.e. (10$\bar{1}$) orientation. In fact, in type 6 H, the slowest
growing monolayer in one orientation should become the fastest
in orientations at 60° to it. This is easily pictured from
Frank's notation, which has mnemonic representation also.
According to this, a monolayer which is represented by △ in
a certain orientation will be represented by ▽ at orientations
60° to it, since a △ changes into a ▽ by rotation
through 60°. Hence on alternate sides of the hexagon, the
growth layers form alternate groupings of

$$(△ △ △ ▽ ▽ ▽) \text{ and } (▽ ▽ ▽ △ △ △)$$

Thus, whichever layer is the slowest growing one in a

particular orientation, say the first $\triangledown$ after a series
of $\triangle$s , then the third layer after it is necessarily the
slowest growing in orientations at $60°$ to it. This alter-
nation of velocities will lead to the interlacing of the
growth steps. This is represented diagrammatically in fig.
(87). Here in the stack of six monolayers the fastest growing
layer is marked F and the slowest S. Between these two mono-
layers there are four other monolayers with intermediate rates
of growth and for the sake of clarity these have not been
drawn. Further the separation between the F and S layers is
exaggerated; actually they are so closely piled up on each
other, that the whole forms a single step 15A high. The F
layer is shown to become S layer and vice versa when the
orientation changes through $60°$. Thus the growth layers will
be 6 layers high i.e. 15A high on the six sides of the hexagon,
and only three layers high on the zig-zags, at the six corners
i.e. the step height will be 7.5A. Amelinckx (1951α)has
measured the step height of an interlaced spiral, similar to
that shown in fig. (88), to be 7 ± 2A. This is in accordance
with the above explanation.

Fig. (88) showing alternate trigonal spirals, assists
in the above interpretation. Here, in any orientation, the
three layers are separated from the other three and the figure
has trigonal symmetry. This is to be expected since the
symmetry of any one of the monolayers, in the stack of monolayers,

advancing over another is trigonal. Fig. (89) is another illustration of interlacing of two trigonal spirals.

9.2. SOME FURTHER EXAMPLES

Figs. (90) and (91) illustrate an example of interlaced spiral in which the structure of the step lines on the alternate sides of the hexagon is markedly different. In three orientations, alternate step lines are rugged and irregular whereas in the other three orientations all the step lines are smooth. In the part ABC of fig. (91), the step lines are smooth, and in part ACD, alternate step lines are irregular and have a rugged structure. The continuity of alternate smooth step lines in ACD can be traced to ABC. The transition along the zig-zag portion AC is clearly shown in the figure. This rugged appearance of step lines may be due to slight surface oxidation, causing the layers to separate out in certain orientations.

Figs. (92), (93) and (94) showing the same feature in three different magnifications illustrate another interesting variation of interlaced spirals. The point of special interest here is that the six corners appear to grow faster than the straight portions. This results in the step lines, between any two corners, having a cusp and a concave form. According to theory, a step with a re-entrant corner or with a negative radius of curvature should rapidly grow out. This cusp in the

step line and its concave form could only have been maintained
by the faster growth at the six corners, this pull along these
corners giving the hexagonal figures the above shape. In
fig. (94), which shows the centre of the spiral, it is seen
that the step lines are convex near the centre, their
curvature decreasing with the increase of the distance, in
accordance with theory.

A point which can be noted in all these figures of
interlaced spirals is that at the six corners, the extent of
the zig-zag or criss-cross pattern varies in different cases.
In some of them e.g. figs. (82), (85) and (86) this is
limited over a small area and the transition appears quite
sharp. Whereas in other figures such as (84) and (91) this
transition from the slowest to the fastest monolayers by
changing the orientation through 60° is gradual and smooth.
Further over this transition area the zig-zag portion of the
interlaced spiral may be composed of small straight lines as
illustrated in figs. (82), (85) and (86) or it may be grad-
ually curved as seen in fig. (84). In the diagram fig. (87),
the transition portion has been drawn, for the sake of sim-
plicity, as straight lines.

This alternation of the velocity of growth with the
change of orientation by 60° will necessarily occur in the
hexagonal type 6 H, but it is possible that it may occur in

118.

the rhombohedral types also, in which case the rhombohedral

types will also display these inter|ed spirals. According
lac

to this explanation since the change of growth velocity will

necessarily occur for spirals developed on crystals belonging

to type 6 H, they should always interlace. But crystals of type

6 H have been observed to exhibit circular, hexagonal, as well

as interlaced spirals. Therefore, this explanation, though

it gives a qualitative explanation, is incomplete and there

must be some other factors also controlling the formation of

these spirals.

9.3. GROUPED INTERLACED SPIRALS AND ITS EXPLANATION

In some of the interlaced spirals a grouping of a

certain number of steps takes place. Several such cases

have bee n studied and the number of steps grouping together

has been found to vary depending upon the number of layers

in the x-ray unit cell of the crystal. Fig. (95) shows part

of an interlaced spiral in which in any one orientation seven

steps are observed to group together having a characteristic

sequence of spacing between them. These steps can be

followed in fig. (98), which shows spiral as a whole at a

lower magnification, to the other side of the interlaced

portion, and the same sequence of spacing repeating itself

is observed. This characteristic spacing between the success-

ive seven steps is seen to repeat itself for the successive

groups. Under low magnification, these grouped steps give

an appearance resembling optical band-spectra. In fig. (96),

showing a different portion of the same spiral, it is seen that the high visibility of the step lines is due to the deposition of some impurity. In fig. (97), the advancing groups of seven steps meet the interlaced steps originating from three new screw dislocations. The figure illustrates their interaction.

On another crystal a similar grouping of five steps has been observed. This is illustrated in fig. (99). Unlike the previous example the grouping of five steps together cannot be followed to the other side of the interlaced portion since the interlaced portion is near the crystal edge. The spacing between the successive five steps is not constant and therefore it does not have the characteristic appearance of figs. (95) and (97).

In addition to these fixed number of steps grouping together, on one face of a crystal, the number of steps grouped together ha s been observed to change in certain regions. Thus in fig. (100) which exemplifies this type of behaviour, it is observed that the number of steps that have grouped together varies greatly on different parts of the crystal.

Explanation

An explanation of these features can be given as follows. (Verma 1951 a). The different polytypes of silicon-

120.

carbide have the Ramsdell's zig-zag sequence or Zhdanov symbol of $(33)_n$ 32 . Using Frank's notation, the structure can be written as:

$$\left[(\triangle \triangle \triangle \triangledown \triangledown \triangledown)_n \triangle \triangle \triangle \triangledown \triangledown \right]$$
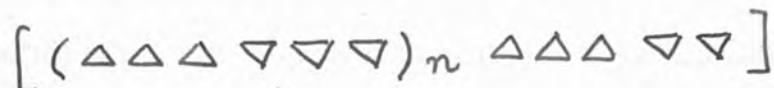
As in the previous case of simple interlaced spirals, the growth conditions will be different for each of the Si-C layers provided atomic interactions are significant as far away as the number of layers involved. The most striking difference will occur at each change in the $\triangle \triangledown$ sequence i.e. when the first $\triangle$ layer occurs after a series of $\triangledown$ layers or vice versa. Now it is not known whether this will make the rate of advance faster or slower. If it makes the layer grow faster, it will not produce an observable change and hence is unimportant. If, however, it makes it grow slower then a certain monolayer in this stack of monolayers will be the slowest one and the faster following layers will pile up on it, upto and excluding the next one which goes at the same rate. Thus if we assume that the first $\triangle$ after a series of $\triangledown s$ (or vice versa) has the slowest velocity in any one orientation, then it will repeat itself after six such layers making the growth steps 15A high, until we reach the last layer which will be 12.5A high, since it is composed of only five monolayers. After this, the whole sequence will go on repeating itself. The case for seven steps grouping together is represented as follows:-

$\triangle\triangle\triangle\triangledown\triangledown\triangledown$ | $\triangle\triangle\triangle\triangledown\triangledown\triangledown$ | $\triangle\triangle\triangle\triangledown\triangledown\triangledown$ | $\triangle\triangle\triangle\triangledown\triangledown\triangledown$ | $\triangle\triangle\triangle\triangledown\triangledown\triangledown$ | $\triangle\triangle\triangle\triangledown\triangledown\triangledown$ | $\triangle\triangle\triangle\triangledown\triangledown\triangledown$

← 15A →   ← 15A →   ← 12.5A →
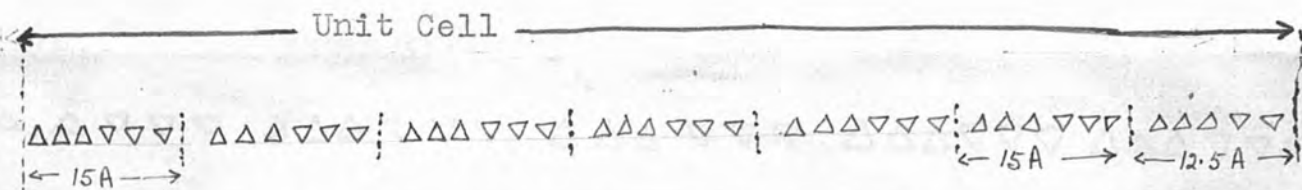
Thus depending upon the number n in the Zhdanov symbol $\left[(33)_n \; 32\right]$ we will have a certain number of steps grouping together.

In figs. (95) and others the seven steps grouped together form the unit cell and hence the step height at successive edges is only a fraction of the unit cell. Similarly the step heights of all other grouped steps is also a fraction of the unit cell. These steps further break up into two parts i.e. each is only 3 monolayers high, over the interlaced or zig-zag part.

The observation of the changing number of steps grouped together suggests a change in type from one part of the crystal to another. The different parts of the crystals showing grouping of say 9, 11, etc., steps means that those parts of crystal are the polytypes with Zhdanov symbol $\left[(33)_8 \; 32\right]$, $\left[(33)_{10} \; 32\right]$, --- etc. This may account for the disagreement between crystal symmetry and x-ray diffraction data sometimes observed (Ramsdell ~~1951~~ & Kohn 1951)

The observation of this grouping of steps is another visual confirmation provided by crystal growth patterns, of the repeat sequence predicted by x-ray phenomena.

122.

INTERFEROMETRIC STUDIES.

CHAPTER X.

RESULTS OF INTERFEROMETRIC STUDIES AND POLYTYPISM

IN SILICON-CARBIDE

By the application of multiple-beam interferometric
techniques as outlined in Chapter Vl, the step heights for
the growth spirals observed on different Si-C crystals were
measured. As shown below, the step height between successive
arms of the spiral differs on the different polytypes and is
characteristic of the particular type, having a direct corres-
pondence with the size of the x-ray unit cell. The step
heights of these growth spirals have been found to be (1)
equal to the size of the x-ray unit cell (2) a multiple (3)
a fraction of the x-ray unit cell, giving the three types of
spirals discussed in Chapters Vll, Vlll and lX respectively.

10.1.   GROWTH SPIRALS WITH ELEMENTARY BURGERS VECTOR

(a)   Si-C Crystals of Type 6H

The spirals belonging to the first type are the
elementary spirals. By far the largest number of these growth
spirals observed were on the commonest variety of Si-C crystals
of type 6H. Since the step height of these spirals is equal
to 15A, it is too small to be measured directly by the shift

123.

of the individual Fizeau fringes at these steps, and, therefore, the methods outlined in Secs. 6.2 to 6.5 for finding the average step heights were utilized. The results of interferometric measurements are summarised below.

The growth spiral of fig. (18b) was observed on a crystal which was quite well developed. By measuring the interfacial angles between the basal plane and other faces, by a one circle goniometer available in the laboratory, it was found that these angles given in Table VI, agree within experimental errors with the data given by Thibault (1944) for type 6 H and, therefore, this crystal was identified to be of type 6 H.

Table (VI)

Angle between the basal plane and the form.		Form	
Experimentally determined value	Thibault's data		
49° 8'	48° 33½'	n - $\bar{n}$	10$\bar{1}$5
54° 53'	54° 47'	r - $\bar{r}$	10$\bar{1}$4
62° 5'	62° 6'	s - $\bar{s}$	10$\bar{1}$3
70° 29'	70° 33½'	x - $\bar{x}$	10$\bar{1}$2
78° 4'	- -		-
89° 53'	90° 00'	m	10$\bar{1}$2
80° 1'	79° 59½'	y - $\bar{y}$	10$\bar{1}$1
Another zone			
62° 0'			
70° 29'			

124.

Three different methods given in Secs. (6.2a), (6.3), and (6.4) were applied for the measurement of step heights. Fig. (18a) shows Fizeau fringes under high dispersion passing over the peak of the spiral hill. That the Fizeau fringe is passing exactly over the centre of the spiral can be seen in fig. (18a), where the spiral turns have been revealed by the effect of diffraction (see Sec. 6.6). By knowing the angle through which the Fizeau fringe bends at the centre, the dispersion i.e. the separation between the successive orders from fig. (18a), and 'd' the separation between the successive steps (changed to the same magnification as fig.(18a)) from fig. (18b), the step height has been measured using equation (20). The result is given in column I of Table(VII). Fig (18c) shows the fringes of equal chromatic order corresponding to fig. (18a), and using equations (29&30), the measured step height is given in column II of Table (VII). In column III is given the average step height by knowing the total difference in the level of the crystal on either side of the discontinuity line at a point A and then dividing this by the difference in number of steps crossed in reaching this point from the centre of the spiral by going round the 'fish' like obstruction in a clockwise or anticlockwise direction.

Table VII

h, the measured step height for the growth spiral in fig. (18a) observed on a crystal of type 6 H		
Use of Fizeau fringes	Use of fringes of equal chromatic order	By counting the steps
15.2 A; 14.1 A	17.1 A	14.8 A

A similar measurement of step-height was done for the growth spiral at the bottom of fig. (44), by the use of Fizeau fringes. The result of four independent trials for the measurement of step-height was:

14.5 A ;   15.5 A ;   15.0 A ;   15.3 A.

These measurements show that the average step height of these growth spirals is 15.2 A with a maximum uncertainty of about 1A. The lattice parameter 'c' for type 6 H is equal to 15.079 A (See Table (II)). This shows that within the limits of experimental accuracy, the step height is equal to the lattice parameter c of the X-ray unit cell. This is to be expected, since for the spirals observed on the basal plane (0001), the step height should be equal to the repeat distance along the 'c' - axis.

(b) Si-C   Crystals of Type 15R

The type of crystal studied next was the second most common variety of Si-C crystal of type 15R. The growth spiral observed on this crystal is illustrated in figs. (19a) and (34). The type of the crystal was again identified goniometrically and the interfacial angles between the basal plane and other faces are given in Table (VIII) below, and are compared with the data given by Thibault (1944).

Table (VIII)

Angle between the basal plane and the form		Form
Experimentally determined value	Thibault's data	
47° $15'$	47° $30'$	M $10\bar{1}13$
54° $44'$	54° $46'$	r $10\bar{1}10$
63° $45'$	63° $42\frac{1}{2}'$	f-$\bar{f}$ $10\bar{1}7$

This crystal had only three well-developed faces, besides the basal plane, suitable for goniometry. However, the measured angles 47° $15'$ and 63° $45'$ show it to be conclusively of type 15R, since these two angles do not occur for type 6 H and occur only for type 15 R.

The growth spiral observed on this crystal has straight edges (except at the centre) and therefore for the measurement of step height, by the application of Fizeau fringes, shown in fig. (19b) equation (26) was used. For greater accuracy, as discussed in Sec. (6.5), figures (19a) and (19b) were superimposed over one another as shown in fig. (19c). The results of the measurement of step height is given in Table (IX).

Table (IX)

Crystal Type	lattice parameter		Measured step height
	c	a_{rh}	
15R or Zhdanov symbol (32)	37.95A	12.78A	13.0 A 11.1 A 13.1 A

This result of measurement shows that the step height is equal to a_{rh}, the size of the actual rhombohedral unit cell, which is equal to $\frac{1}{3}$ the length of the 'c'- axis referred to the hexagonal axes. This is in accordance with the true stacking sequence, which for type 15 R is in Zhdanov's notation (32) or in Frank's notation ($\triangle \triangle \triangle \nabla \nabla$).

128.

(c) <u>Si-C Crystal of Type 33R.</u>

This interesting result needed some further con-firma tion. To verify this, the type of a large number of crystals showing growth spirals was determined amongst which one crystal which was determined to be of type 33R was found. Since the measurement of step height on this crystal wa s crucial, the type of this crystal was determined accurately with the goniometer. Fortunately, this crystal had a number of faces quite well developed giving excellent reflections. In Table (X) the results of the measurement of the interfacial angles between the basal plane and the successive faces are reproduced and are compared with the data given by Ramsdell (1945).

Table (X)

Angle between the basal plane and form		Quality	Form
Experimentally determined value with possible error	Ramsdell's data		
53° 37' ± 2'	53° 32') 53° 39')	A	B 0.1.Ī.23. B̄ 1.0.Ī.23.
61° 26' ± 2'	61° 22½') 61° 24')	A	W 0.1.Ī.17. W̄ 1.0.Ī.17.
70° 41' ± 2'	70° 34') 70° 33½')	A	x 0.1.Ī.11. x̄ 1.0.Ī.11.
75° 48' ± 5'	- - - -	B, thin face	- - - - - -
81° 1' ± 2'	80° 53½') 80° 52')	B, very thin face	υ 0.1.Ī. 5. ῡ 1.0.Ī. 5.
54° 54'	- - - -	-	- - - - - -
62° 47'	62° 49½') 62° 46½')	A	u 1.0.Ī.16. ū 0.1.Ī.16.
67° 19'	67° 14') 67° 24')	B	t 1.0.Ī.13. t̄ 0.1.Ī.13.
Two very thin faces not measurable		-	- - - - - -
90° 5'	- - - -	-	- - - - - -
79° 48'	- - - -	-	- - - - - -

This close agreement between the experimentally measured interfacial angles and the data given by Ramsdell was taken to prove conclusively that the crystal was of type 33R.

The growth spiral observed on this crystal is shown in fig. (101) or (75). The behaviour of the growth fronts and the resulting shape of the spiral have already been commented upon in Sec. (8.2). Fizeau fringes passing over this spiral are shown in fig. (102). In accordance with the method of Sec. 6.5 for greater accuracy, Fizeau fringes are shown superimpos ed over the growth spiral in fig. (103). Since it is a polygonal spiral, again using the Formula (26) the step height was determined, the results of which are summarised in Table (XI).

Table (XI)

Ramsdell's Notation	Zhdanov and Frank's Notations	Lattice parameter		Measured step height
		c	a_{rh}	
33R	(33 32) (△△△▽▽▽△△△▽▽)	82.94A	27.704A	27.8 A 23.0 A 28.3 A 31.0 A

The measurement within limits of experimental accuracy shows conclusively that the step height for type 33R crystal is equal to a_{rh} of the actual rhombohedral unit cell which is equal to $\frac{1}{3}$ its length along the c - axis referred to the hexagonal axis.

Thus it seems reasonably established that in silicon-carbide crystals the step heights for elementary spirals on

the hexagonal crystals is equal to the lattice parameter 'c'
and in rhombohedral crystals the step height is equal to
a_{rh} of the rhombohedral unit cell, which corresponds to the
actual stacking arrangement. Thus in both the cases so far
studied, the step height is equal to the size of the actual
X-ray unit cell. Such spirals, therefore, originate from
dislocations with unit Burgers vector i.e. these are the
elementary spirals.

In another crystal, the growth spiral on which is
illustrated in fig. (16b), it has been possible to measure
the step height by the shift of the Fizeau fringes (fig.16a)
on these individual steps. The step height is equal to 130 A.
Taking the step height h = a_{rh}, this crystal should be of
type 159 R with Zhdanov symbol $\left[(33)_8 \ 32\right]$. However, to confirm
this prediction X-ray diffraction data would be needed.

10.2. GROWTH SPIRALS ORIGINATING FROM DISLOCATIONS OF MULTIPLE STRENGTH

Often the growth spirals observed on silicon-carbide
crystals having a high visibility, belong to this class. A
typical example of such a spiral is shown in fig. (104), which
is a part of fig. (70). Fizeau fringes passing on these
spiral steps are shown in fig. (105). For photographing these
Fizeau fringes a lightly silvered glass flat was used with
the advantage that the spiral turns are visible simultaneously
with the Fizeau fringes. The step height as measured by the

132.

shift of Fizeau fringes at these steps is equal to 620 A.
The crystal was identified by usual goniometric measurements
to be of type 6 H. The step height, therefore, is a multiple
of the X-ray unit cell. This conclusion is further supported
by the observation that these steps dissociate into component
steps as shown in fig. (71).

Fig. (106) or (40) which shows the case of two screw
dislocations of opposite hand generating closed loops is of
interest. The shift of the Fizeau fringes (see fig. (107))
passing over these steps, gives the step height or the thickness
of each layer = 120 A. Since the ledges originating from the
two screw dislocations fuse with one another without marking
out a fault surface, it may be concluded that the steps
originating from the two dislocations are identical and there-
fore the two dislocations have the same structure and strength.
Since it is improbable that both these dislocations are the
same multiple of a dislocation with a smaller Burgers vector,
it may be concluded that the two dislocations are elementary
dislocations and the crystal is a polytype with a large unit
cell. If indeed the step height is equal to the a_{rh} of the
rhombohedral types, the crystal will be a polytype 141 R with
Zhdanov symbol $\left[(33)_7 \, 32 \right]$.

10.3. INTERPRETATION OF POLYTYPISM

These observations on growth spirals lead readily
to an understanding of polytypism as observed on silicon-

carbide crystals, in terms of dislocations. The above inter-
ferometric studies have shown that the step height of the
growth spiral is characteristic of the type of crystal on
which it is observed, and is equal to the size of the X-ray
unit cell. According to Burton, Cabrera and Frank's theory,
the spiral form is obtained, when during the process of growth,
the initial ledge formed on the face of the crystal by the
emergence of the screw dislocation, winds itself into that
shape. Thus the crystal growing by the presence of dislocations,
is not composed of an indefinite number of layers stacked upon
each other as ideally considered, but of a finite number of
interleaved helicoids. Each helicoid axis is a dislocation.
The structure necessarily repeats with a period corresponding
to the pitch of the screw. Thus the step height will be
equal to the height of the initial ledge. The step heights
have already been shown to be equal to the size of the X-ray
unit cell, which therefore becomes the crystal building unit
giving rise to the different polytypes.

It, therefore, remains to explain the creation of
the initial ledge. Frank (1951α)suggests that silicon-carbide
crystals may initially grow into plates by surface nucleation
mechanism. These plates will become self stressed, through
non-uniform distribution of impurities or thermal stresses
due to partially screened intense radiation, ultimately upto
its theoretical yield stress, when the thin plate will buckle
and shear. This will raise terminated steps on the crystal

face, and if the shear is by a uniform amount terminating fairly abruptly a ledge will be exposed. The crystal subsequently growing will have necessarily the structure corresponding to that of the ledge. So if the original crystal has a simple initial structure like that of type 6 H, with Zhdanov symbol (33), and the slip is an integral multiple of the repetition period of this structure, the crystal growing will be of type 6 H. If, however, the slip is by a non-integral multiple of this period, the resulting structure will be a polytype. This will explain the structure with Zhdanov symbol $[(33) n\ 32]$. Since a non-integral slip will leave a misfit on the slipped surface, it should be less common than the integral slip. This explanation, however, does not explain the non-occurrence of structures with Zhdanov symbol $[(33)_n\ 31]$, $[(33)_n\ 35]$ etc.

Vand (1951) has also given an explanation on similar lines. An alternative explanation for polytypism is possible. If the initial structure contains a stacking fault in the region whose ledge becomes exposed, we will get a polytype with period equal to the step height.

Whatever be the cause of intitial ledge, the X-ray unit cell forms the crystal building unit giving rise to the different polytypes.

CHAPTER XI

CONCLUSIONS

PRESENT POSITION OF EXPERIMENTAL OBSERVATIONS.

11.1. CONTRIBUTIONS BY THE PRESENT INVESTIGATIONS

As stated in Chapter III, when the present investigation was started the only experimental evidence available in support of the spiral mechanism of crystal-growth due to the presence of dislocations, were the observations by Griffin (1950) on beryl crystals. These observations were meagre and qualitative. Because of the small number of turns which the spiral was developed (only two turns) it was not possible to make any measurements on the spiral itself. It was shown that the step height at the 'line markings' was less than 34 A i.e. less than 4 unit cells. It could only be inferred that these features are growth features in accordance with the theory.

In the present investigation, using improved experimental techniques, numerous growth spirals have been observed and many of the theoretical predictions have been confirmed and new experimental facts and data have been obtained which have supplemented the theory and lead to the understanding of new facts.

The theory of crystal growth as developed by Burton,

Cabrera and Frank (1951) predicted that the crystals growing by the presence of screw dislocations will exhibit on their faces flat spiral growth pyramids, the step heights being "monomolecular", the exact shape and step height being left as an unsettled question. The present investigations soon revealed that these spirals could be classified into three types. Firstly, elementary growth spirals originating from screw dislocations with unit Burgers vector. Secondly, growth spirals originating from screw dislocations of multiple strength. Thirdly, interlaced growth spirals. The last two types had not been anticipated by theory. Further, the idea of unit Burgers vector needed clarification. The growth spirals were said to be "monomolecular" which is by no means the case. It is the X-ray unit cell that acts as the crystal building unit which forms the step height. Those spirals which have a step height equal to the X-ray unit cell are called the spirals originating from dislocations with unit Burgers vector. It should be made clear, that even in such a spiral the step height is equal to several molecular thicknesses e.g. for type II or 6 H, the step height is equal to 15 A which is equal to 6 molecular layers.

The spirals, whose step heights were determined to be equal to a multiple of the X-ray unit cell showed that it is possible for dislocations to be of multiple strength and, therefore, for defining a dislocation in any material, the strength or Burgers vector has to be specified.

137.

The third type of spiral viz: the interlaced spirals were entirely new. It demonstrated that under certain conditions of growth, step heights could also be a fraction of the unit cell in certain parts of the growth spiral. Further it demonstrated the variation of the dependence of growth rate on the crystal surface in different orientations.

In addition, the microscopic observations gave information about the shape of the spirals. For the first time it was demonstrated by the growth spirals observed on silicon-carbide crystals that the same crystal could exhibit both circular and polygonal spirals (regular hexagonal) and also intermediate cases. This has not yet been observed in any other study - nearly in all observed cases the spirals are polygonal.

Besides giving information about the shapes of the spirals, microscopic observations have illustrated the different properties of growth fronts; the interaction of growth fronts originating from different sources on the same crystal face and the fault surfaces produced. This leads to the explanation of the complex growth patterns when 2, 3 or larger number of screw dislocations emerge on the crystal face. The curves of intersections when the series of growth fronts meet each other and several complex geometrical patterns resulting from groups of dislocations arranged in different ways have been illustrated. When a very large

number of dislocations emerge on the crystal certain
statistical properties like density of dislocations have
been studied. A significant observation is that it is char-
acteristic that in any one region of the crystal, the dis-
locations are predominantly of the same sign and have the
same strength.

Experimentally pairs of dislocations of opposite
sign are seldom observed. Amongst all such pairs observed
so far on silicon-carbide, a pair of dislocations close to
each other and equally developed has not been observed for
dislocations of elementary Burgers vector with small step
heights. However, such a rare case was observed for dis-
locations giving rise to step heights 120 A. This observation
could be explained that in addition to the attractive forces
between the two dislocations of opposite sign, there must be
a constraining force trying to anchor these dislocations to
their equilibrium positions between the lattice rows. This
observation leads to the conclusion that this constraining
force which was taken by Peierls (1940) and Nabarro (1947)
to depend upon elastic constants only depends upon the
strength of the dislocation, so that the attractive and the
anchoring forces can balance each other at a certain distance
of separation between the dislocations.

The step heights have been measured accurately by
the application of multiple-beam interferometry. It is

found that the step heights of the growth spirals observed on the different types have a direct correspondence with the X-ray unit cell. This leads to the understanding of the interesting property of polytypism as observed on silicon-carbide crystals, in terms of dislocations.

11.2. PRESENT POSITION OF OBSERVATIONS

The volume of experimental observations in support of the theory of spiral mechanism of crystal growth has grown considerably in the interim period, and a brief description in the chronological order will be given.

Dawson and Vand (1951) using electron microscopic techniques have observed the growth spirals of long-chain paraffin crystals ($C_{36} H_{74}$). These spirals are rectangular in shape. By metal shadow casting they have shown the step height to be equal to 47 ± 5 A, which, within experimental errors is equal to the size of the X-ray unit cell.

The growth of cadmium-iodide from aqueous solution was first studied by Bunn and Emmett (1949) to study the layer formation. The spiral mechanism of growth of cadmium-iodide crystals was demonstrated by Forty (1951,1952). The step heights of the growth spirals on cadmium-iodide crystals are not of molecular thicknesses, but are several hundred angstrom units high. Many growth patterns on cadmium-iodide were found to have marked resemblance with the growth patterns

observed on silicon-carbide crystals, and it is concluded that cadmium-iodide also exhibits polytypism similar to that observed on silicon-carbide.

Haematite ($Fe_2 O_3$) crystals also show growth spiral features (Verma 1952). Both polygonal and curvilinear spirals were observed. By the application of the multiple-beam interference fringes, step heights have been measured and shown to be equal to the value of the repeat distance predicted by X-ray phenomenon.

Triangular spiral features have been observed by Amelinckx (1952) on chemically deposited gold and from their visibility it is inferred that the step heights are large. Spiral features have also been observed by Forty (1952α)on magnesium formed in a furnace. No measurements of step heights have been reported. From the visibility it is inferred that these originate from dislocations of small Burgers vector. Amelinckx (1952α)also reports a spiral formation on mica.

These are the observations reported up-to-date. However, it is thought that a number of crystals will demonstrate this spiral mechanism of growth, the observations on which may be awaited.

11.3. COMPARISON OF THE OBSERVATIONS ON SI-C WITH OTHER
OBSERVATIONS

The observations on silicon-carbide crystals are
unique. No other crystal has yet been observed to exhibit
all the three types of growth spirals viz: growth spirals
originating from dislocations of unit Burgers vector, growth
spirals originating from dislocations of multiple strength,
and interlaced spirals. The only other crystal observed to
exhibit the interlaced spiral is cadmium-iodide.

The measurement of step heights of elementary growth
spirals has been done on only a few crystals. The available
data of step heights on long-chain paraffin crystals (Dawson
and Vand 1951) and on haematite (Verma 1952) show that the
step heights are equal to the predicted X-ray values. The
large step heights on cadmium-iodide crystals (Forty 1952)
have been shown to be large integral multiples of the smallest
repeat unit.

A noteworthy point in the spirals on Si-C crystals
is that the centre of the spirals is marked visibly by a hole,
the size of which is observed to vary. (Compare fig. (22)
with (35) etc.). According to Frank (1951 b), a dislocation of
Burgers vector exceeding about 10 A will be in equilibrium
only with an empty tube at its core so that there will be
a hollow at the point of emergence of the dislocation on the
crystal surface. However, in the growth spirals observed on

paraffins which have a step height of 47 A, the points of emergence of dislocations are not marked by a hole. This may be attributed to the dissociation of a complete dislocation into weak partial dislocations. It is interesting to note that the point of emergence of dislocation in haematite crystals of step heights nearly 14 A is not marked by a hole.

References

Acheson, E. G.,   1893 Chem. News 68, 179.

"   1893 J. of Franklin Inst. 136, 196, 279.

Amelinckx, S.,   1951 Nature 167, 939.

"   1951a Nature 168, 431.

"   1952 Comptes Rendus 234, 113.

"   1952a Nature. 169, 580.

Baumhauer, H.,   1911 Z. Krist. 50, 33.

"   1915 Z. Krist. 55, 249.

Becker, R., &
Döring, W.,   1935 Ann. Physik 24, 719.

Bennett, A.H.,   Jupnik, H., Osterberg, H., Richards, O.W.,

                     1951. Phase Microscopy (New York: John Wiley
                                                        & Sons).

Bunn, C.W. & Emett, H., 1949 Discussions of the Faraday Society

                     No. 5, Crystal Growth .. p. 119

Burch, C.R., &
Stock, J.P.P.,   1942 J. Sci. Inst. 19, 71.

Burgers, J.M.,   1939 Proc. Roy. Acad. Sci. Amsterdam 42, 293,
                                                               378.
"   1940 Proc. Phys. Soc. 52, 23.

Burton, W.K., Cabrera, N., & Frank, F.C., 1949 Nature 163, 398.

"   "   "   1951 Phil. Trans. Roy.
                                              Soc. A. 243, 299.

Burton, W.K., & Cabrera, N., 1949 Discussions of the Faraday
                               Society No.5. Crystal Growth..p. 33.

Cottrell, A.H.,   1949 Theory of Dislocations; Progress in Metal
                          Physics Vol.I (London: Butterworth's
                          Scientific Publication) ... p. 77.

Dawson, I.M., & Vand, V., 1951 Nature 167, 476.

    "   "   1951 Proc. Roy. Soc. A., 206, 555.

Frank, F.C.,   1949 Discussions of the Faraday Society

                         No.5 Crystal Growth .. p. 48, 67.

    "   1951 Phil. Mag. 42, 809.

    "   1951a Phil Mag. 42, 1014.

               1951b Acta Cryst. 4, 497.

Frenkel, J.,   1945 J. Phys. U.S.S.R. 9, 392.

    "   1946 Kinetic Theory of Liquids (Oxford: Clarendon Press).

Forty, A.J.,   1951 Phil. Mag. 42, 670.

    "   1952 Phil. Mag. 43, 72, 377.

               1952a Phil. Mag. 43, 481.

Gibbs, J.W.,   1878 Collected Works, 1928, (London: Longmans Green & Co.,) . p. 325, footnote.

Griffin, L.J.,   1950 Phil. Mag. 41, 196.

Hamy, M.,   1906 J. Phys. Radium 5, 789.

Haward, R.N.,   1939 Trans . Far. Soc. 35, 1401.

Holden, J.,   1949 Proc. Phys. Soc. B 62, 405.

Jagodzinski, H., 1949 Acta Cryst. 2, 201, 299.

Kalb, G., &
Wittborg, W.,   1951 Naturwiss. 38, 156.

Kohler, A., &
Loos, W.,   1941 Naturwiss. 29, 49.

Kossel, W.,   1927 Nachr. Ges. Wiss. Gottingen, p. 135.

Kowarski   1935 J. Chim. Physique, 32, 303, 395, 469.

Levinstein, H.,   1949 J. App. Phys. 20, 306.

Linfoot, E. H.,   1945 Nature 155, 76.

Marcelin, R.,   1918 Ann. Physique 10, 185.

Menzies, A.W.C.,
& Sloat, C.A.,   1929 Nature 123, 348.

Miers, Sir H.A.,   1903 Proc. Roy. Soc. 71, 439.

"   1904 Phil. Trans. Roy. Soc. A 202, 459.

Nabarro, F.R.N.,   1947 Proc. Phys. Soc. 59, 256.

Orowan, E.,   1934 Z. Physik 89, 634.

Ott, H.,   1911 Z. Krist. 50, 33.

"   1915 Z. Krist. 55, 249.

Padurow, N.N.,   1949 Neuen Jahrbuch f. Min. etc.,
                           Monatschefte A. 9, 203.

Payne, B.O.,   1947 J. Sci. Instrum. 24, 163.

Peierls, R.,   1940 Proc. Phys. Soc. 52, 34.

Picard &
   Duffendack,   1943 J. App. Phys. 14, 291.

Polanyi, M.,   1934 Z. Physik, 89, 660.

Ramsdell, L.S.,   1945 Am. Min. 30, 519.

"   1947 Am. Min. 32, 64.

Ramsdell, L.S., &
Kohn, J. A.,   1951 Acta Cryst. 4, 111.

Stranski, I.N.,   1928 Z. Phys. Chem. 136, 259.

Strong, J.,   1940 Modern Physical Laboratory Practice.
                           (London: Blackie & Son).

Taylor, E.W.,   1947 Proc. Roy. Soc. A. 190, 422.

"   1949 J. Roy. Micr. Soc. 69, 49.

Taylor, G.I.,   1934 Proc. Roy. Soc. A, 145, 362.

Thibault, N.W.,   1944 Am. Min. 29, 249, 327.

Tolansky, S.,   1946 High Resolution Spectroscopy (Methuen &
                                                            Co).

Tolansky, S.,   1948   Multiple Beam Interferometry of
                            Surfaces and Films. (O.U.P.).

Vand, V.,   1951   Nature, 168, 783.

    "   1951   Phil. Mag. 42, 1384.

Verma, A.R.,   1951   Nature 167, 939; 168, 430.

    "   1951   Phil. Mag. 42, 1005.

    "   1951a Nature 168, 783.

    "   1952   Nature 169, 540.

Volmer, M.,   1923   Z. Phys. Chem. 102, 267.

    "   1939   Kinetic der Phasen bildung (Dresden &
                            Leipzig : Steinkopff).

Volmer, M., &
Schultze, W.,   1931   Z. Phys. Chem. A, 156, 1.

Weigel, O.,   1915   Nachr. Ges. Wiss. Göttingen,
                            Math - phys. Kl., p. 264, 299.

Zernicke, F.,   1934   Physica 1, 689.

    "   1934   Roy. Astron. Soc. M.N., 94, 377.

Zhdanov, G.S.,   1945   C.R. Acad. Sci. U.R.S.S. 48, 39.

ACKNOWLEDGMENTS

*Observations on Carborundum of Growth Spirals Originating
from Screw Dislocations.*

By AJIT RAM VERMA,
Royal Holloway College, University of London*.

[Plates XXV.–XXVIII.]

ABSTRACT.

Numerous growth spirals with shapes ranging from circular to regular
hexagonal have been observed on carborundum crystals of types I. and II.,
by coating the crystal faces with a thin film of silver of reflectivity nearly
90 per cent and then working in reflection, using phase contrast
illumination. The shapes of these spirals, in relation to the crystal
structure, are shown to be in accordance with the predictions of Frank's
theory. On a type II. crystal, hexagonal interlaced spirals have been
observed. The annihilation of growth fronts where they meet, and other
properties of growth fronts are illustrated and hence the observed patterns
for two or more screw dislocations are explained. The observed density
of dislocations ranges from small values up to a maximum of
10^4 per sq. cm. For a typical circular spiral the calculated values of the
radius of the critical nucleus is 2μ and supersaturation is 0·2 per cent.
By the application of multiple-beam interference, using both Fizeau
fringes and fringes of equal chromatic order, the step heights in spirals
have been measured accurately for type II. crystal and found to be
15 Å. This is equal to the height of the unit cell, proving that these are
growth spirals originating from screw dislocations, in exact accordance
with theoretical prediction.

* * *

§ 1. INTRODUCTION.

ACCORDING to Burton, Cabrera and Frank (1949) growth of crystals at
low supersaturations can take place only in the presence of dislocations.
A crystal should, therefore, have a number of dislocations with a screw
component terminating on the crystal face. Frank (1949) showed that
when growth takes place on the molecular terraces so exposed, the edges
of monomolecular layers develop as " growth spirals " centred on the
dislocation. Experimental evidence supporting this was found on beryl
by Griffin (1950). The present paper deals with dislocations and " growth
spirals " found on the faces of carborundum crystals.

---

* Communicatd by Pofessor S. Tolansky.

§2. The Crystal Structure and Types of Carborundum.

Carborundum, a strongly homopolar crystal, occurs in at least eight known types. One of these is cubic, sometimes called β-Sic. All other types (α-SiC) are based on either hexagonal or rhombohedral unit cells. All types have identical layers, but differ in their arrangements. Each type is distinguished by the number of layers in the unit cell. The basal pinacoid is predominantly developed, and it is on this that these growth spirals have been observed.

The crystals studied were either pale green, dark green or black. Some, which have a few well developed faces, have had their structural types determined by a goniometric method (Thibault 1944). X-ray diffraction methods will be required for the others.

No cubic crystal has been studied. Most of the crystals examined were of the commonest type, carborundum II. Its unit cell is hexagonal with six layers, and in Ramsdell's notation is 6 H (Ramsdell 1947). The lattice parameters are

$$a = 3 \cdot 073 \text{ Å}, \quad c = 15 \cdot 079 \text{ Å}.$$

In this work the only other type available was carborundum I. This has a rhombohedral unit cell and referred to the hexagonal axes consists of fifteen layers. In Ramsdell's notation it is 15 R with

$$a = 3 \cdot 073 \text{ Å}, \quad c = 37 \cdot 70 \text{ Å}.$$

§3. Visibility of Growth Spirals.

Numerous "growth spirals" have been observed on the faces of carborundum (SiC) crystals. These spirals are well developed; over thirty turns of the spiral can be traced in some cases. The spirals are centred on a dot which must mark the point of emergence of a screw dislocation on the crystal face.

The clean surface of the crystal when examined by a metallurgical microscope, using bright field illumination, does not show up these features, the surface appearing smooth. A little amount of impurity makes these features slightly visible (fig. 8, Pl. XXVI. has been taken by this method). Breathing lightly on the crystal face, while it is under observation, increases the visibility and the " lines " flash out, but soon disappear when the water re-evaporates. The " lines " seen by breathing are dotted and slightly diffuse, but the visibility obtained by this method is high. Though convenient for visual observations, the procedure is not suitable for photography.

Following Griffin's technique, contrast was increased by deposition of a thin film of silver on the crystal face using thermal evaporation. This was improved by the use of phase contrast illumination. The photographs have been taken using positive phase contrast, the absorption of the phase plate being 80 per cent and phase retardation equal to $\frac{1}{2}\pi$. With this equipment many features are often still faint and only

Spiral Growth on Carborundum Crystal Faces

IN 1949 Frank[1,2] pointed out the possibility that growth of crystals at low supersaturations, essential for good crystals, could take place because of the formation of dislocations in the crystal so that any real crystal should have a number of dislocations with a screw component, terminating on the face. When growth takes place on these exposed molecular terraces, the edges of these layers develop into spirals centred on the dislocation.

Griffin[3] has observed these 'monomolecular' layers on the $(10\bar{1}0)$ face of a beryl crystal, and has shown by multiple-beam interferometry that the height of these steps is less than 34 A., that is, less than four unit cells of the crystal. It was inferred that these steps are only one unit cell high.

In the present investigation, numerous 'growth spirals' have been observed on the faces of carborundum and measured with the aid of phase-contrast microscopy and multiple-beam interferometry.

Carborundum[4] occurs in at least eight known types, one of which is cubic, whereas the rest are either hexagonal or rhombohedral and have identical layers but differ in their arrangement and are uniquely distinguished by the number of layers in the unit cell. The crystals studied here are of type I (rhombohedral, fifteen layers, with lattice parameter $c = 37 \cdot 7$ A.), and type II (hexagonal, six layers, $c = 15 \cdot 1$ A.).

These spirals were studied by coating the crystal faces with a thin film of silver of reflectivity nearly 90 per cent, deposited by thermal evaporation, and then examining these faces in reflexion.

Theory shows that for growth taking place from vapour, the ledge extending from the point of emergence of the dislocation to the crystal boundary has a rate of advance independent of the crystallographic orientation, thus forming a simple Archimedean spiral which can be calculated and from which the constant of spacing between turns can be predicted. These predictions have been completely confirmed numerically by the circular spirals shown in Fig. 1.

The dependence of the rate of advance of a growth front on the orientation of the step line should impose a characteristic distortion of the growth of spirals, exhibiting the crystal symmetry. In accordance with this, Fig. 2 shows a hexagonal spiral (crystal type II). The straight edges correspond to a sharp minimum in the growth-rate as a function of orientation.

The complex growth patterns predicted for two or more screw dislocations ending on a crystal face and depending on the property of growth fronts which annihilate each other where the two edges meet are illustrated in Fig. 1. Thus for two screw dislocations of opposite hand, with the unfolding of the two spirals the ledges starting from one terminate on the other, generating closed loops.

Various other growth patterns for two, three and larger numbers of dislocations ending on crystal faces of type I and type II have been photographed and explained.

Interlacing of hexagonal spirals observed on a crystal face of type II is illustrated in Fig. 3.

The observed density of dislocations varies widely on different specimens, ranging from a few to a maxi-

mum of $\sim 10^4$ per sq. cm. On any crystal they are predominantly of one hand.
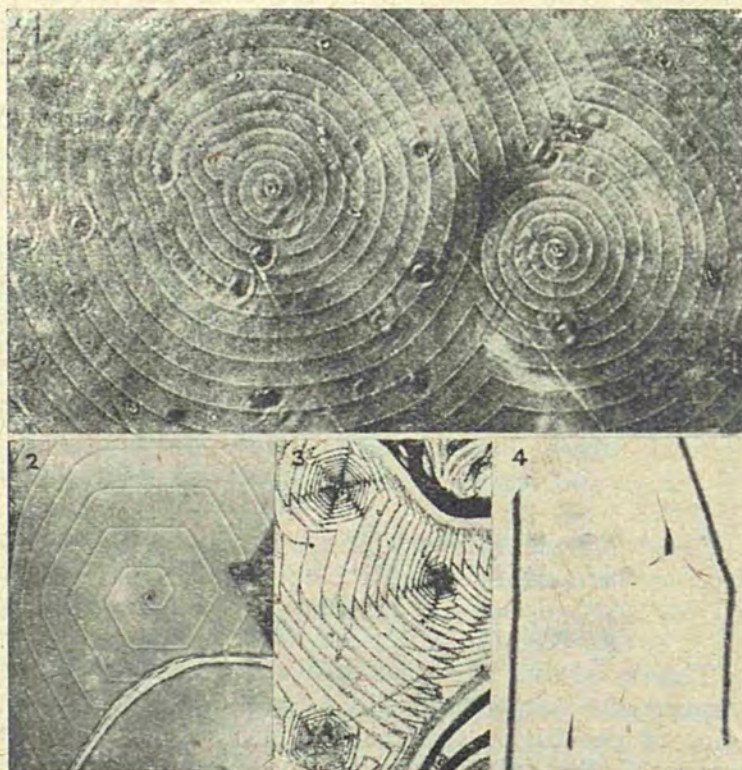
The calculated radius of the critical nucleus is $2\,\mu$ and the supersaturation $0\cdot2$ per cent.

To measure the step height of these spirals, multiple-beam interference (Tolansky[5]) has been employed. Fig. 4 shows the Fizeau fringes for $\lambda\,5,461$, passing over a circular spiral, in which the height can be accurately measured; and as the number of turns is readily visible, the height of each single step can be deduced with precision. Analogous measurements

have been made also with fringes of equal chromatic order. The step heights on a type II crystal measured from two different spirals are respectively 15·2 A. and 15·1 A., with a maximum uncertainty of 2 A. It is already known from X-ray analysis that, for type II, $c = 15·1$ A. Thus it has been proved here that the step is a single unit-cell high.

The observation of spiral markings on carborundum has already been reported[6]. The observed shapes of these spirals are in accordance with the predictions of theory, and their step height is equal to that of a unit cell, showing that these are growth spirals originating from screw dislocations.

A more detailed account of this work has been communicated elsewhere. I am grateful to Prof. S. Tolansky for his interest and encouragement in the course of this work, and to the British Council for the award of a scholarship.

AJIT RAM VERMA

Royal Holloway College,
Englefield Green,
Surrey.

[1] Burton, Cabrera and Frank, *Nature*, **163**, 398 (1949).
[2] Frank, F. C., Farad. Soc. Discuss., Crystal Growth, No. 5 (1949).
[3] Griffin, L. J., *Phil. Mag.*, **41**, 196 (1950).
[4] Ramsdell, L. S., *Amer. Min.*, **32**, 64 (1947).
[5] Tolansky, S., "Multiple-beam Interferometry of Surfaces and Films" (Oxford Univ. Press, 1948).
[6] Mellor, J. W., "A Comprehensive Treatise on Inorganic and Theoretical Chemistry", **5**, 879 (1924).

just visible. Usual photographic methods for increasing the contrast have been employed in some of the photographs given.

In fig. 13 (Pl. XXVIII.), it is seen that the visibility and contrast is high compared with other photographs. The surface of this crystal was not very clean when it was silvered. The silver deposit was not uniform, the surface appearing mottled. Examination with phase contrast illumination gave high visibility. This suggests that impurity can make the steps more visible.

§4. Shape of the Spiral for a Single Screw Dislocation.

The growth spiral will have a shape depending upon the rate of advance of a growth front in different crystallographic directions.

For growth taking place in accordance with Frank's ideas two cases arise :—

(*a*) when the Frenkel kinks on the step (exchange sites) are close together and the distance moved by an adsorbed molecule before it hits a step is large ;

(*b*) when the kinks are few or the distance moved by the adsorbed molecule is small.

When the former conditions exist, which are more likely to occur in growth from vapour, the molecule will have a high probability of adhering to the step if adsorbed near it, irrespective of the crystallographic orientation of the step. Thus for growth from the vapour, taking the rate of advance of the ledge to be independent of direction, the ledge will form a simple spiral under steady uniform supersaturation. The form of the spiral can be represented by the Archimedian equation

$$r = 2\rho_c \theta,$$

and the constant spacing between turns is

$$\delta r = 4\pi \rho_c,$$

where ρ_c is the radius of critical nucleus, equal to $a\phi/2k\mathrm{T}\ln\alpha$, and where α is the supersaturation ratio, a is the interatomic distance and ϕ is the neighbour-neighbour binding energy of the crystal.

These predictions are confirmed by the circular spirals shown in figs. 1, 2, 3 and 8 (Pls. XXV., XXVI.). It is to be noted, however, that the spiral turns are more closely spaced at the centre, and the spacing gradually increases on going away from the centre until it becomes nearly constant. This is in accordance with the prediction of theory (Burton, Cabrera and Frank 1951).

Any dependence of the rate of advance of a growth front on the orientation of the step-line could impose a distortion of the growth spirals, so that they exhibit the symmetry of the crystal face. Such an effect has been found in fig. 4 (Pl. XXVI.), where the spiral is nearly circular at the centre, and gradually takes on the hexagonal symmetry of the

crystal face (carborundum type II.). In fig. 7 (Pl. XXVI.) is a hexagonal spiral observed on a crystal identified to be of type II. This is a regular hexagonal spiral, showing clearly the dependence of the growth rate on the crystallographic orientation. The step-lines very near the centre show a curvature, which, as predicted by theory, decreases with distance from the centre. However, soon the straight step-lines start rounding off at the corners and become gradually curved on moving away from the centre. These step-lines do not meet the line of discontinuity sharply, but tend to curve away from it, as shown in fig. 7, for the outer five or six step-lines.

The straight edges show that under certain conditions there is a sharp minimum in the growth rate as a function of orientation.

In figs. 10 and 11 (Pl. XXVII.) further spirals are shown. Fig. 10 has been observed on a rhombohedral crystal type I.

§5. Properties and Behaviour of Growth Fronts.

The growth pattern for two or more screw dislocations ending on a face is complex and depends on the properties of the growth fronts. The growth fronts starting from a single screw dislocation will spread on the surface of the crystal face in regular shapes, but the presence of a boundary or an obstruction will distort its regular shape. When the advancing growth fronts meet an obstruction they can propagate round corners, as shown at the upper end of the obstruction in fig. 4; this point behaves almost as a source of secondary growth fronts.

The growth fronts emitted by two sources of opposite sign annihilate each other where they meet. Numerous examples of this can be seen in figs. 2 and 3 (Pl. XXV.). When there are several screw dislocations actively emitting growth fronts, a point on the crystal face will be in the dominant field of only one of these, and this alone determines the number of growth fronts passing through it. This is exemplified in fig. 2 where there are five screw dislocations. By choosing the point of observation, say, near the bottom screw dislocation, the number of growth fronts passing through it is solely determined as if this alone were active.

§6. Growth Spirals for Two or More Screw Dislocations.

In fig. 17 is drawn schematically the growth pattern for two screw dislocations A and B of the same hand. The ledge starting from A goes on rotating and generating the spiral until it meets at p_1 the ledge originating from B where it terminates. At p_1 the two ledges fuse with one another. As the spirals unfold themselves the ledges meet at p_1, p_3, p_5 . . . in the upper half and at p_2, p_4, p_6 . . . in the lower half of the figure. The locus of points of intersection for two equal spirals has been shown to be a cartesian oval (Burton, Cabrera and Frank 1951). Between p_1 and p_2 (p_3, p_4), etc., the missing parts of the two spirals are shown by the dotted lines. The resultant figure is the solid line curve.

Starting from A and going round the spiral we descend by one step in each complete turn till we come to the point p_1. From p_1 we go round the spiral B to the point p_4 and then again on the spiral A to the point p_5. Thus in going round the resultant curve once, we descend by two steps from p_1 to p_5 to p_9 and so on. Similarly, starting from B and going round we will descend by two steps, from p_2 to p_6, etc. . . . As the curves gradually smooth out at the points of contact, the figure will appear to be two spirals alternately spaced. Fig. 17 has been drawn for circular spirals, and the case for spirals with straight edges can similarly be drawn where the behaviour will be the same. In fig. 3 (Pl. XXV.) the case for circular spirals is illustrated.

Fig. 17.
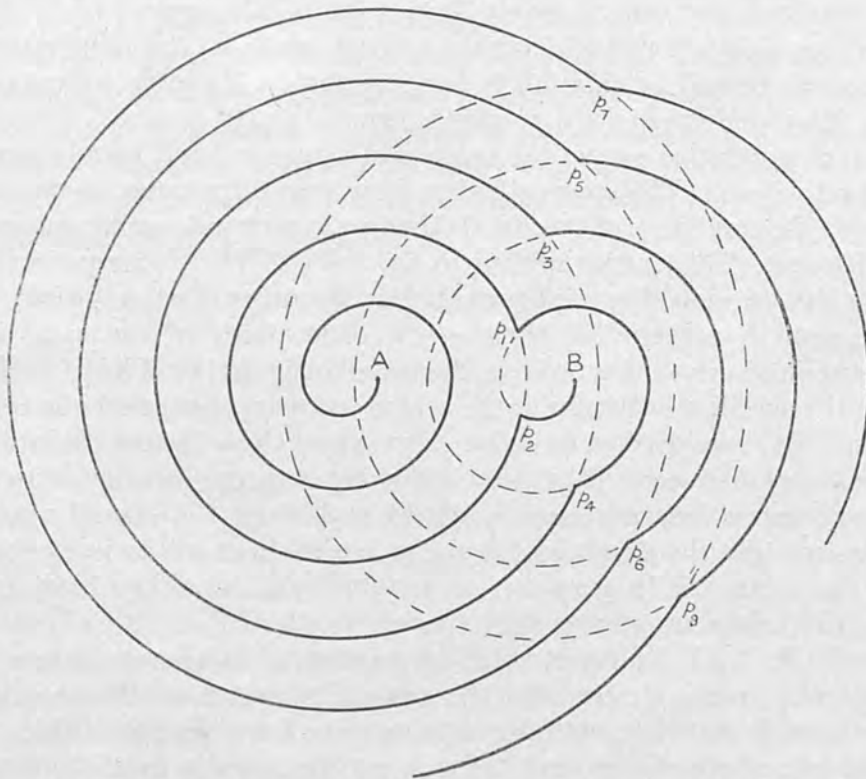
Fig. 8 (Pl. XXVI.) illustrates a unique example in which the spiral is doubled with the members strictly " parallel ". It may be that the twin form arises from two close-by dislocations of the same sign, cooperating closely.

In fig. 9 (Pl. XXVII.) is illustrated the case of two screw dislocations of the same sign close to each other. The spirals are circular and developed for two or three turns after which the ledges from other neighbouring dislocations interact with them.

In fig. 10 (Pl. XXVII.) is shown another case of two similar screw dislocations close to each other, so that growth starts from both of them. The spirals are circular at the centre for one or two turns after which they settle down as spirals with straight edges. The meeting of the growth fronts

from the two screw dislocations results in small kinks in the innermost straight edges. As in the case of circular spirals, here also by going round we descend by two steps, and the figure has the appearance of two spirals alternately spaced. However, the step height between successive lines in any particular direction is just one unit.

Fig. 11 (Pl. XXVII) shows the case in which the central screw dislocation has developed several turns before reaching the point where the second small screw dislocation emerges. They quickly accommodate each other and the behaviour is similar to the previous cases. The central screw dislocation is dominant and would determine the rate of crystal growth of the face. Near the edge of the figure it is seen that some more screw dislocations emerge on the crystal face, and are situated in the same direction from the central screw dislocation as the second one. These new screw dislocations yield within a short while to the domination of the central one and quickly fall in line, passing on the growth fronts with slight delay and in slightly modified form.

Now consider two screw dislocations of opposite hand terminating on the crystal face. The ledge starting from one terminates on the other, and with the unfolding of the spirals the two arms join together generating closed loops. This is exemplified in fig. 3 (Pl. XXV.), where one of the spirals has developed several turns before the other starts growing.

The growth pattern for three screw dislocations of the same hand observed on a crystal of type II. is illustrated in fig. 12 (Pl. XXVII). Here, again, the spirals are circular at the centre and soon change into hexagonal spirals. It can easily be seen that, for three screw dislocations cooperating with each other, by following any one of the edges, the resultant curve descends three units in each turn. It should again be emphasized that the step height in the successive lines will be just one unit.

At the centre the ledges are closely spaced and, once they have settled down, the ledges are more widely spaced.

Fig. 2 (Pl. XXV.) illustrates the interaction of five screw dislocations. The growth fronts emitted by the screw dislocation at the top of the figure meet, first, the growth fronts advancing from the screw dislocation on the left of the figure and then, later, the growth fronts advancing from the bottom screw dislocation. Annihilation occurs over portions of the resultant growth fronts which assume characteristic shapes composed of arcs of circles with these dislocation points as centre. Near the centre of the figure, due to the interaction of different growth fronts a crowding occurs. Here the compound growth fronts are not arcs of circles with the different dislocation points as centres, but instead there is a gradual change in curvature.

§7. HEXAGONAL INTERLACED SPIRAL.

These features observed on a crystal face of carborundum type II. are shown in figs. 13 and 15 (Pl. XXVIII). In each of these hexagonal spirals the edges fork out at the corners and meet the two neighbouring edges.

This interlacing gives the hexagonal spiral the " spider web " structure shown clearly in fig. 13 which shows the interlinking of four such spirals.

A double interlaced spiral is shown in fig. 14 (Pl. XXVIII.) in which the edges do not meet each other. The lines are broad with inner edges sharp and the outer diffuse.

An explanation of this interlacing has been given by Frank (1951).

§8. Measurement of Step Height.

The step height has been measured by the use of multiple-beam interference fringes using both Fizeau fringes of equal thickness and the fringes of equal chromatic order (Tolansky 1948).

A rounded spiral, effectively a spiral conical hill, may be considered as a circular conical hill made of a series of concentric steps with a constant spacing d and step height h. It can be shown that if a Fizeau fringe passing over the peak of such a hill appears to bend through an angle 2θ, and if X is the dispersion, *i. e.* the distance between successive fringes, then the step height h is given by

$$h = d\lambda \sin \theta / 2\mathrm{X}.$$

By measuring X, θ and d, h can be evaluated. Fig. 5 (Pl. XXVI.) shows the Fizeau fringes passing over the spiral of fig. 4 ($\lambda 5461$).

For examination with fringes of equal chromatic order, the image of the peak of the hill is projected on to the spectrograph slit. This was arranged to prodce a system of fringes of equal chromatic order parallel to the spectrum line in one half of the field and sloping towards the red in the other (fig. 6, Pl. XXVI).

Since the step height is obtained from the mean of all those contributing to form the peak, irregularities of the optical flat and the lack in faithfulness of silver contouring are averaged out.

In one case another determination of the step height has been possible. In fig. 4 (Pl. XXVI) starting from the centre of the spiral we can reach any point A on the line of discontinuity, either by going round the " fish-like " obstruction in a clockwise or an anti-clockwise direction. In the former, we encounter, say, N_1 steps. Therefore the point A is N_1 steps lower with respect to the centre of the spiral. In the latter case we go down, say, N_2 steps from the peak of the hill in order to arrive at A. Thus at A the difference in level on the two sides of the line of discontinuity is that corresponding to $(N_2 - N_1)$ step heights. This difference is quite large (over 50) and is therefore capable of being measured accurately and easily either by Fizeau or fringes of equal chromatic order. Knowing this, the step height has been evaluated, but is subject to uncertainty due to the possible presence of hidden dislocations in the obstacle and discontinuity surfaces.

§ 9. Result of Measurement of Step Height.

It is seen below that the step height measured in the cases so far is equal to just one unit cell.

Fizeau fringes	Fringes of equal chromatic order	Method by counting No. of steps	Crystals
15·2 Å 14·1 Å	17·1 Å	14·8 Å	Spiral in fig. 4, Type II.
14·5 Å 15·5 Å 15·0 Å 15·3 Å			Circular spiral, right of fig. 2.

§10. Discussion of Results.

From fig .2 (Pl. XXV), which is at magnification $\times$ 90, the spacing between the successive arms of the circular spiral when it is nearly constant is approximately 2·5 mm. Using $\delta r = 4\pi \rho_c$ we have

$$\rho_c = \frac{2\cdot5}{90 \times 4\pi} \text{ mm.} \approx 2\mu.$$

From $\rho_c = a\phi/2k\text{T} \ln \alpha$ and using Trouton's rule to estimate $\phi/k\text{T}$ according to which $\phi/k\text{T} = 3\cdot5\text{T}b/\text{T} = 6$ at an absolute temperature of 0·6 of the boiling point of the material we get

$$\alpha \approx 0\cdot2 \text{ per cent.}$$

§11. Density of Dislocations.

The density of dislocations varies widely on different specimens of carborundum. In fig. 4 (Pl. XXVI.) there is only one which dominates the growth of the face. In figs. 1, 2, 3, 11 and 12 (Pls. XXV., XXVII.) there are several. The largest density of dislocations observed is shown in fig. 16 (Pl. XXVIII). Here there are nearly 10^4 screw dislocations per square centimetre.

Another noteworthy point is that in fig. 16 (Pl. XXVIII.) there are nearly twenty screw dislocations, most of which are of the right-handed type. It is characteristic that in any one region there is a large predominance either of right-handed or of left-handed screw dislocations.

§12. Summary.

Numerous growth spirals starting from points of emergence of screw dislocations have been photographed on the surfaces of carborundum crystals. These spirals have characteristic shapes. The shape is discussed in relation to the crystal structure. The behaviour and properties of

VERMA

Phil. Mag. Ser. 7, Vol. 42, Pl. XXV.

Fig. 2.

Fig. 1.

×72

×72

Fig. 3.

×200

VERMA

Phil. Mag. Ser. 7. Vol. 42, Pl. XXVI.

Fig. 4.

Fig. 5.

×72

Fig. 6.

Fig. 7.

Fig. 8

×72

×120

VERMA

Phil. Mag. Ser. 7, Vol. 42, Pl. XXVII.
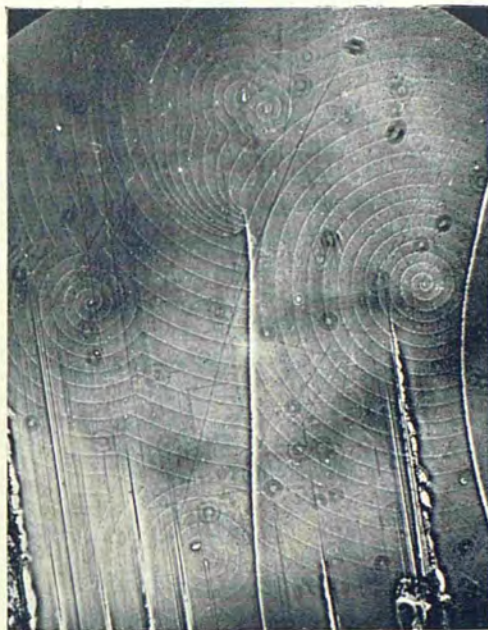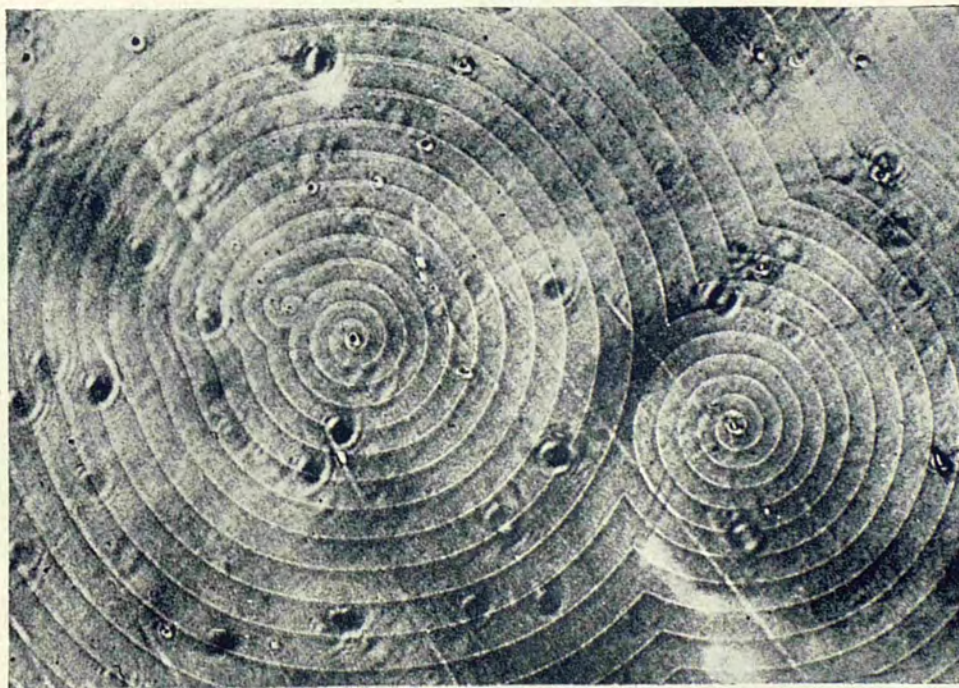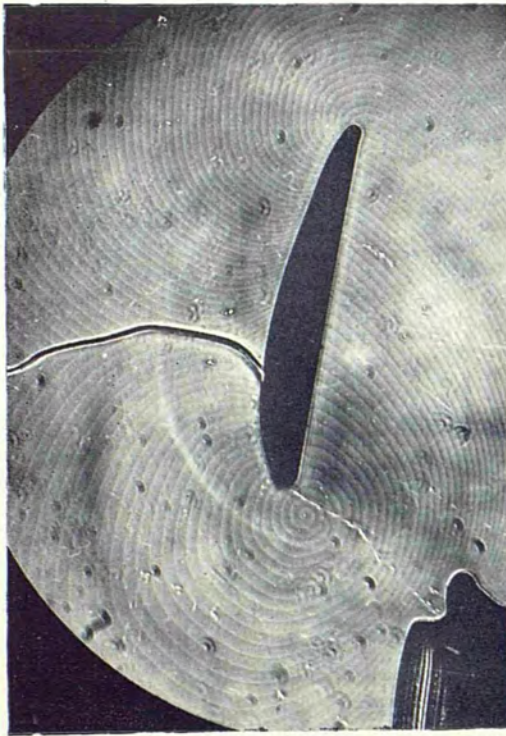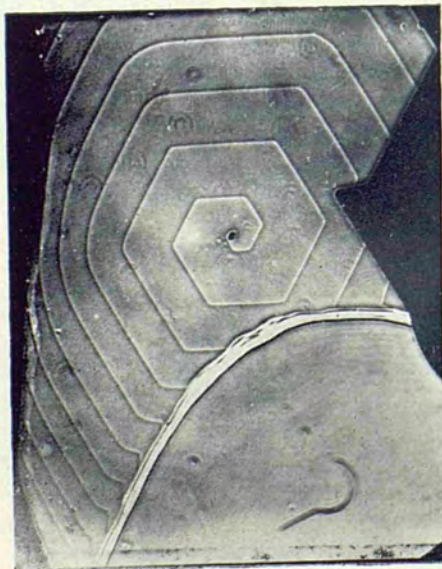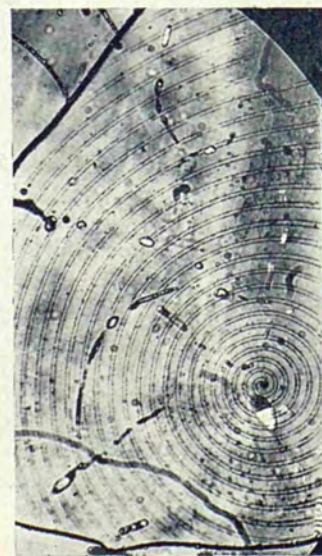
Fig. 9.

×112

Fig. 10.

×72

Fig. 11.

×72

Fig. 12.

×280

VERMA

Phil. Mag. Ser. 7, Vol. 42, Pl. XXVIII.

Fig. 13.

Fig. 14.

×72

×120
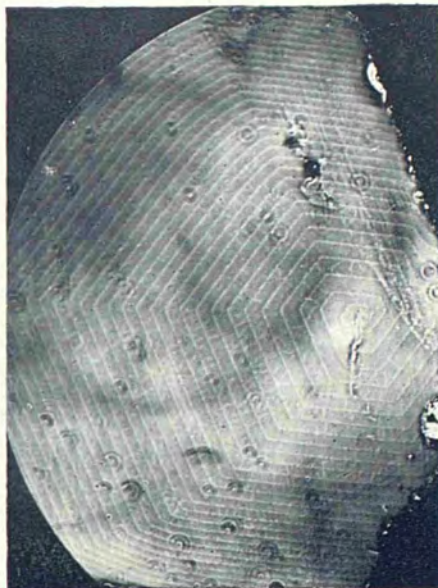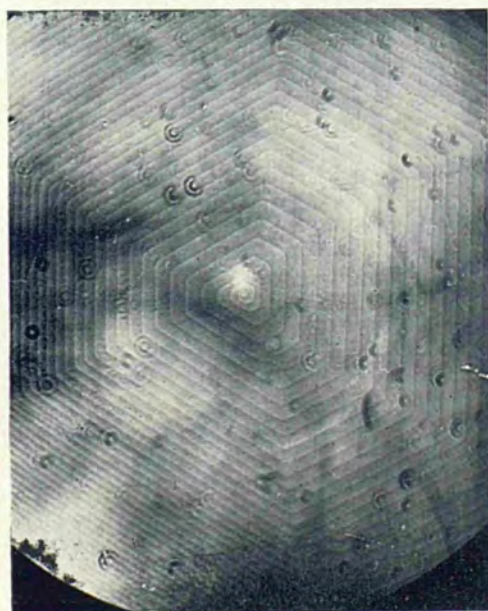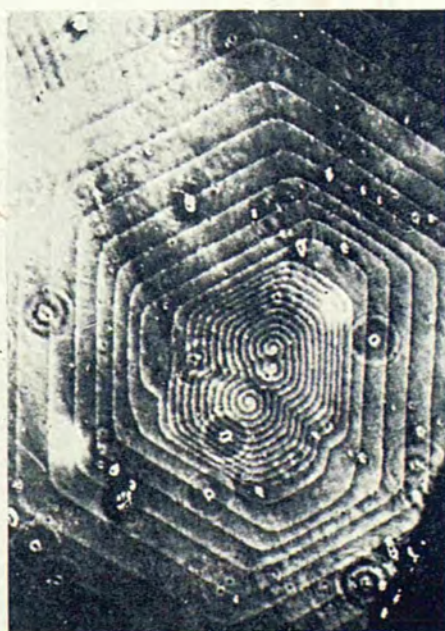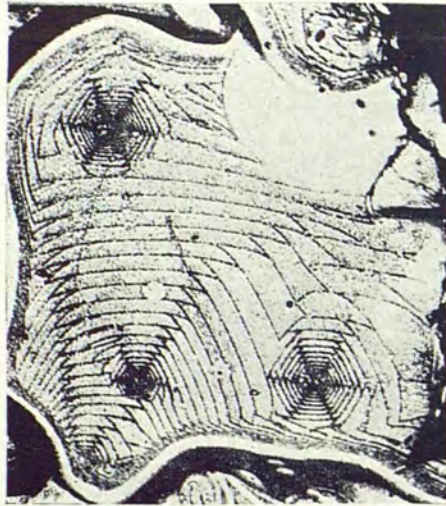
Fig. 15.
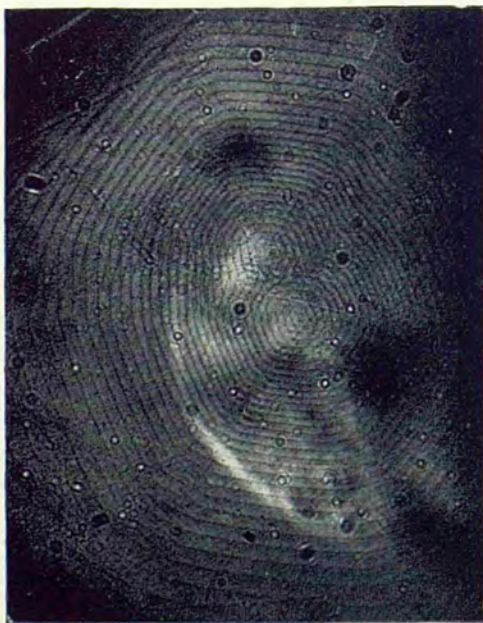
Fig. 16.

×960 nearly

×132

growth fronts and the growth patterns for two and more screw dislocations are illustrated. From the observations on the photographs it is shown that the type of information that can be derived is the determination of the radius of the critical nucleus, the supersaturation and density of dislocations.

The step height has been measured accurately by multiple-beam interference fringes. The step height at the edges of these growth spirals is found to be one unit cell.

References.

Burton, W. K., Cabrera, N., and Frank, F. C., 1949, *Nature, Lond.*, **163** 398 ; 1951, *Phil. Trans. Roy. Soc.* (in press).
Frank, F. C., 1949, *Discussions of the Faraday Society*, **5**, " Crystal Growth " ; 1951, this journal, page
Griffin, L. J., 1950, *Phil. Mag.*, **41**, 196.
Ramsdell, L. S., 1947, *Amer. Min.*, **32**, 64.
Thibault, N. W., 1944, *Amer. Min.*, **29**, 249.
Tolansky, S., 1948, *Multiple-beam Interferometry of Surfaces and Film* (Oxford : University Press).

Vol II

CONTENTS

OPTICAL AND INTERFEROMETRIC ARRANGEMENT.

TECHNIQUES AND SOME APPLICATIONS

EMEMENTARY SPIRALS AND THEIR INTERACTION

TWO SCREW DISLOCATIONS OF OPPOSITE SIGN

GEOMETRICAL GROWTH PATTERNS

SPIRALS ORIGINATING FROM DISLOCATIONS OF

MULTIPLE STRENGTH AND MULTIPLE DISLOCATIONS

INTERFEROMETRIC STUDIES

Schematic Description of a Crystal Surface.

Fig 1.   Crystal Surface at low temperatures.

Fig 1a.   Surface at low

temperatures.

Fig 3.   Surface with

an island.

Fig 2.   Surface at higher temperatures.

Fig 4. An edge dis-
location.
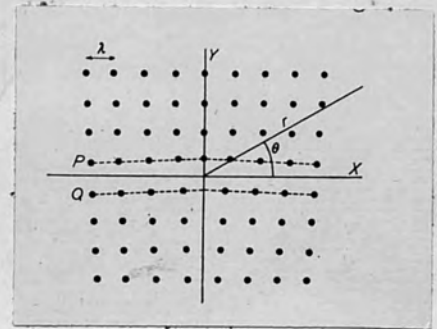
Fig 5. The structure of
an edge dislocation.
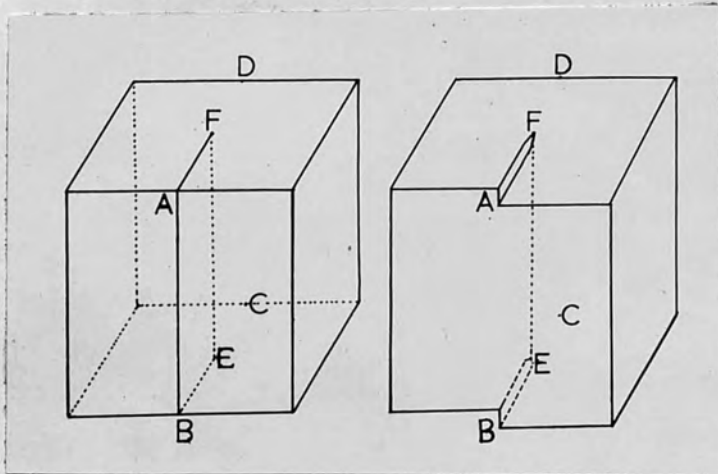
Fig 6.   Fig 7.

Illustrating the formation of a
screw dislocation.
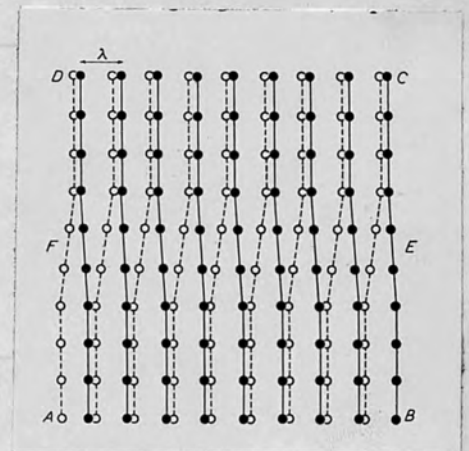
Fig 9.

The structure of a
screw dislocation.
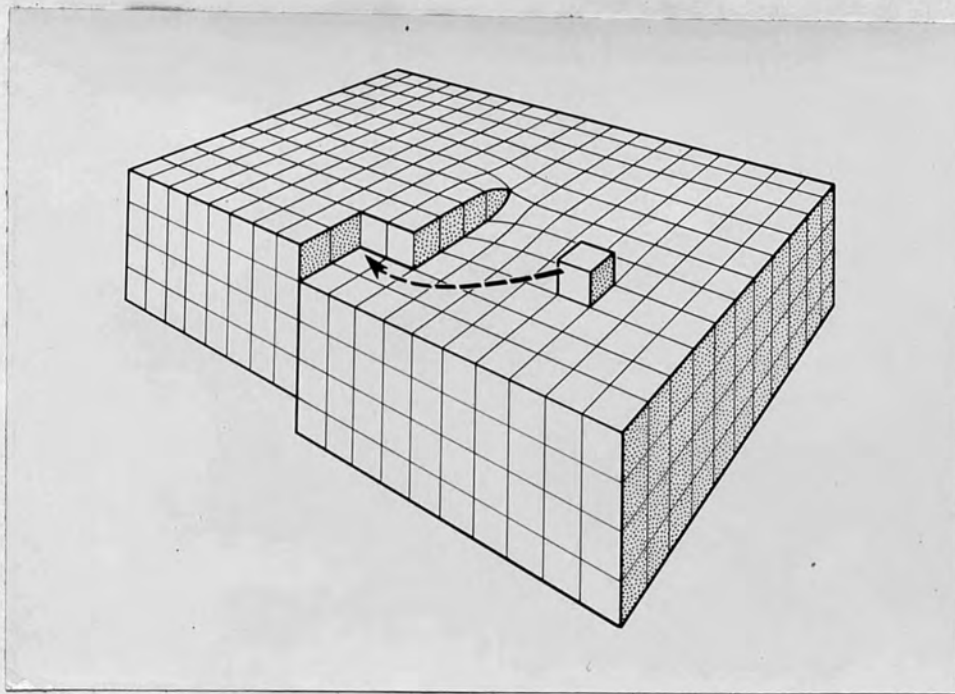
Fig 8. End of a screw dislocation.
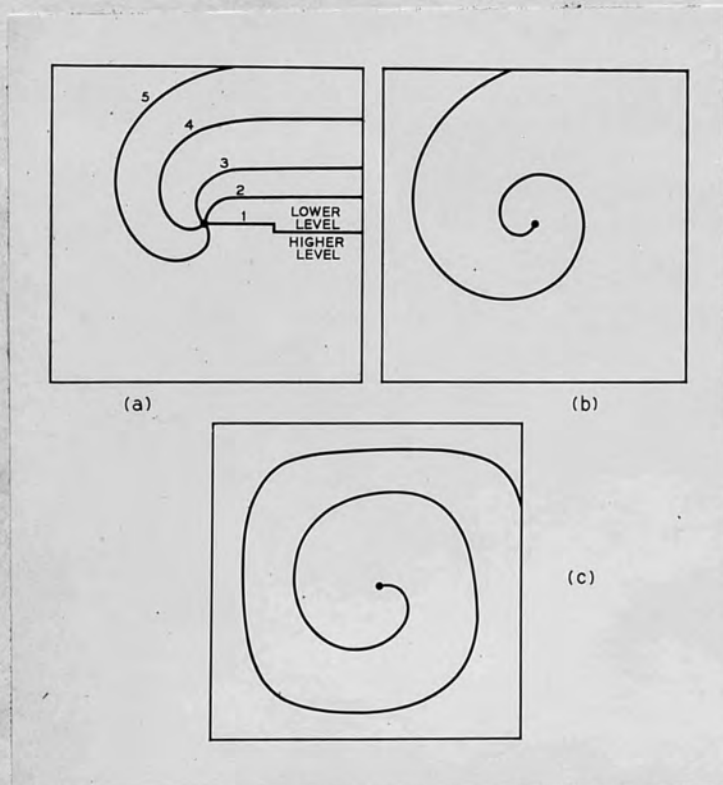
Fig 10. Development of a growth spiral.
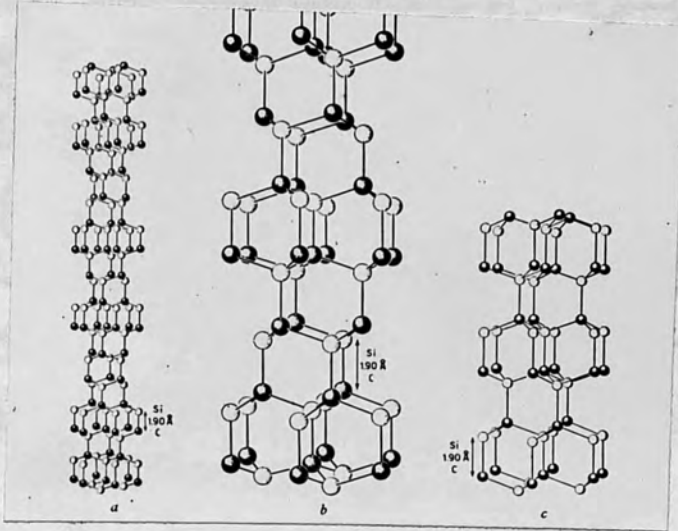
Fig 11. Lattice of silicon-carbide

(a) modification 15 R. (b) modification 6 H. (c) modification
4 H.
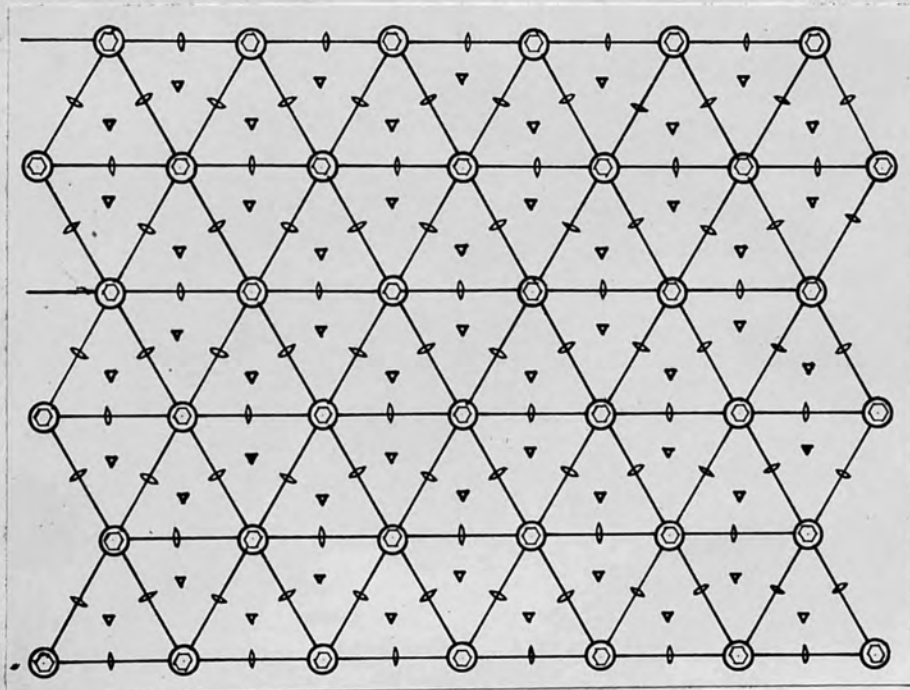
Fig 12a. Symmetry elements in the projection

on (0001) plane.
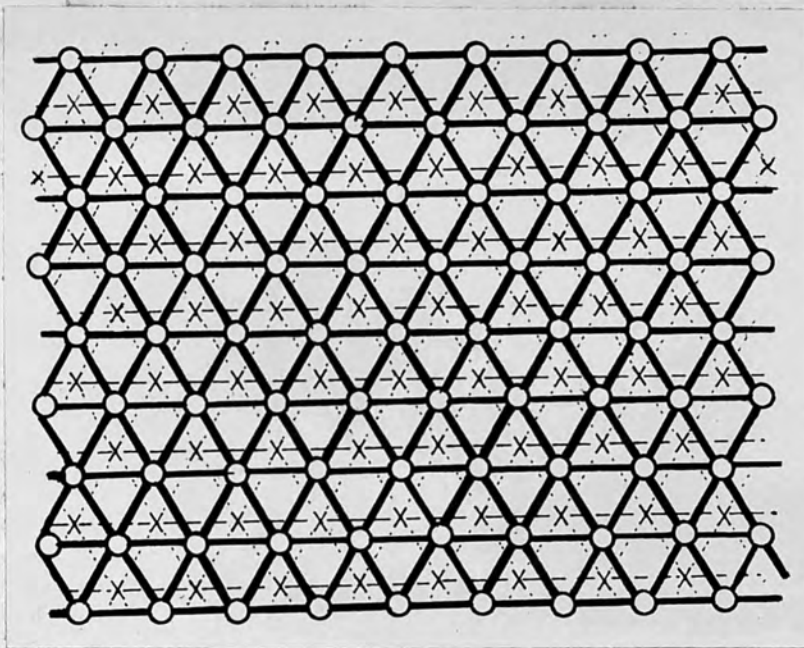
Fig 12b.   Projection on (0001) plane.

A layer marked by o

B layer marked by x
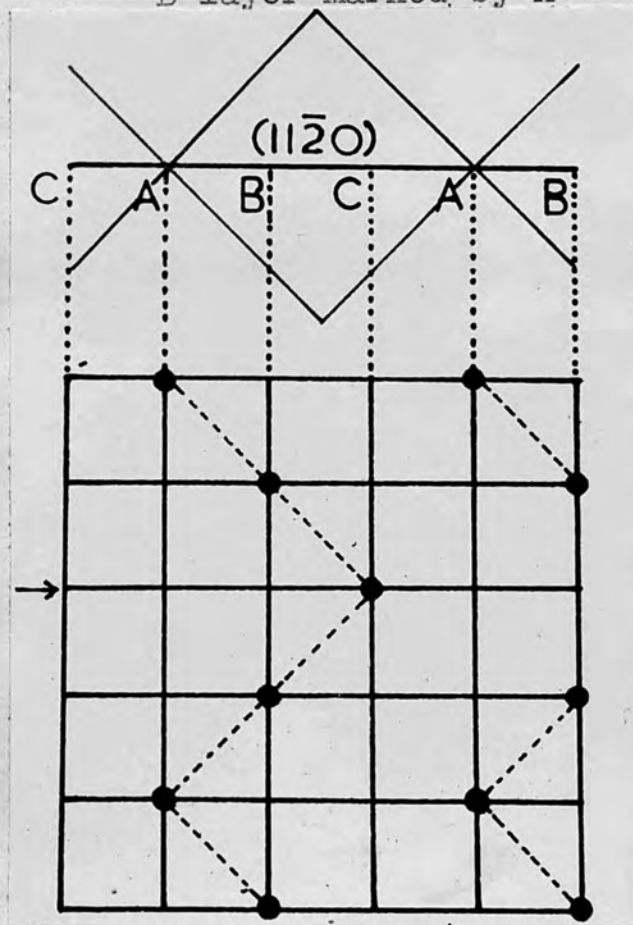
Fig 13.   (11$\bar{2}$0) section showing zig-zag

arrangement.
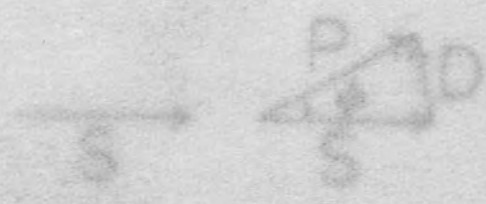
OPTICAL AND INTERFEROMETRIC ARRANGEMENT:

TECHNIQUES AND SOME APPLICATIONS

Fig 14a. Diagram of
light path through a
phase-contrast micro-
scope.
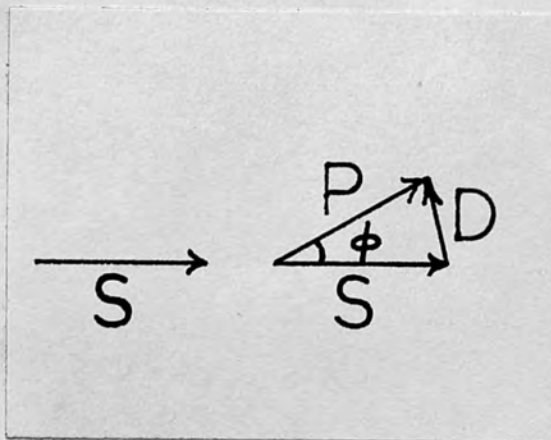
Fig 14b.

Light vectors.

S - Undeviated wave through
the surrounding medium

P - through the particle

D - deviated wave

Plan view of the condenser
diaphragm.

Plan view of phase plate
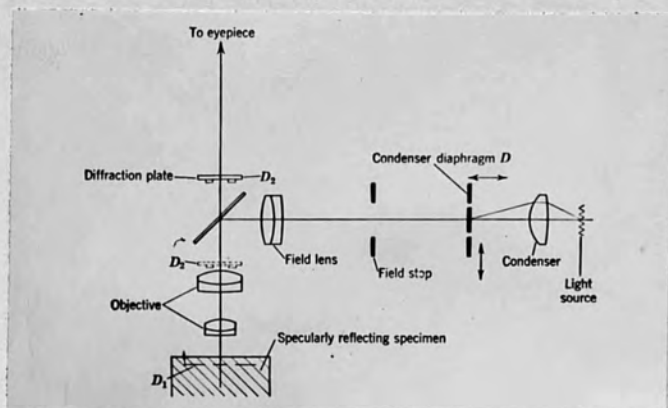
Fig 14c. Optical system of the phase-contrast

vertical-illumination microscope.
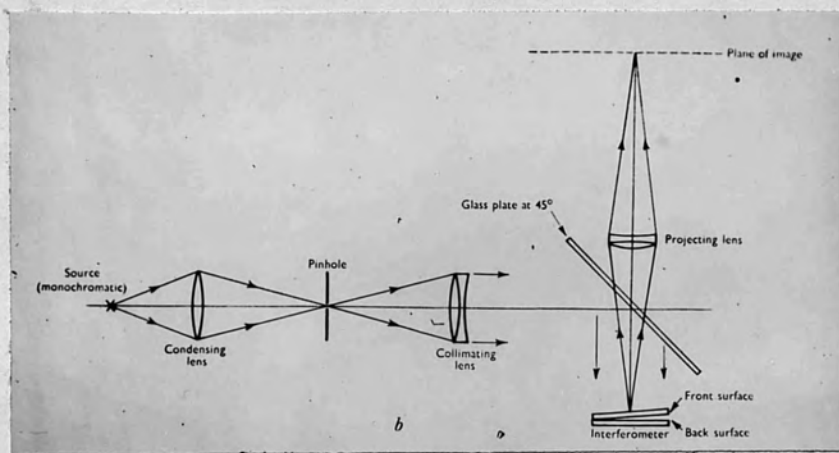
Fig 15. Optical arrangement for Fizeau
fringes in the reflected system.
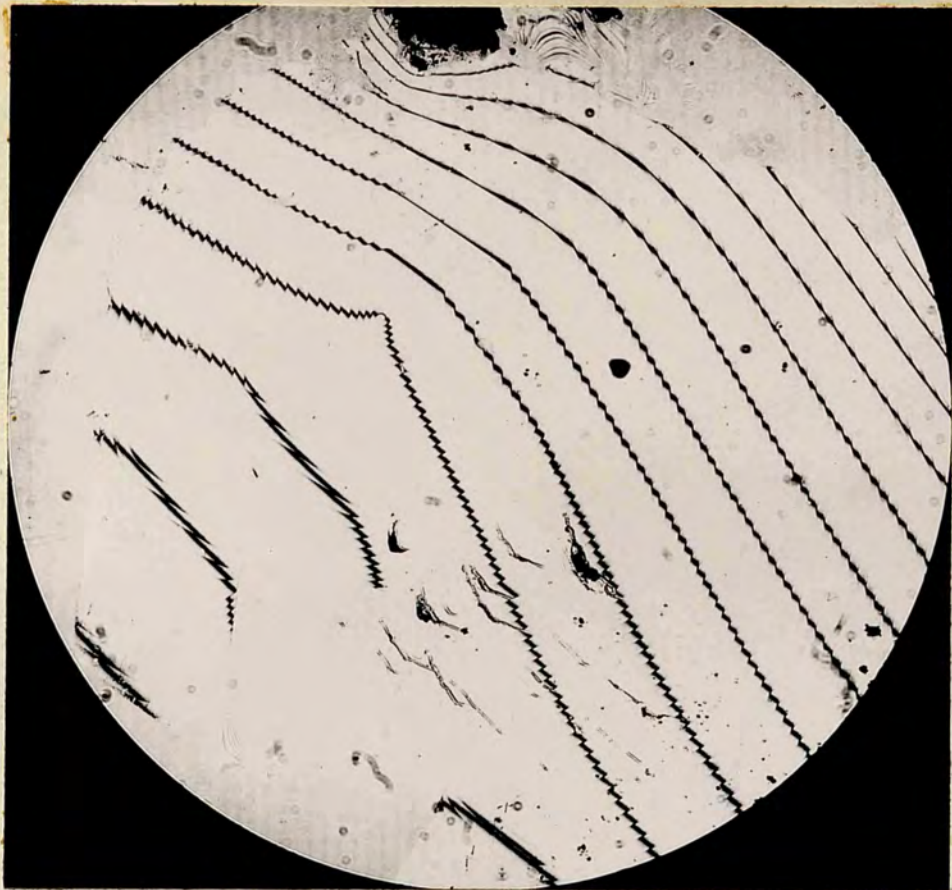
Fig 16a.
Showing shift
of Fizeau
fringes pass-
ing over the
spiral steps
of fig 16b.

X45

Fig 16b.
Hexagonal
spiral with
step height
130 A.

X90

8.

Fig 17a.   Diagrammatic representation of a spiral
conical hill as a circular conical hill and
a Fizéau fringe passing over the peak.

Fig 17b.   Fizeau fringe passing over a hill composed
of a series of parallel steps.
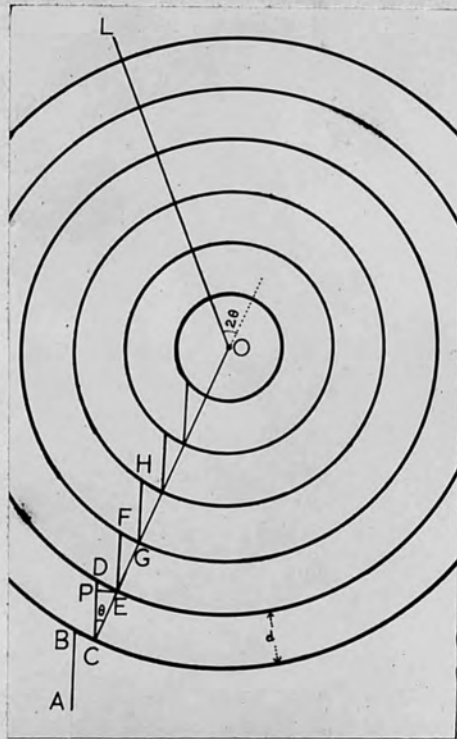
Fig 18a. showing
Fizeau fringes
passing over the
spiral of fig 18b.

X45

A
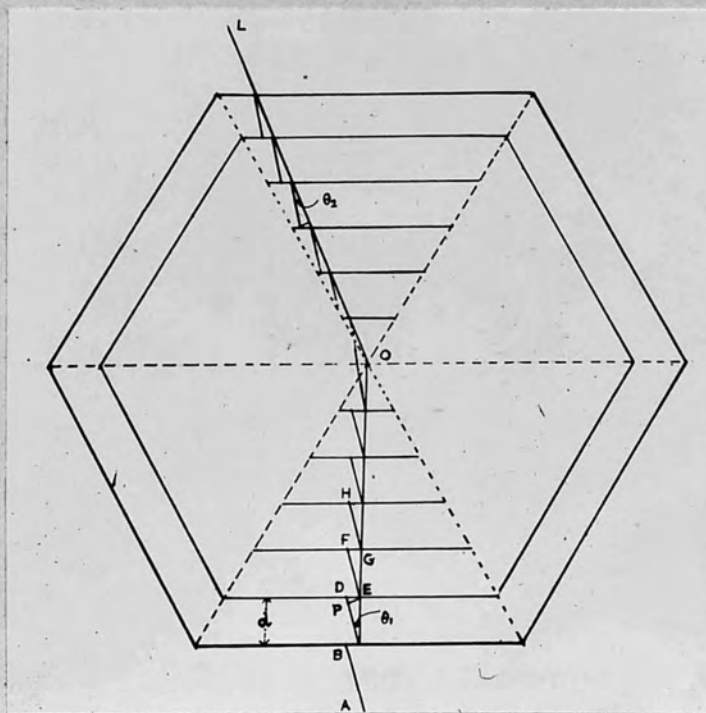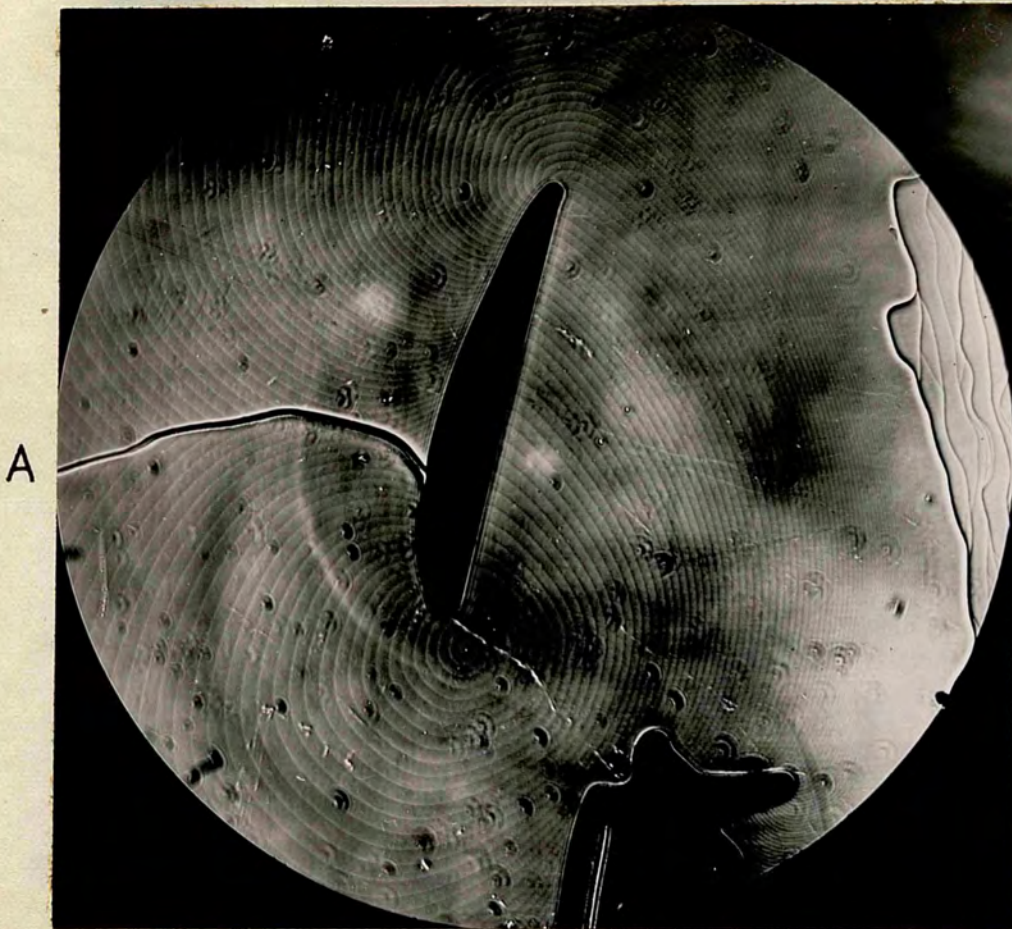
Fig 18b.
A spiral
with rounded
edges.

X90.

10.

X25
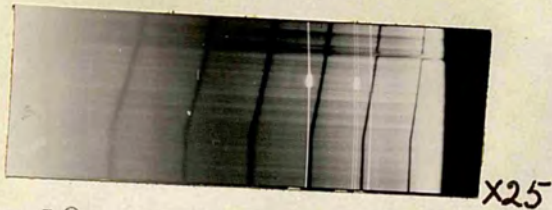
Fig 18c. Fringes of equal

chromatic order

corresponding to

fig 18a.

X45
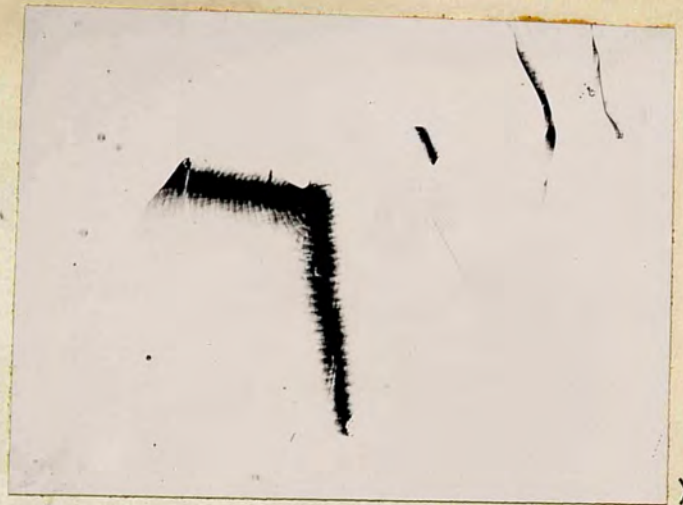
Fig 18e. Fizeau fringes under

high dispersion revealing topo-

graphical features due to

diffraction at the edges.

X90 .
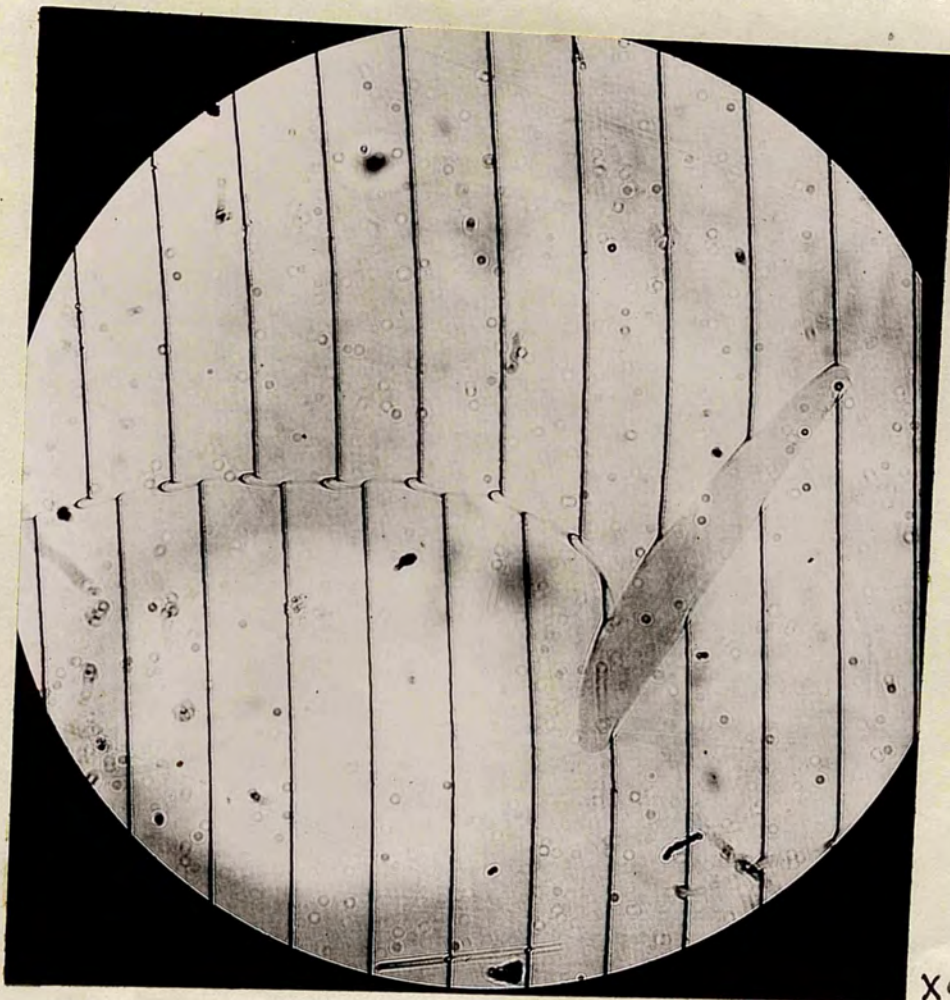
Fig 18d.   Fizeau fringes showing the difference in
crystal level at the point A of fig 18b. on
either side of the line of discontiniuty.
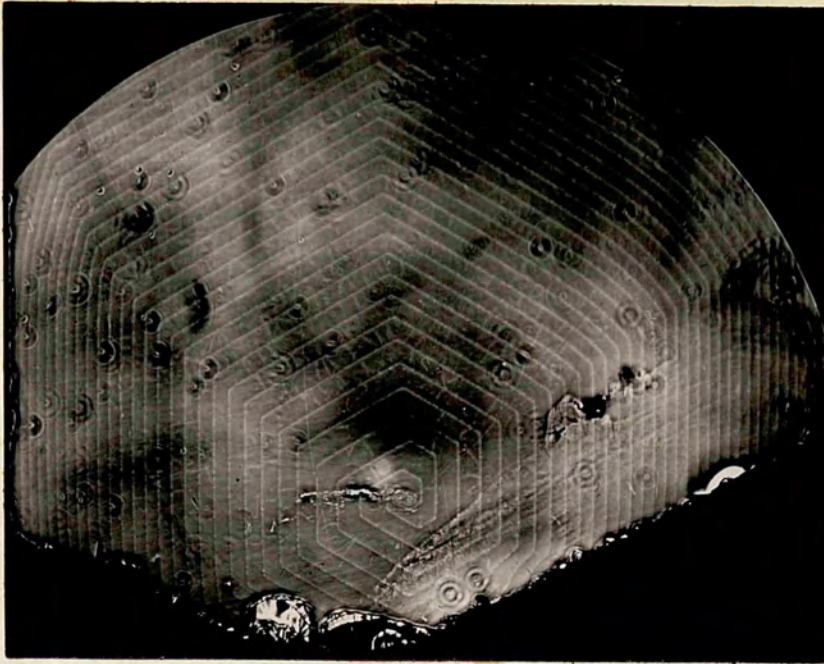
X90

Fig 19a.   A double spiral with straight edges.

(except at the centre).

X90

Fig 19b.   Fizeau fringes passing over the

spiral steps of fig 19a.

12.
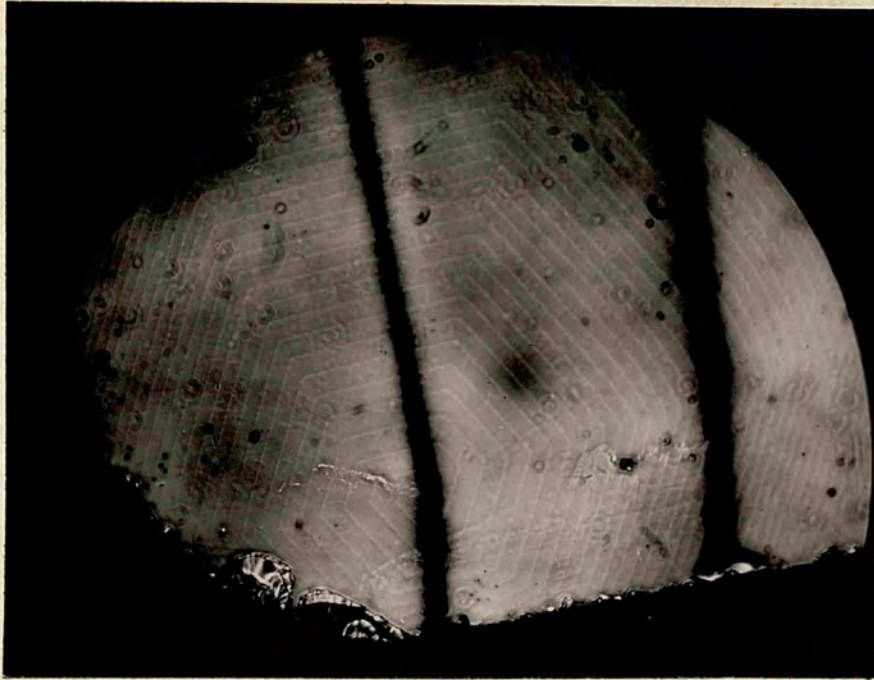
X90

Fig 19c.   Superposition of figs. 19a and 19b.

OPTICAL   FLAT

$\delta t/2$

t

$\delta t/2$
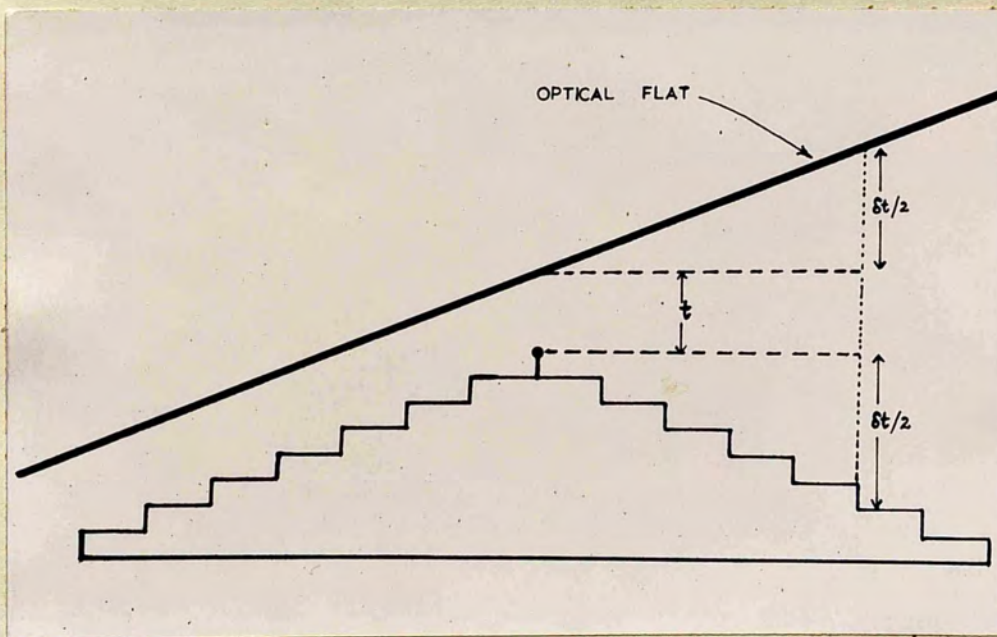
Fig 20. showing increase in the interferometer

gap $\delta t = 2Nh$, N being the number of

steps (each of height h) crossed.

ELEMENTARY SPIRALS

AND

THEIR INTERACTION

Fig 21. Circular spirals.
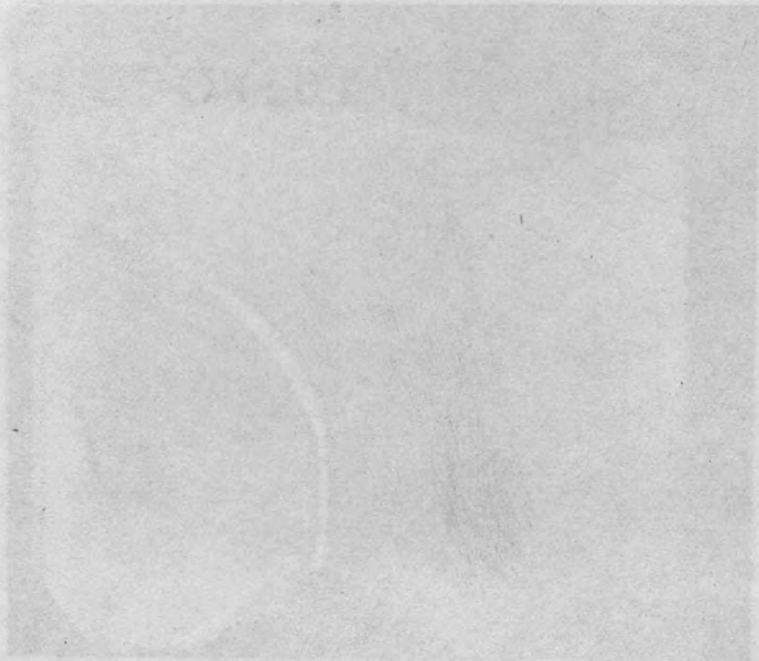
Fig 22. Regular hexagonal spiral.
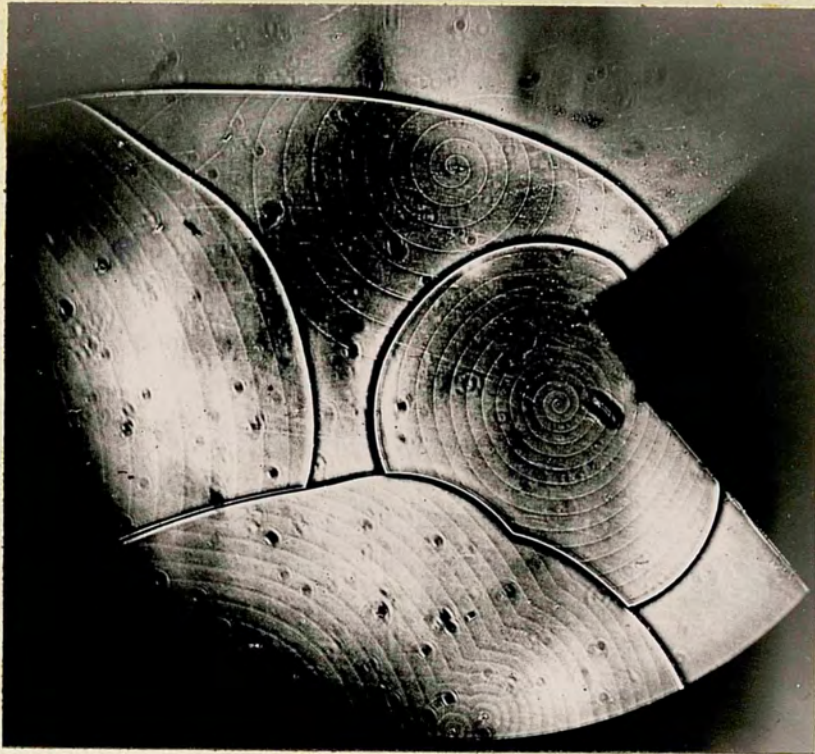
X 90

Fig 21. Circular spirals.
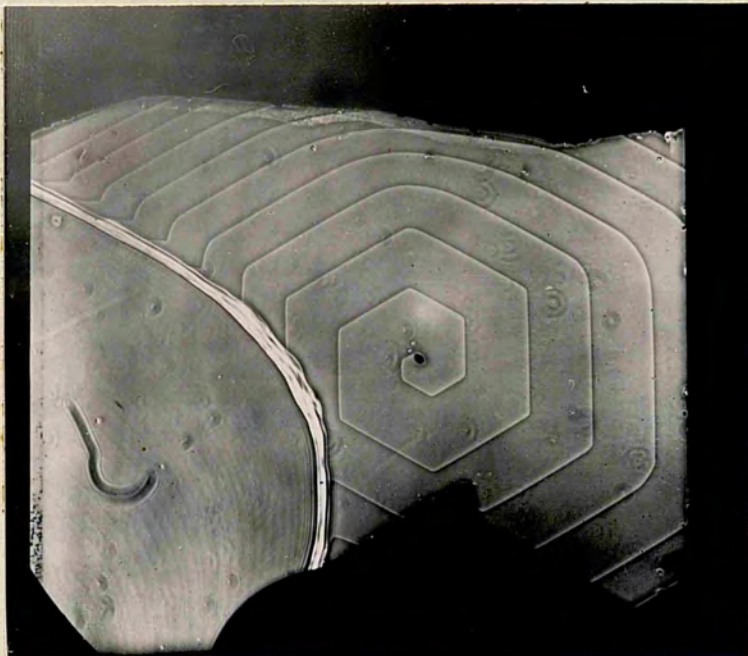
X 90

Fig 22. Regular hexagonal spiral.
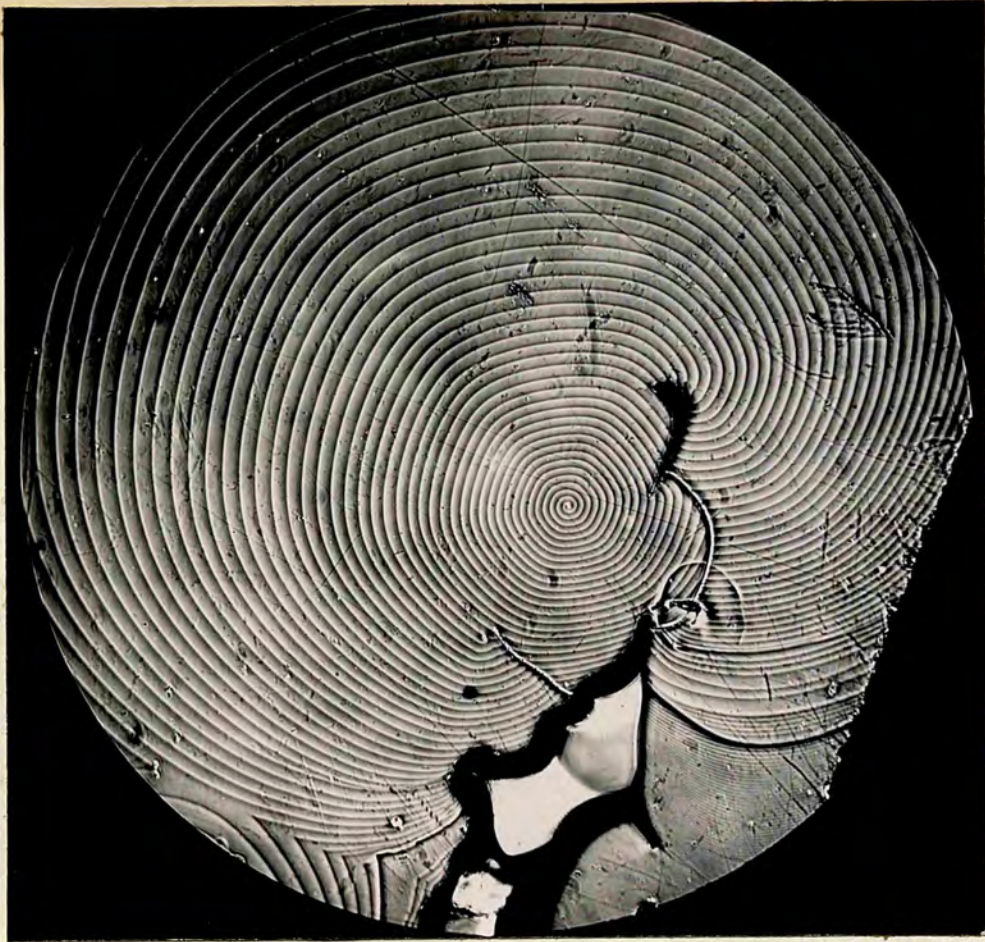
Fig 23.

Spiral with six rounded edges.
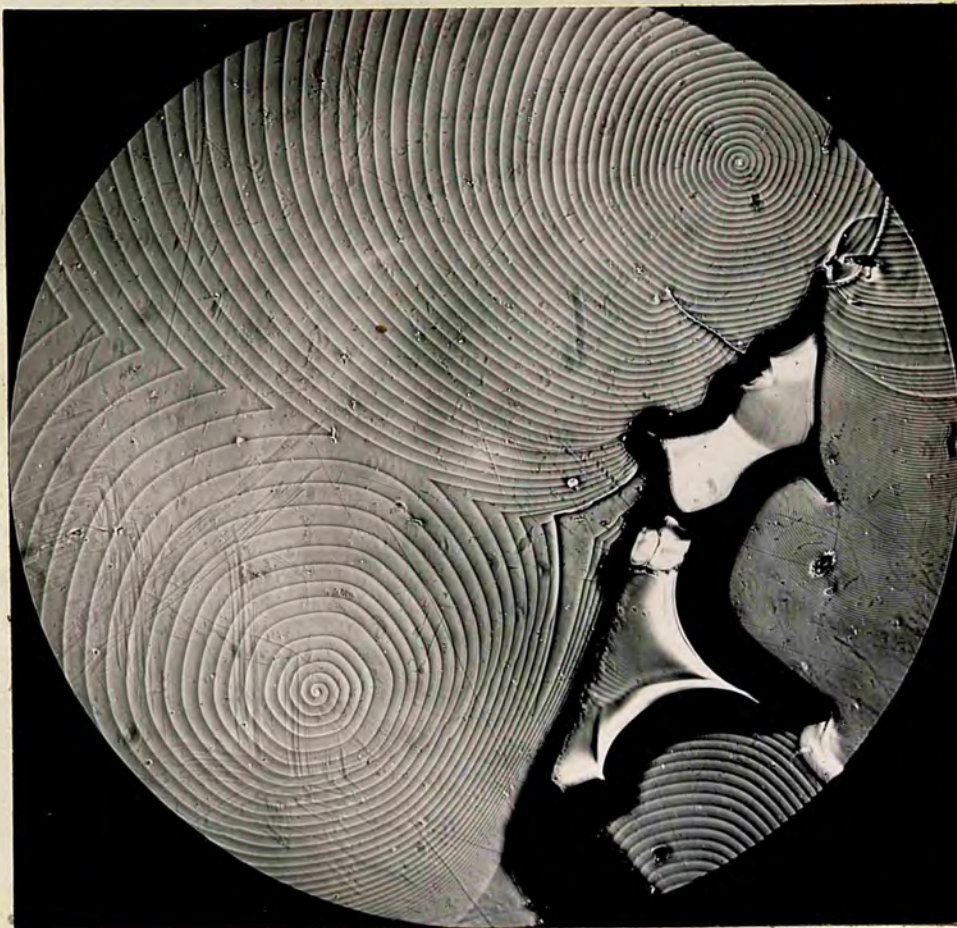
X90

Fig 24.

Two hexagonal spirals with rounded edges.

X90

15.
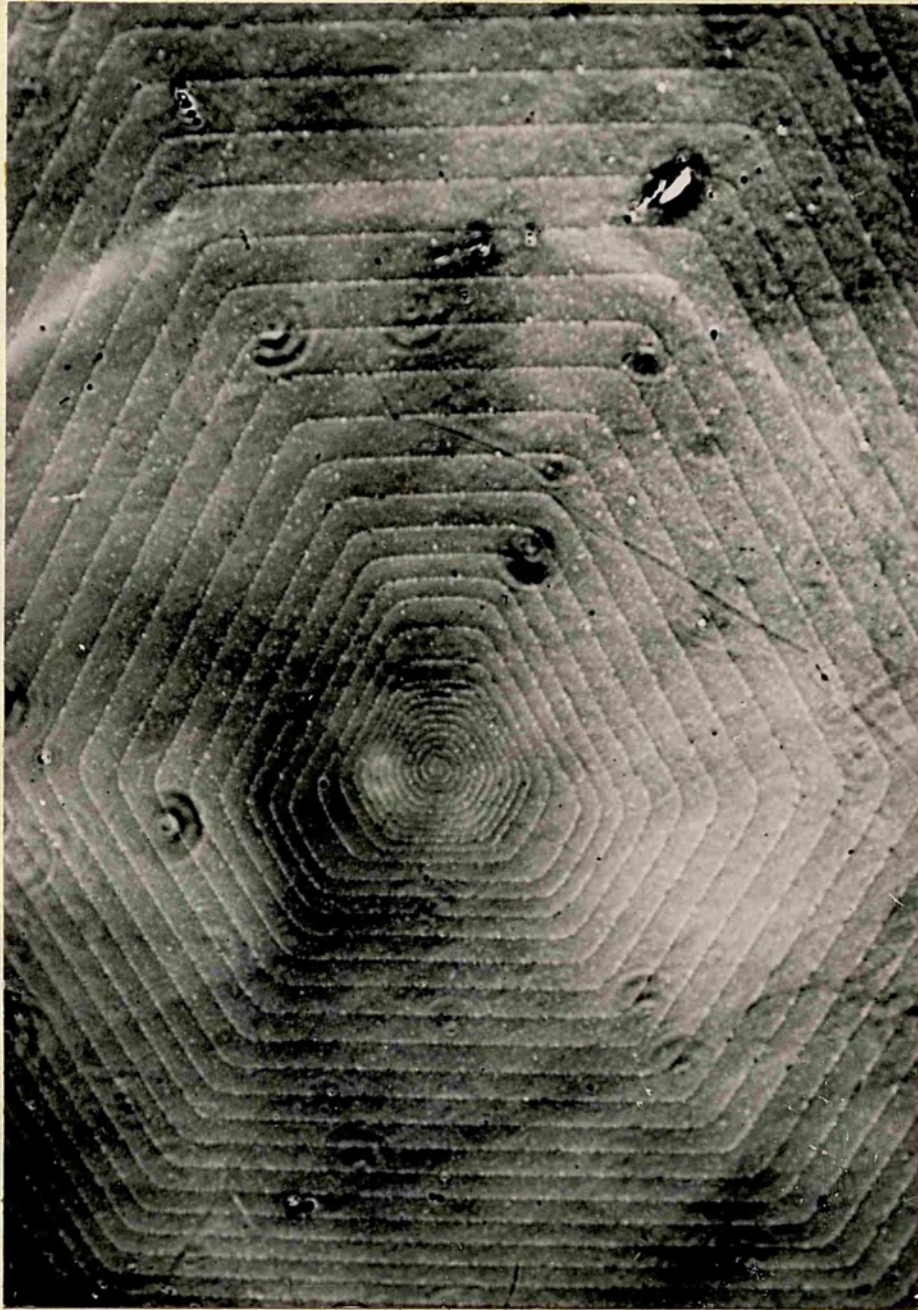
X220

Fig 25. Hexagonal spiral. At the centre
several turns are rounded and closely
spaced.
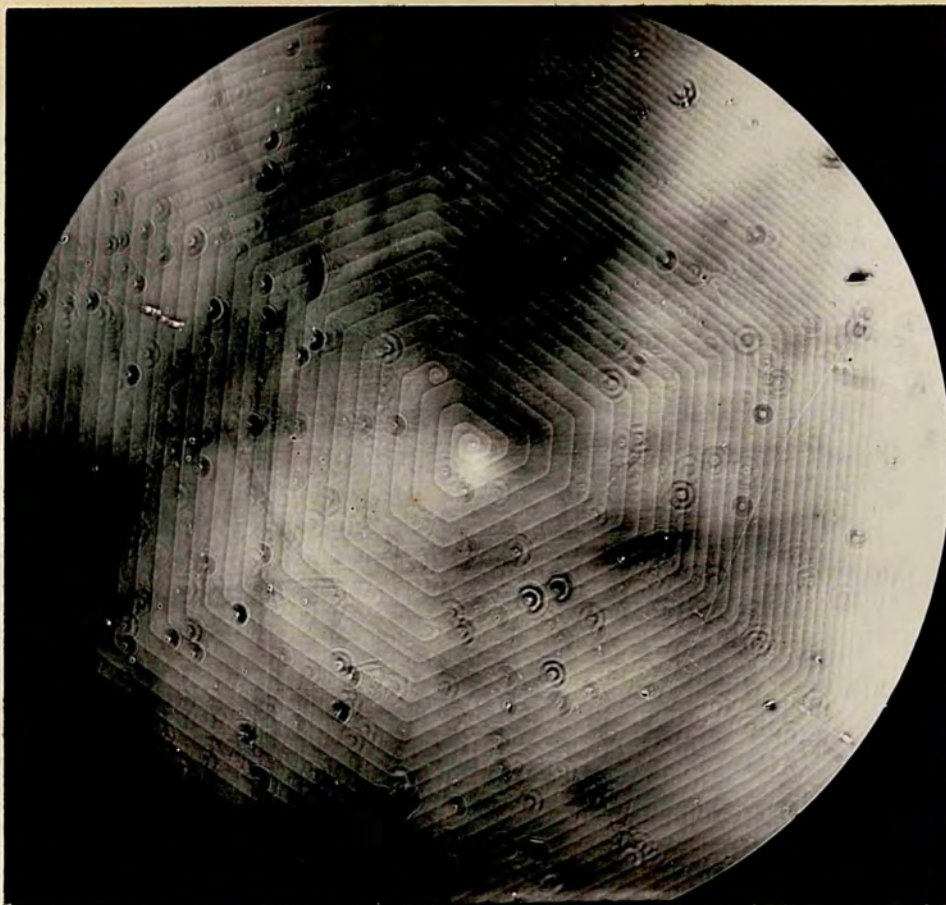
X90

Fig 26. illustrating the phenomenon of "domination"
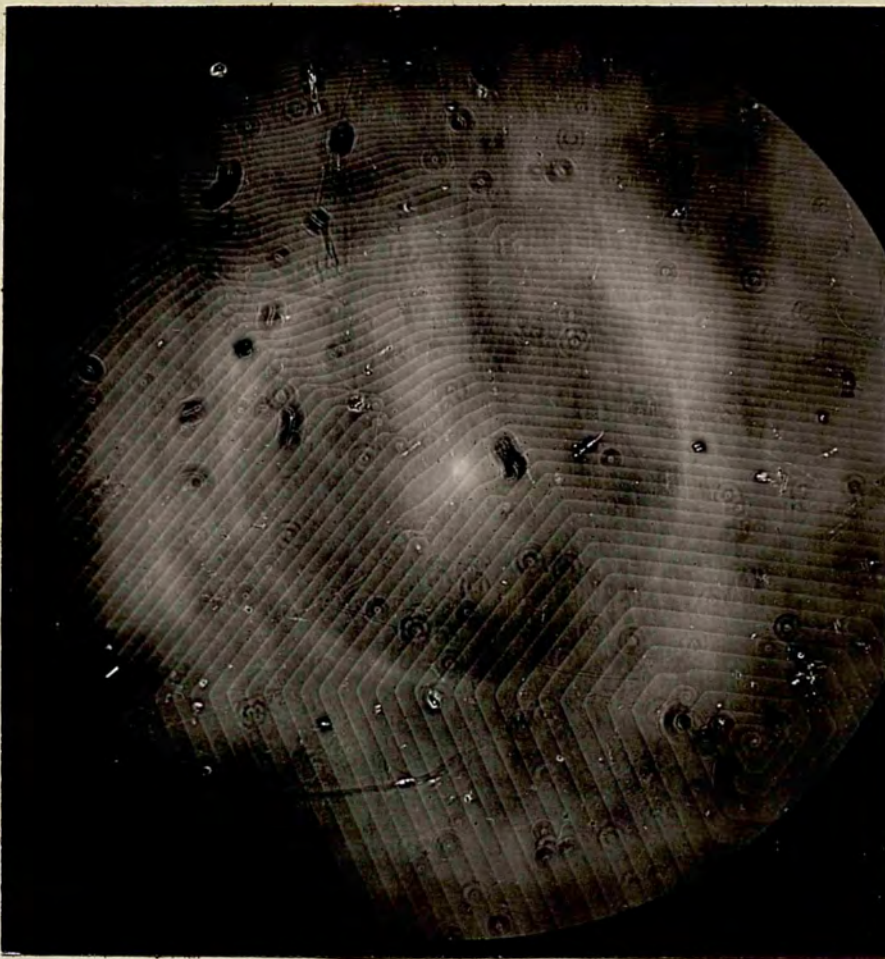
Fig 27.
showing the
upper part
of fig 26.

X90

17.
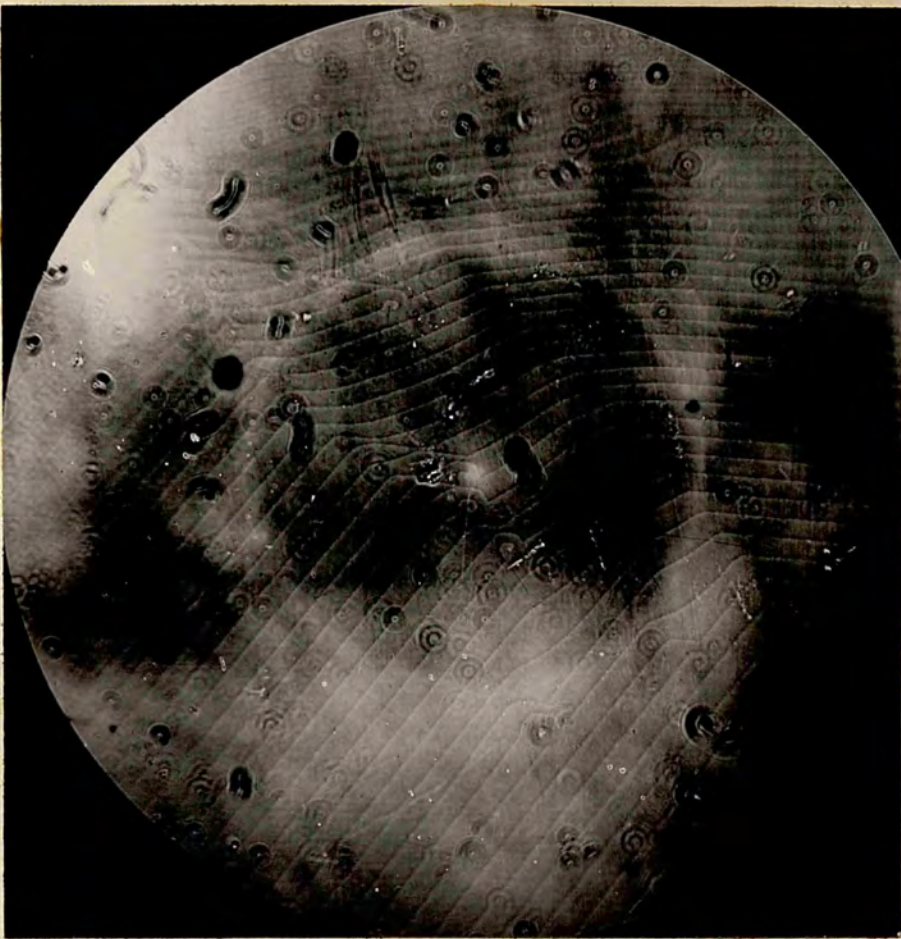
Fig 28.
Enlargement
of part of
fig 27.

X150
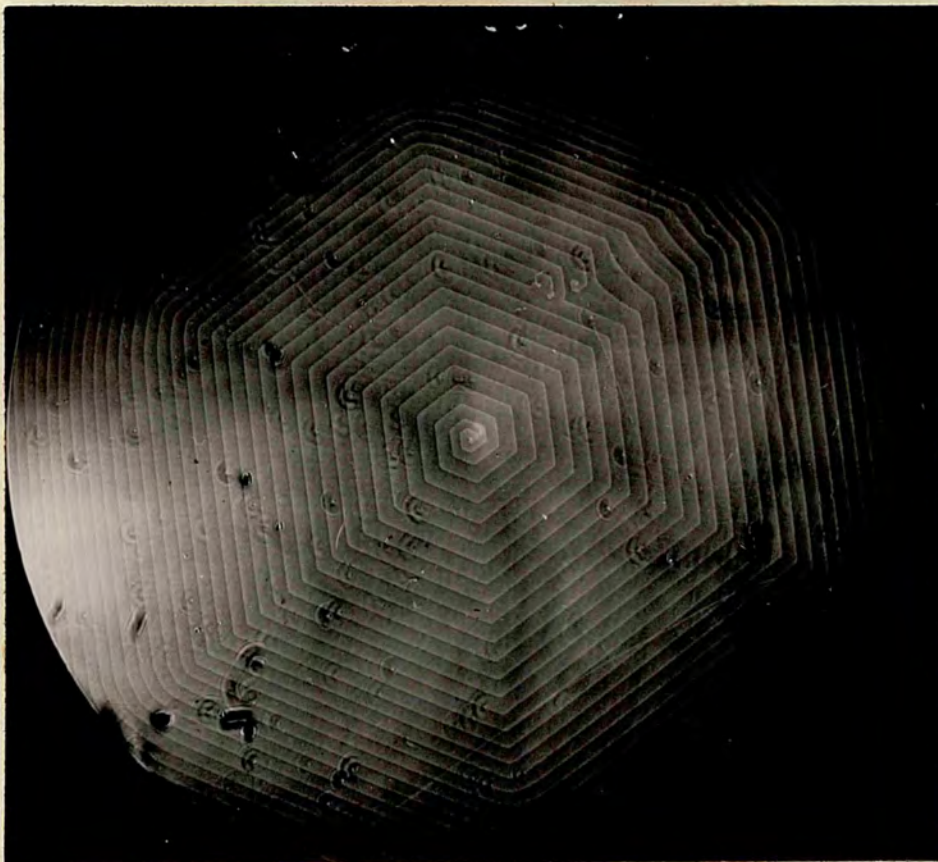
X90

Fig 29. Another example of the phenomena of "domination".

18.

X150

Fig 30.   Two screw dislocations of the same sign at

a distance $< \rho_c$, co-operating with each other.
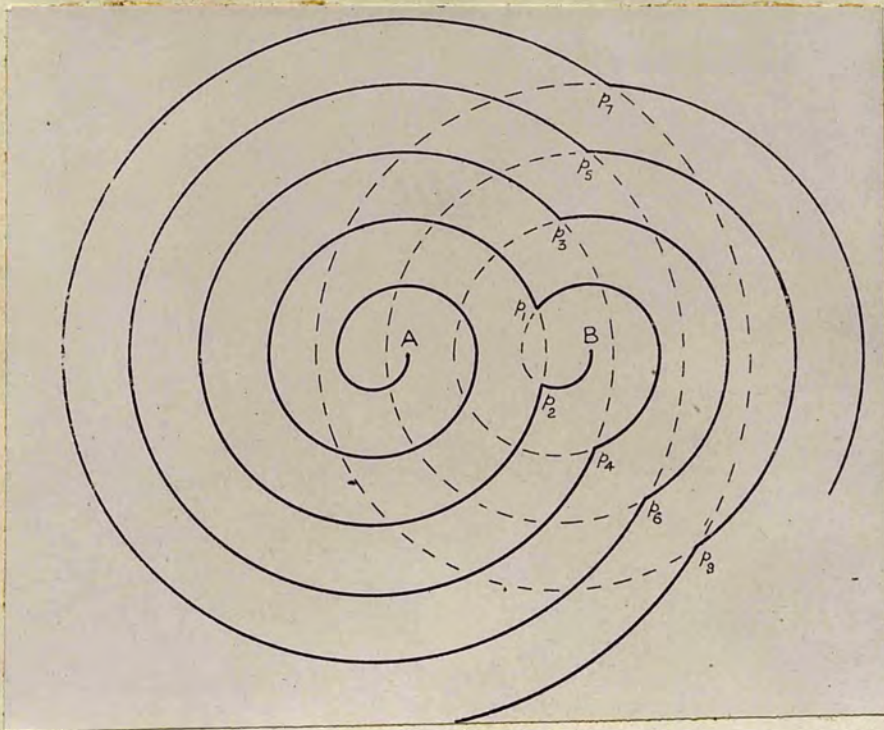
Fig 31.   Schematic representation of the resultant growth
pattern, originating from two dislocations of the
same sign at a distance $> \rho_c$.

X150

Fig 32. Two left-handed dislocations at a distance $> \rho_c$.
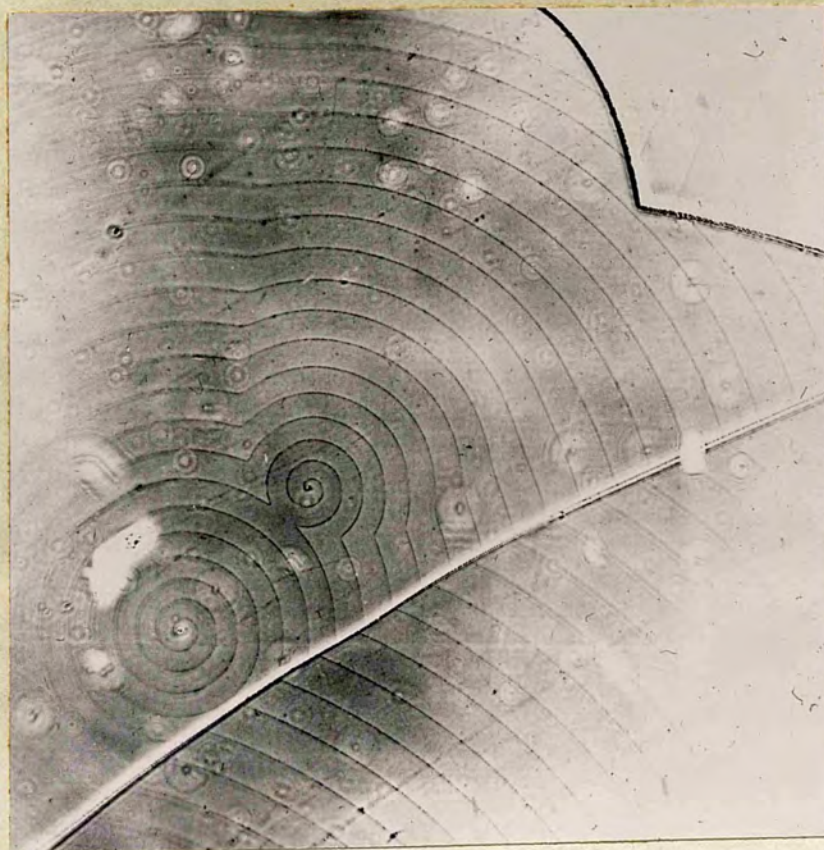
X150

Fig 33. Two right-handed dislocations at a distance $> \rho_c$;
illustrating hyperbolic curve of intersection.

X260

Fig 34. A pair of 'alternately spaced' hexagonal
spirals with the central turns rounded
observed on a crystal of type 15 R.

X250

Fig 35. Circular growth spirals; left half illustrating
        the formation of closed loops (nearly circular)
        due to two dislocations of opposite sign.
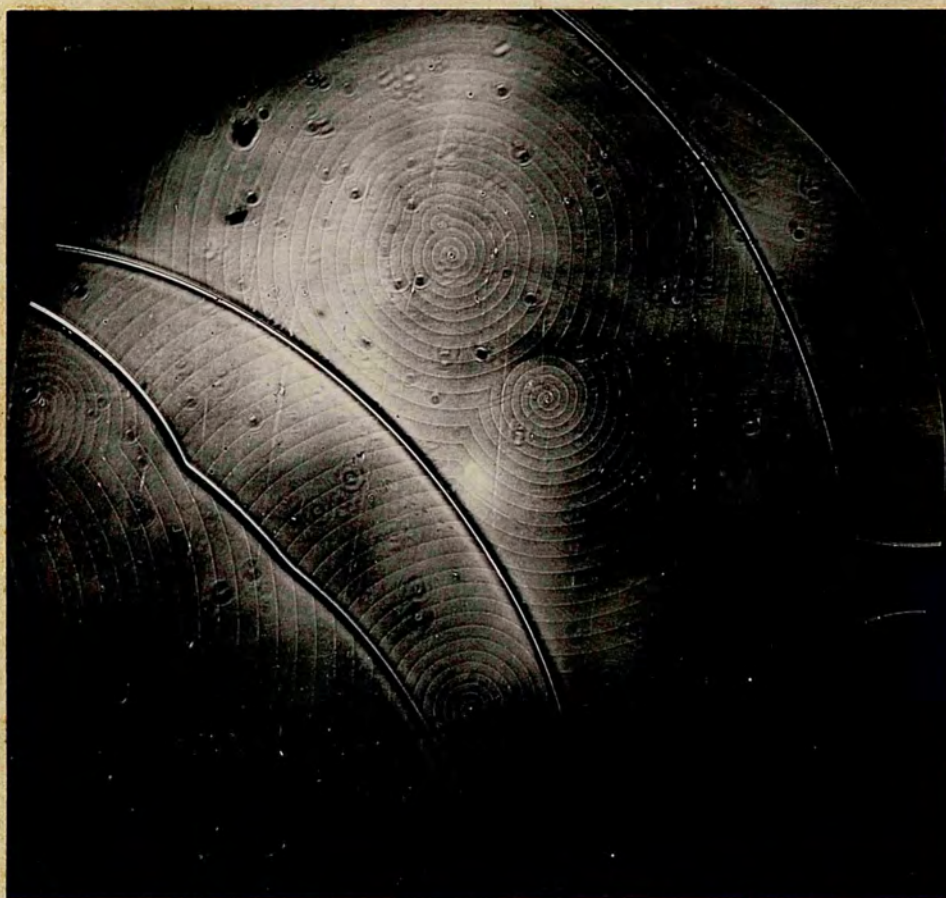
X90

Fig 36.   Interaction of circular growth spirals
         and their curves of intersection;
         Note the lines of discontinuity running
         across the figure.
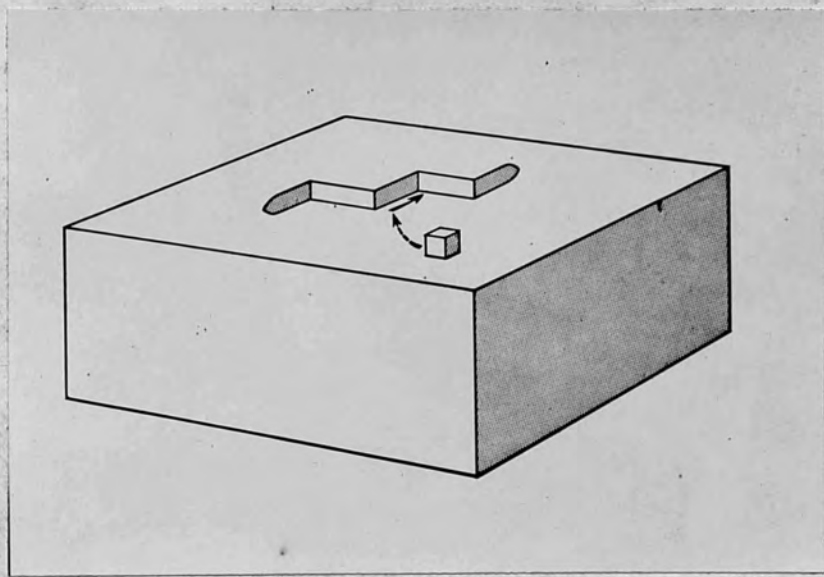
Fig 37.   A ledge running between two dislocations
          of opposite sign ending on a crystal
          face.
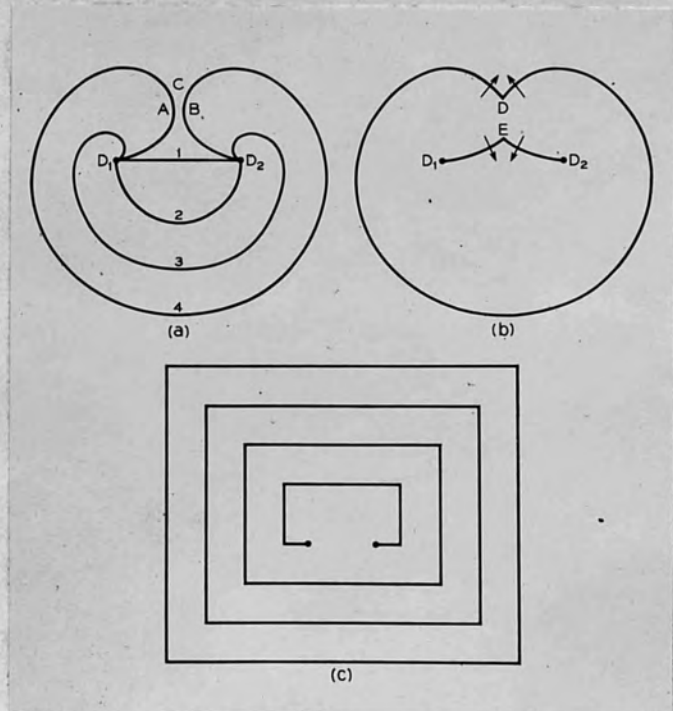
Fig 38.   Schematic representation of the formation
          of closed loops from a pair of unlike
          dislocations.
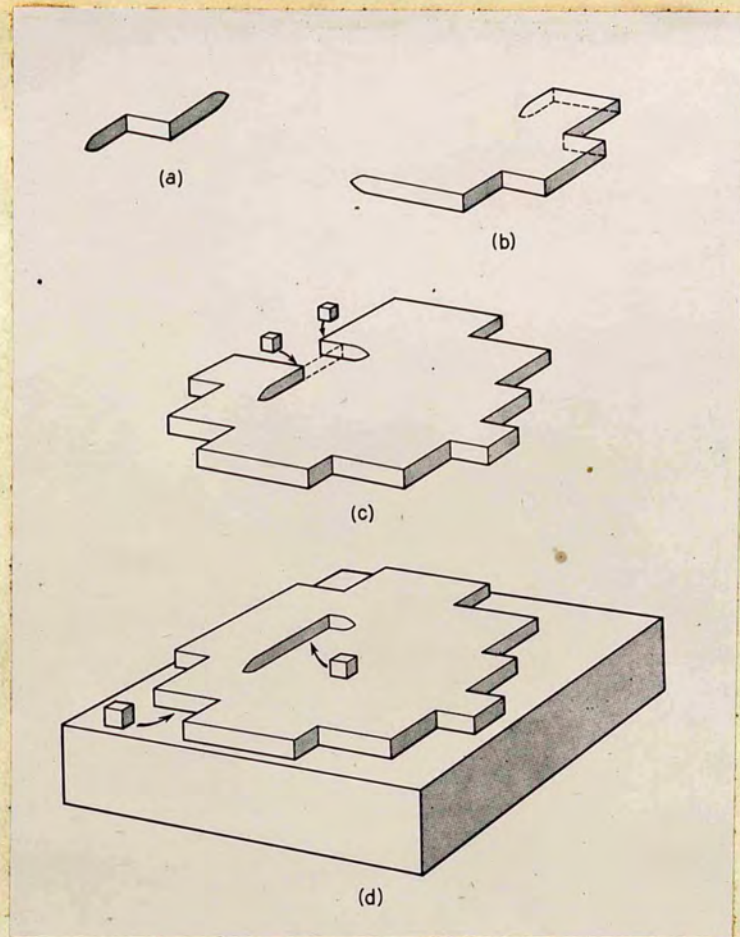
Fig 39. Schematic representation in three dimensions of
several stages of growth from two dislocations
of opposite sign.

X90

Fig 40. Closed triangular and hexagonal loops from a
pair of unlike dislocations.

25.
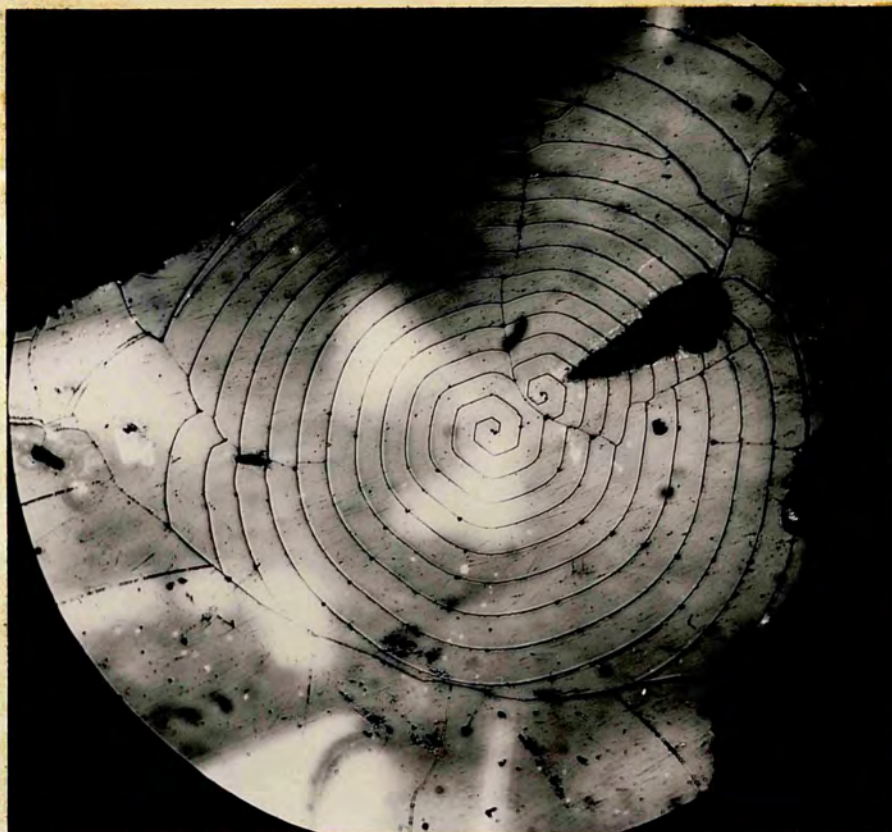
X90

Fig 41. A pair of unlike dislocations of unequal strength
forming closed loops with an edge running at the
points of contact.
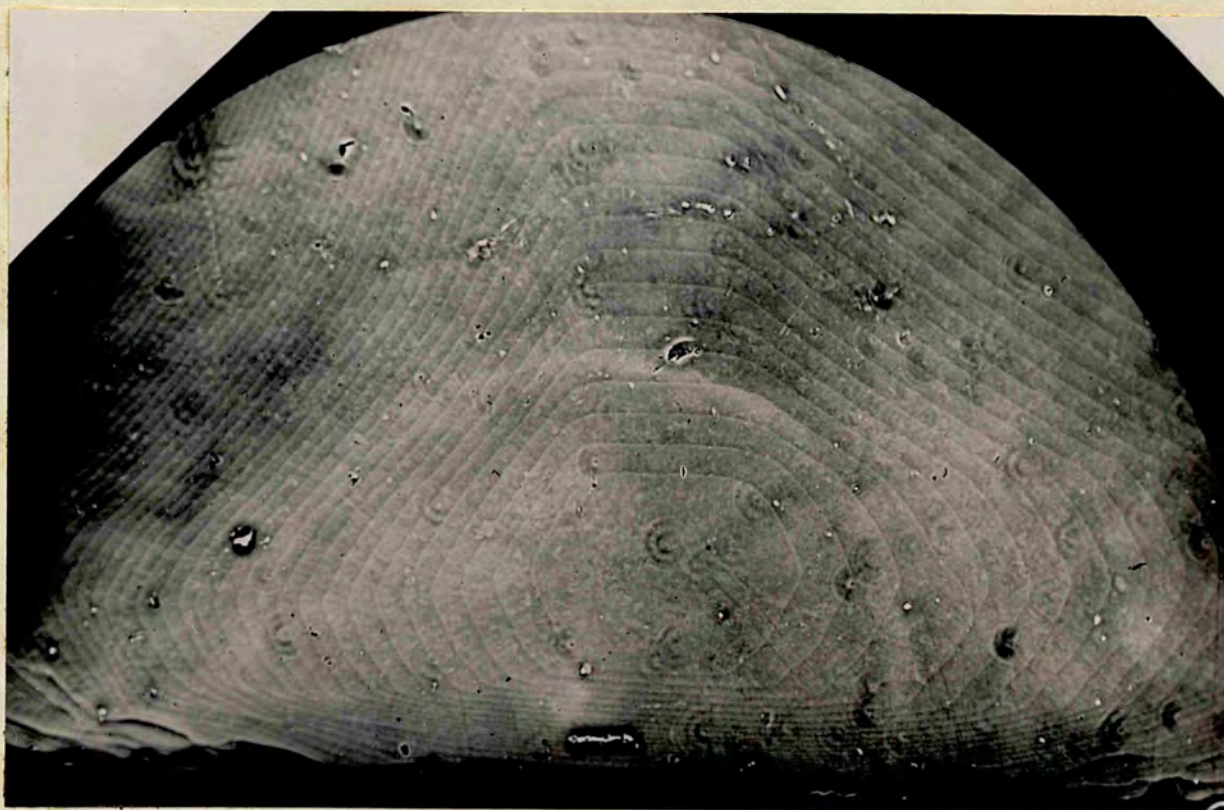
X120

Fig 42. Closed hexagonal layers with no trace of dislocations
at the centre.

26.
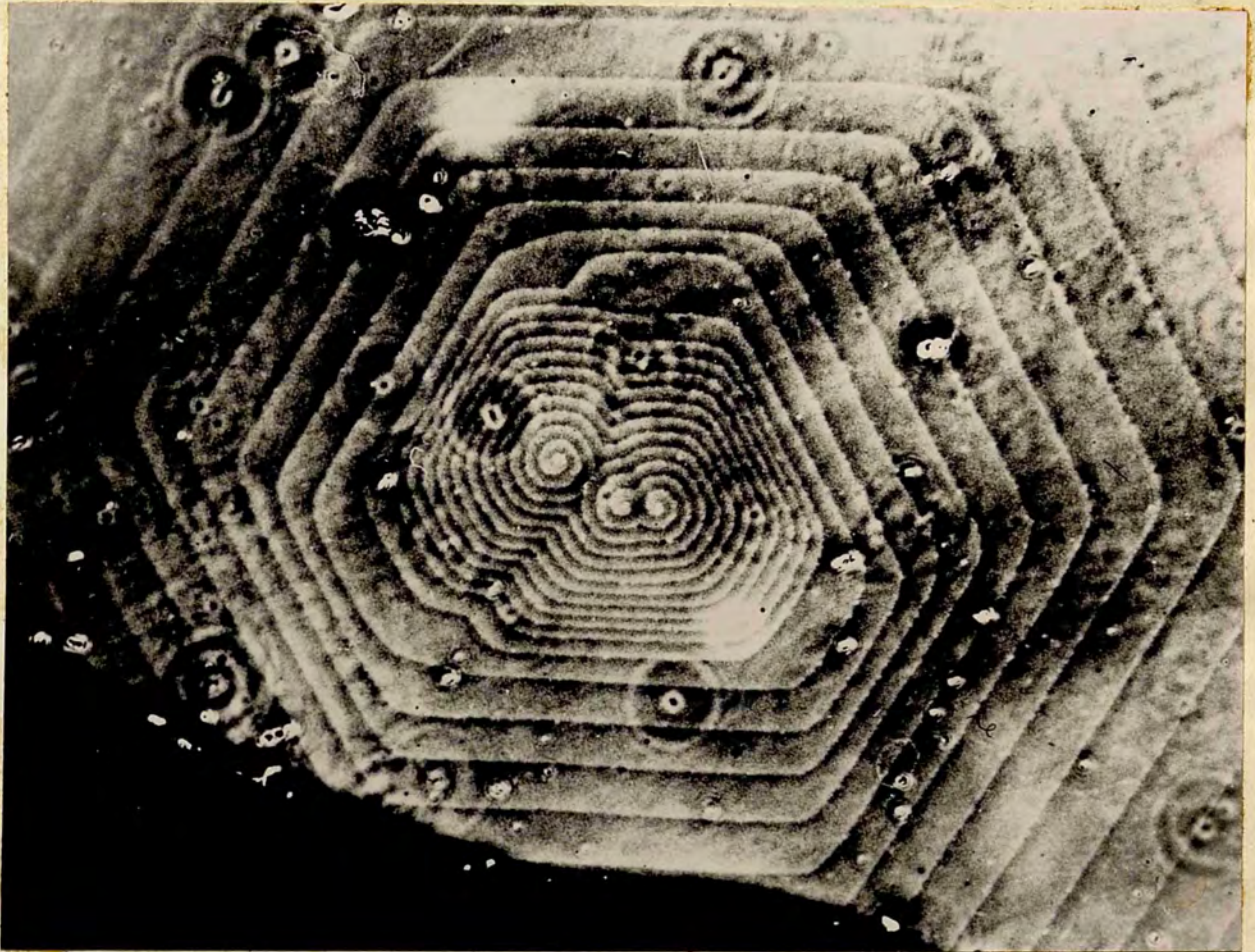
X550

Fig 43. Three dislocations of like sign close together
giving rise to three co-operating spirals. The
central or the last part of growth spirals is
circular, the rest being hexagonal.
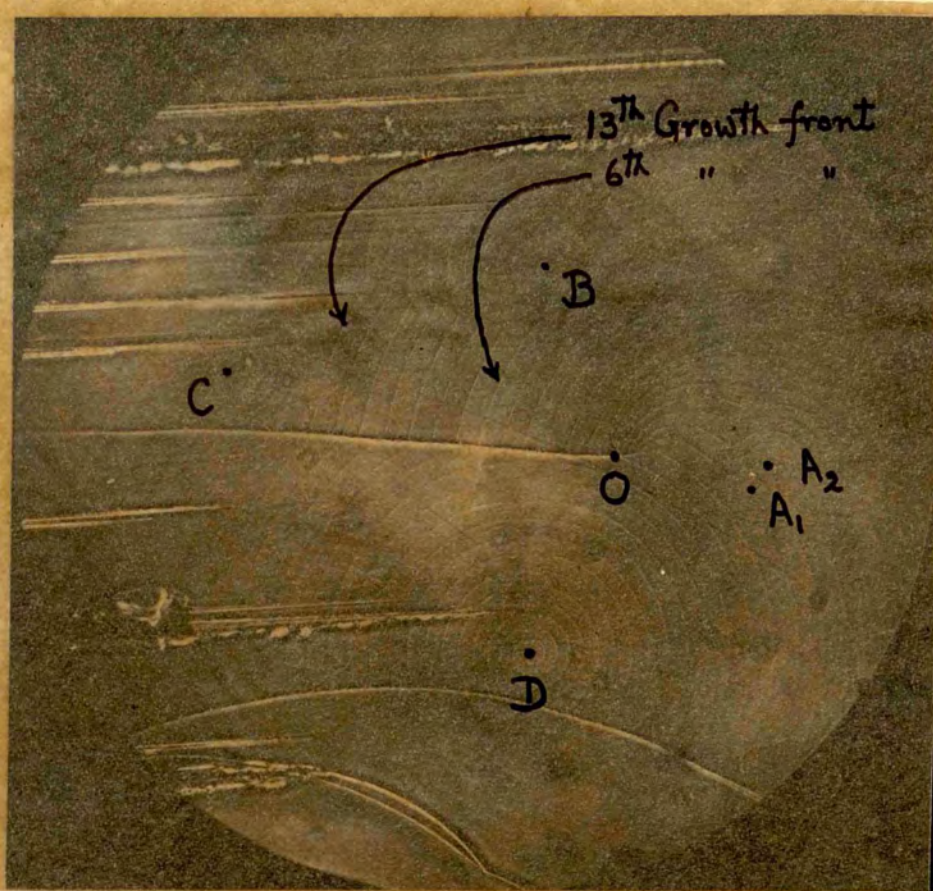
13th Growth front
6th " "

B

C

O

A₂
A₁

D

X90

Fig 44. Resultant growth pattern from five
separated screw dislocations.
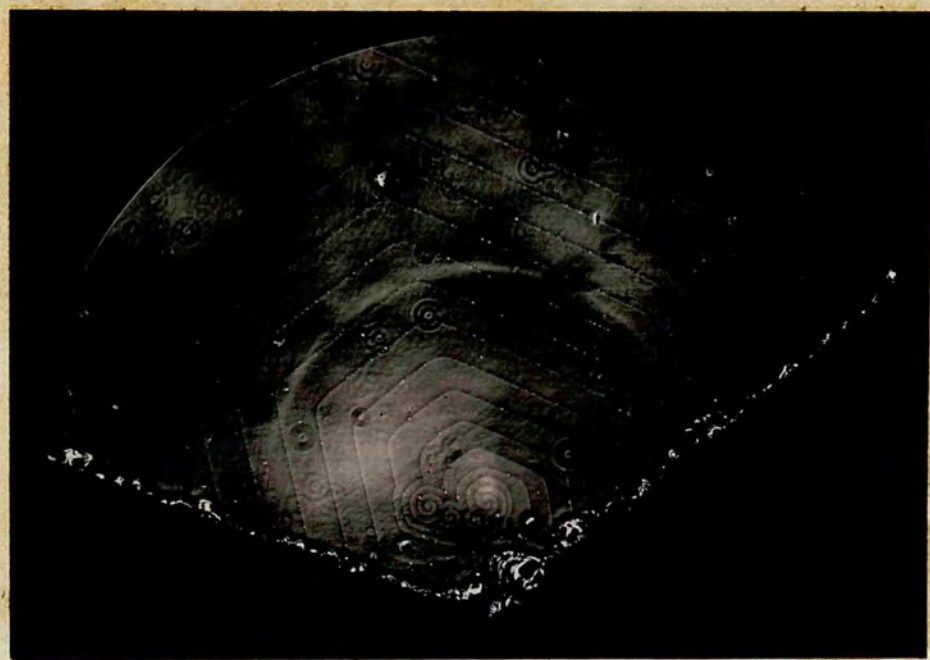
X200

Fig 45. A group of six close dislocations.

X90
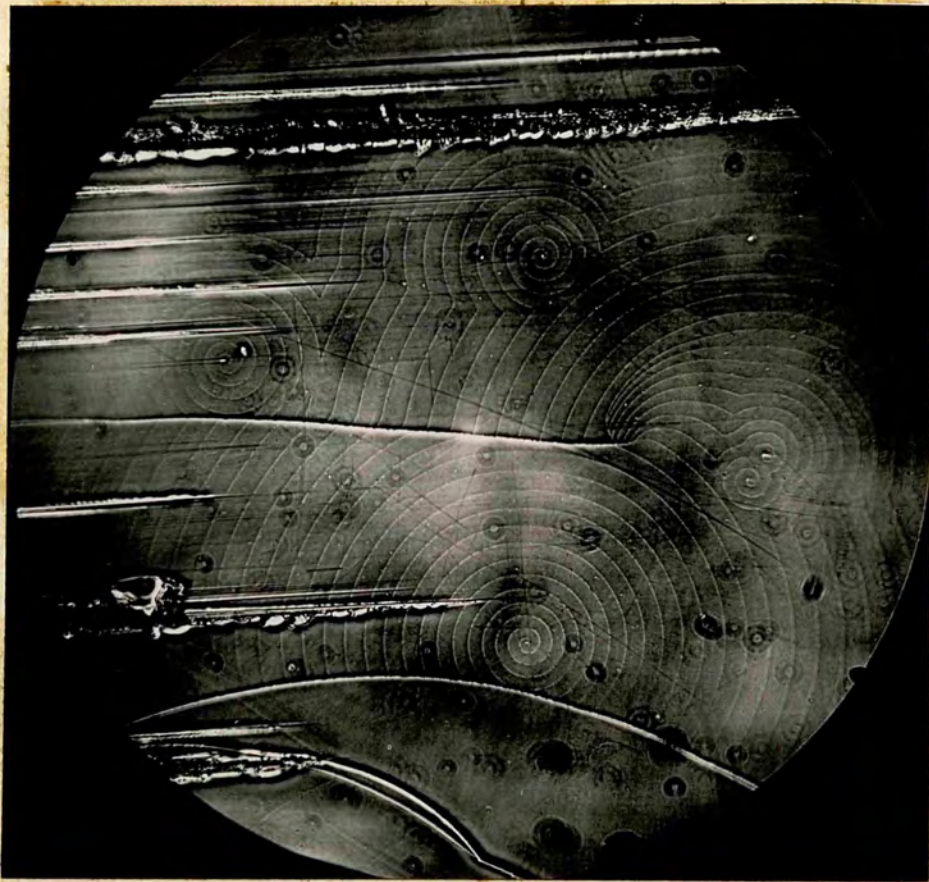
Fig 44.   Resultant growth pattern from five
separated screw dislocations.
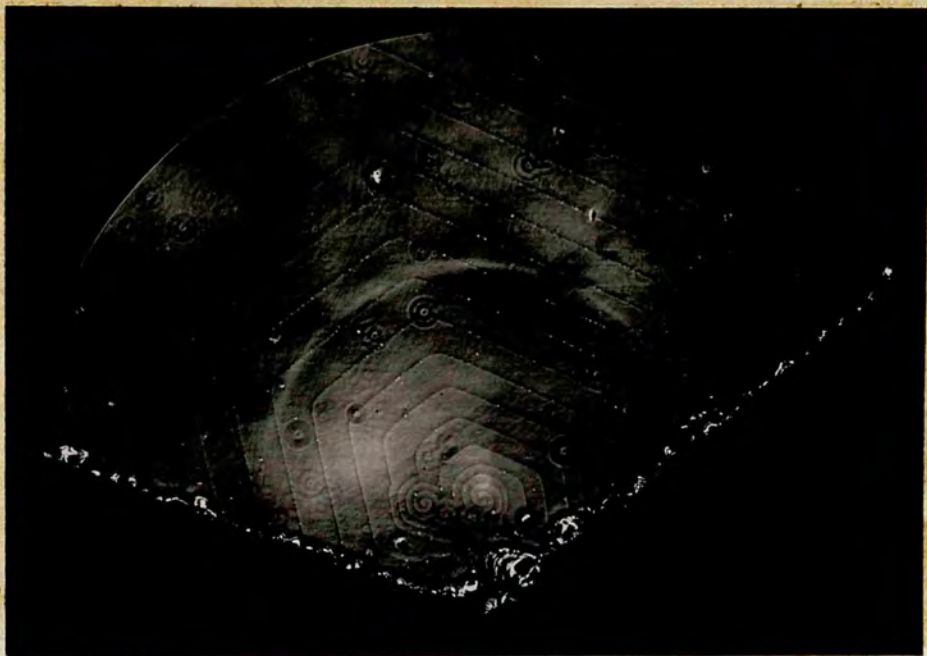
X200

Fig 45.   A group of six close dislocations.

X220

Fig 46. A number of circular growth spirals
originating from dislocations of the
same sign. Density of dislocation $\sim 10^4/cm^2$.

X500

Fig 47. Polygonal spirals originating from dislocations
with density $\sim 10^5 / cm^2$, all of the same sign.
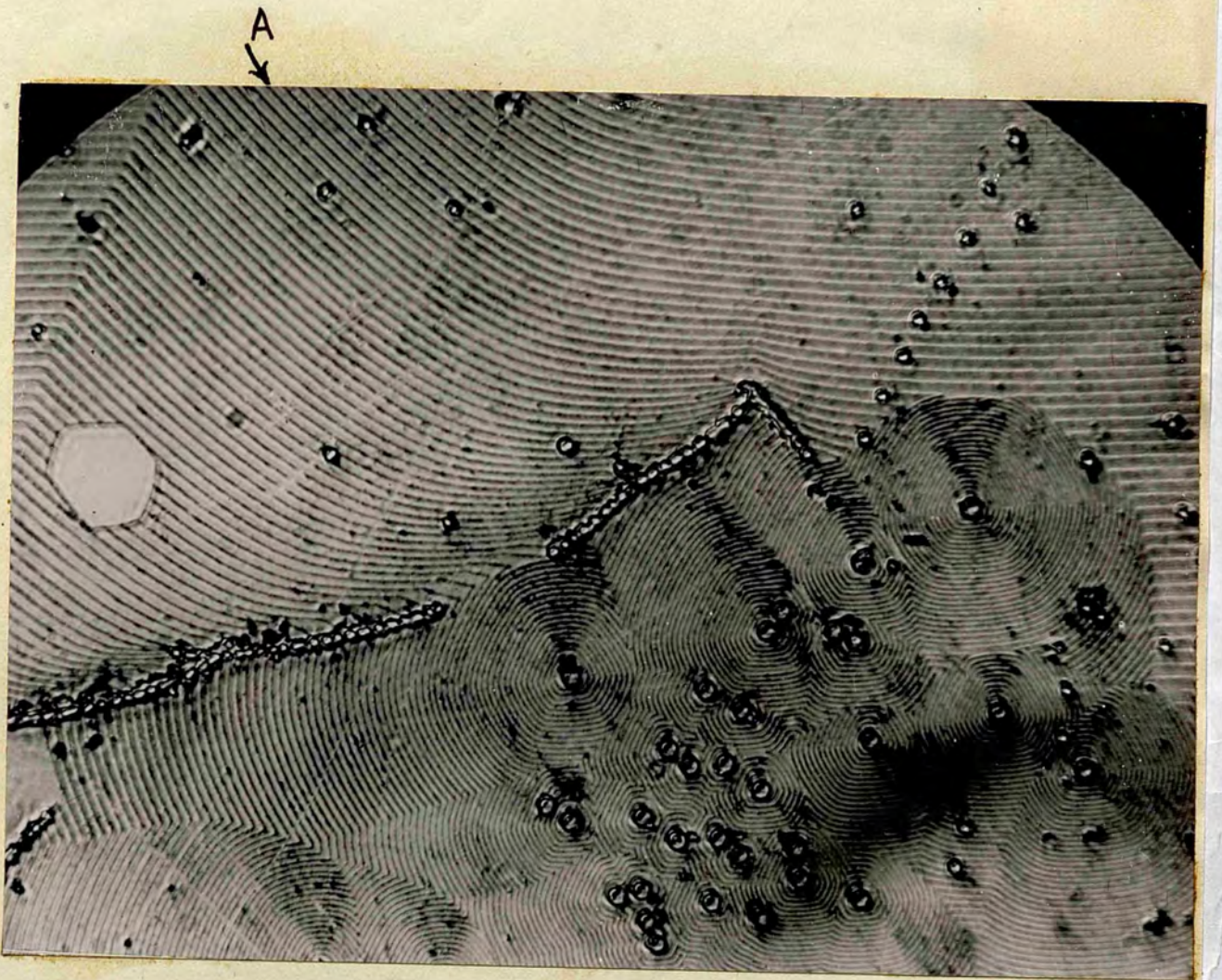
X580

Fig 48. Large number of polygonal spirals with a barrier
of dislocations.
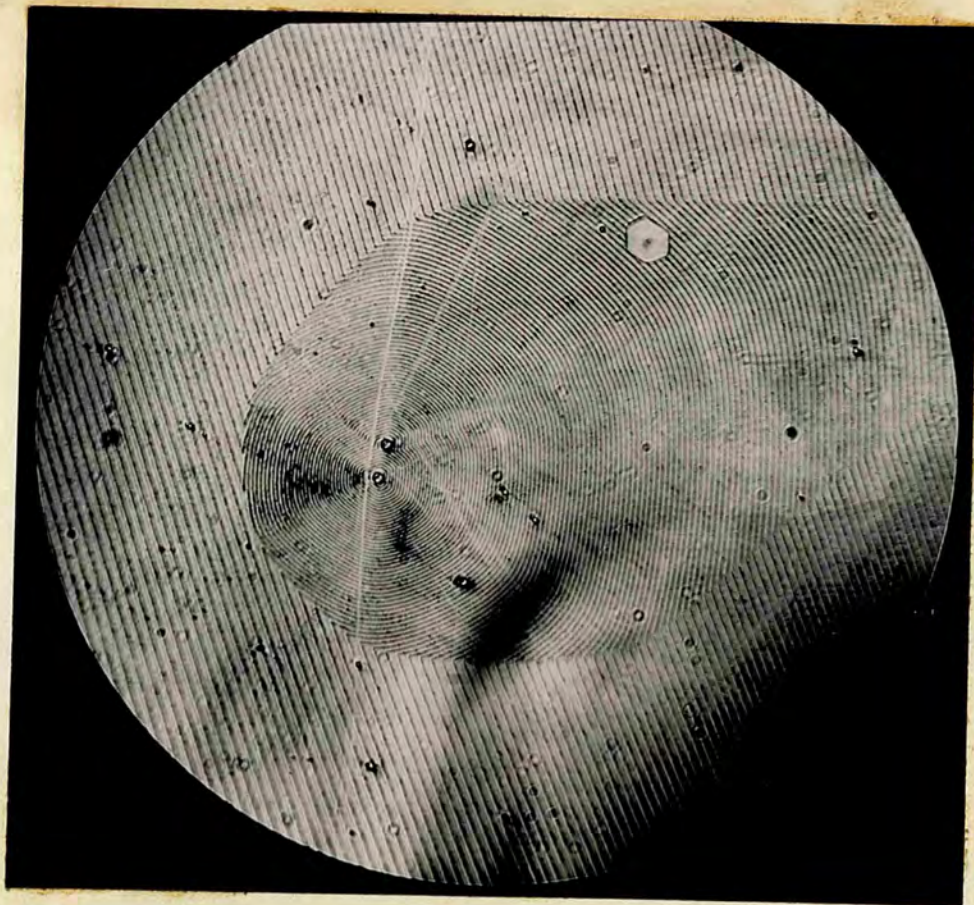
X300

Fig 49. Illustrating curve of intersection.
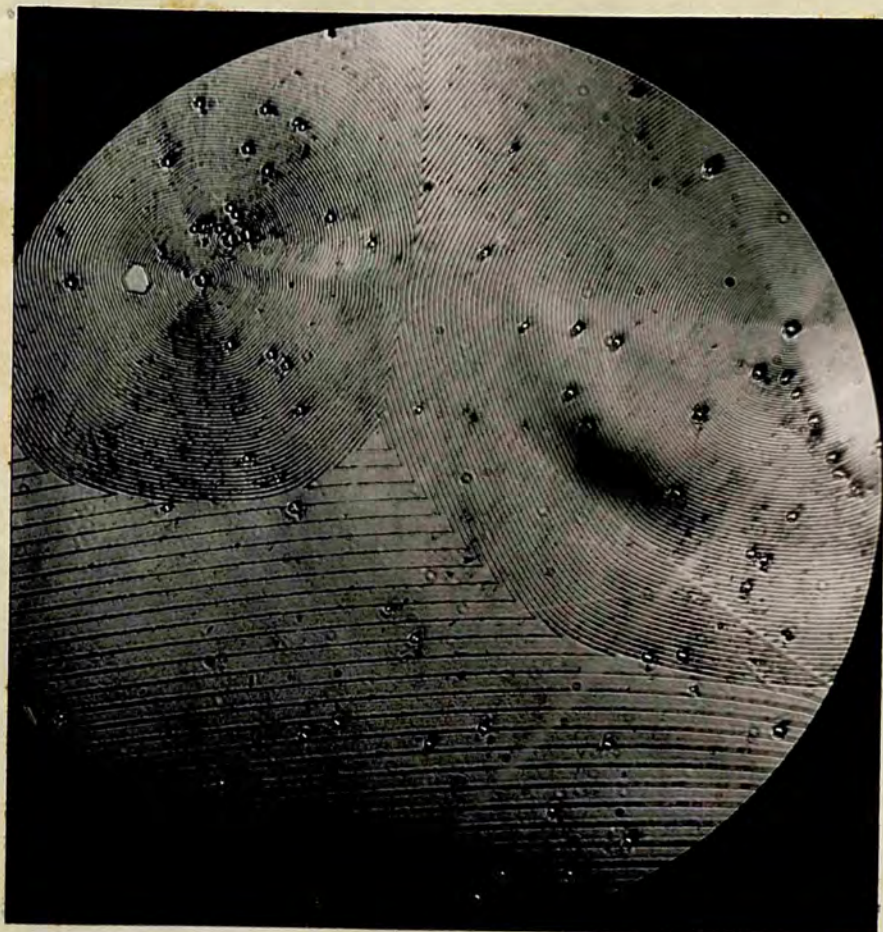
Fig 50.
Formation
of closed
△ loops
by growth
fronts from
three dis-
locations.

X300

32.
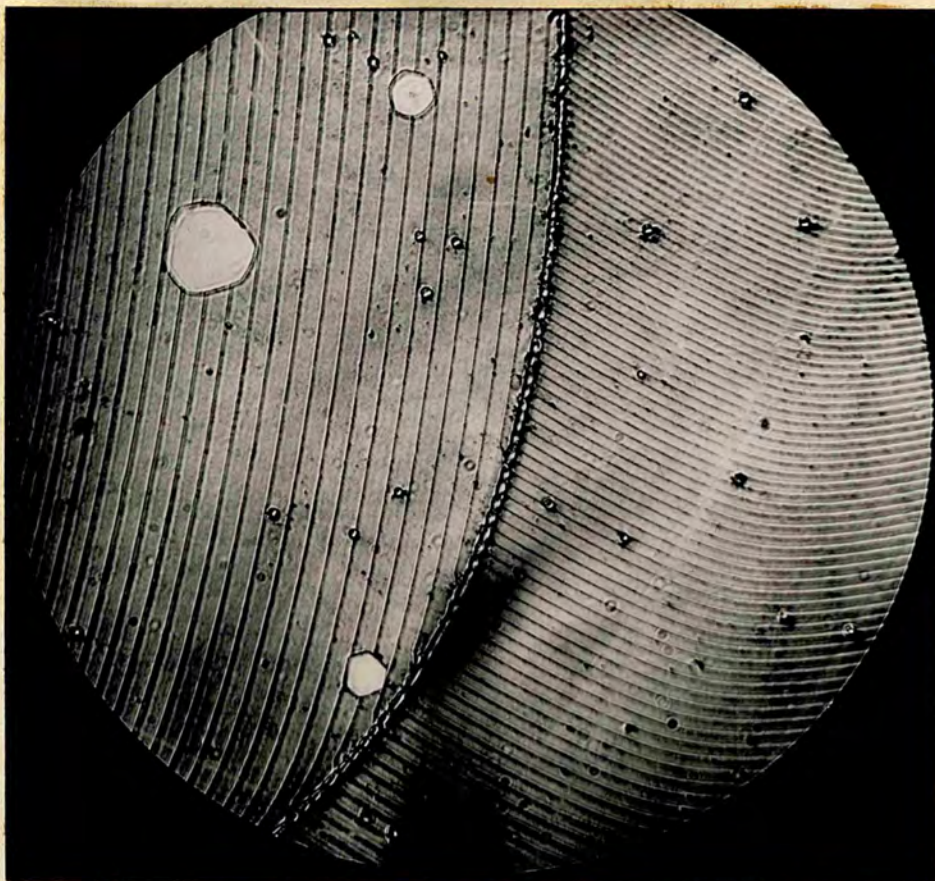
X300
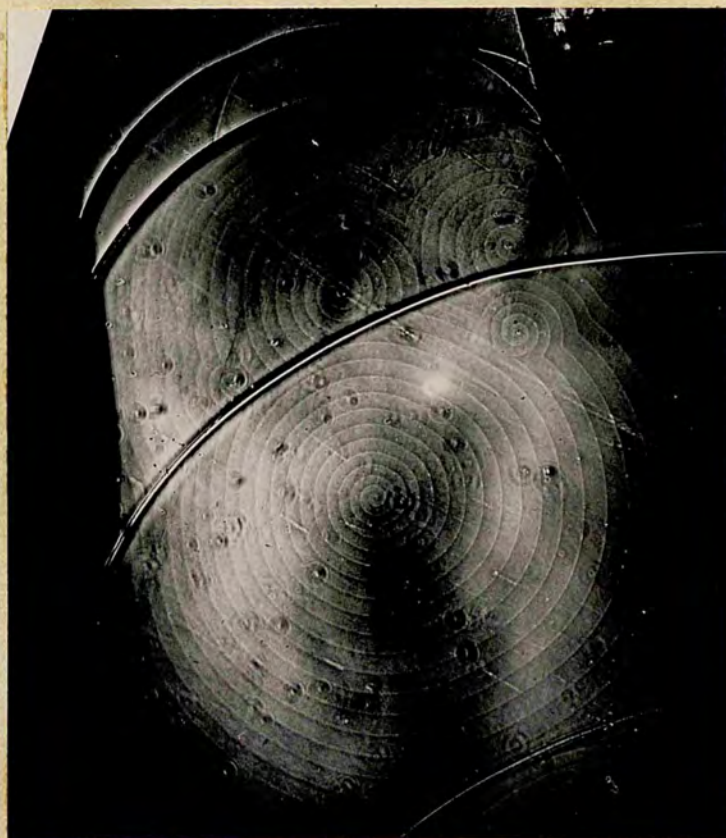
X90

Fig 52.   Upper half of the fig., illustrates the interaction
of two circular spirals equally developed. The
curve of intersection is a straight line perpendicular
to the line joining the two dislocation points and
passes through their middle point.

33.

Fig 53.

X 300

X 900

Fig 54. Growth steps terminating at points marked by a series of dots.

34.

Fault Surfaces.

Fig 55.

X90

Fig 56.

X90
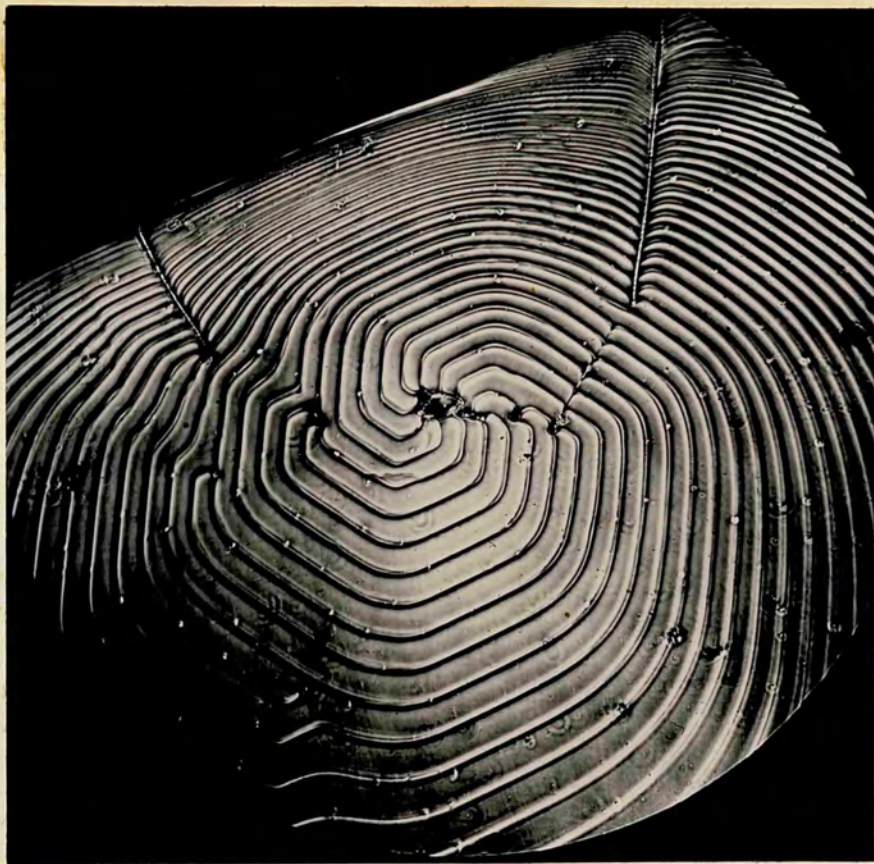
Fig 57.

X150

Fig 58.

X150

36.
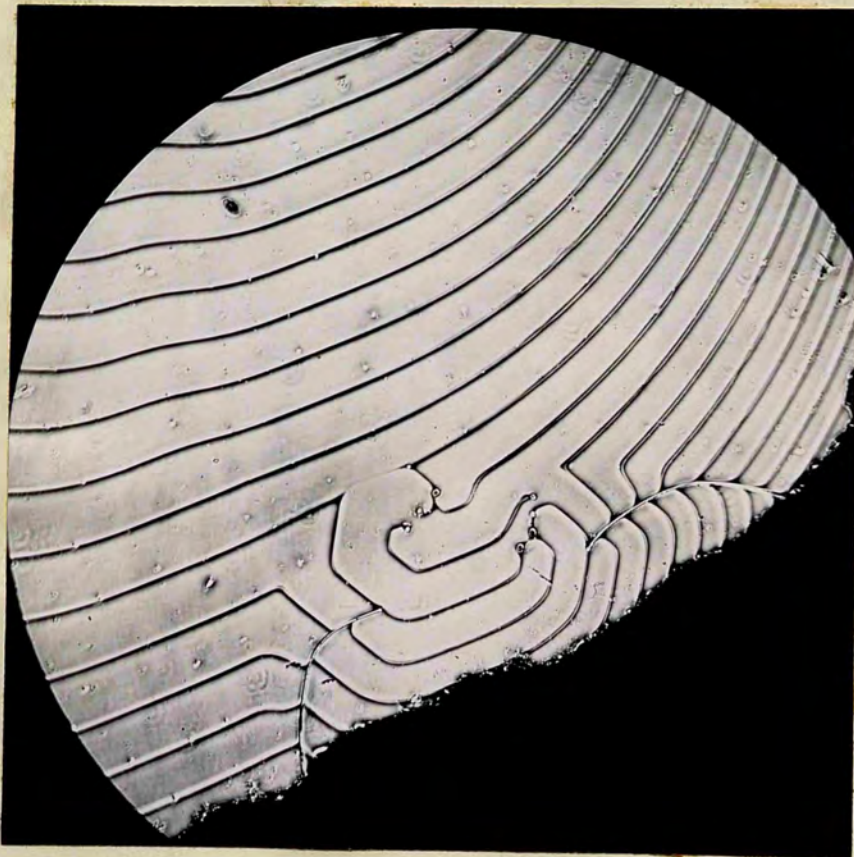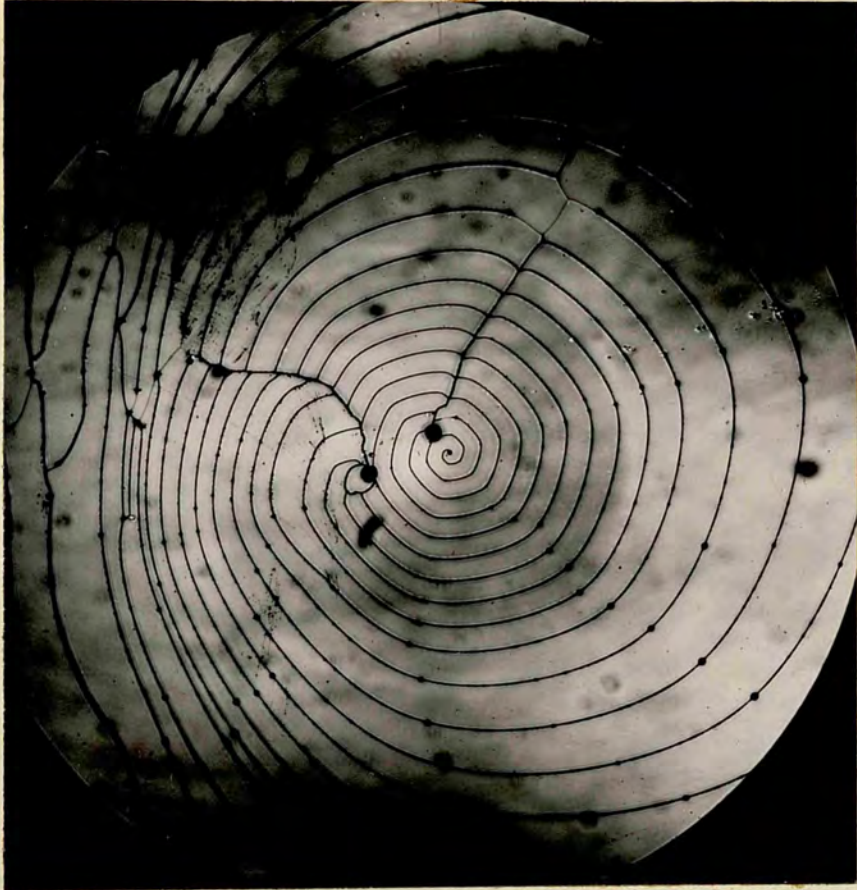
Fig 59.

X90
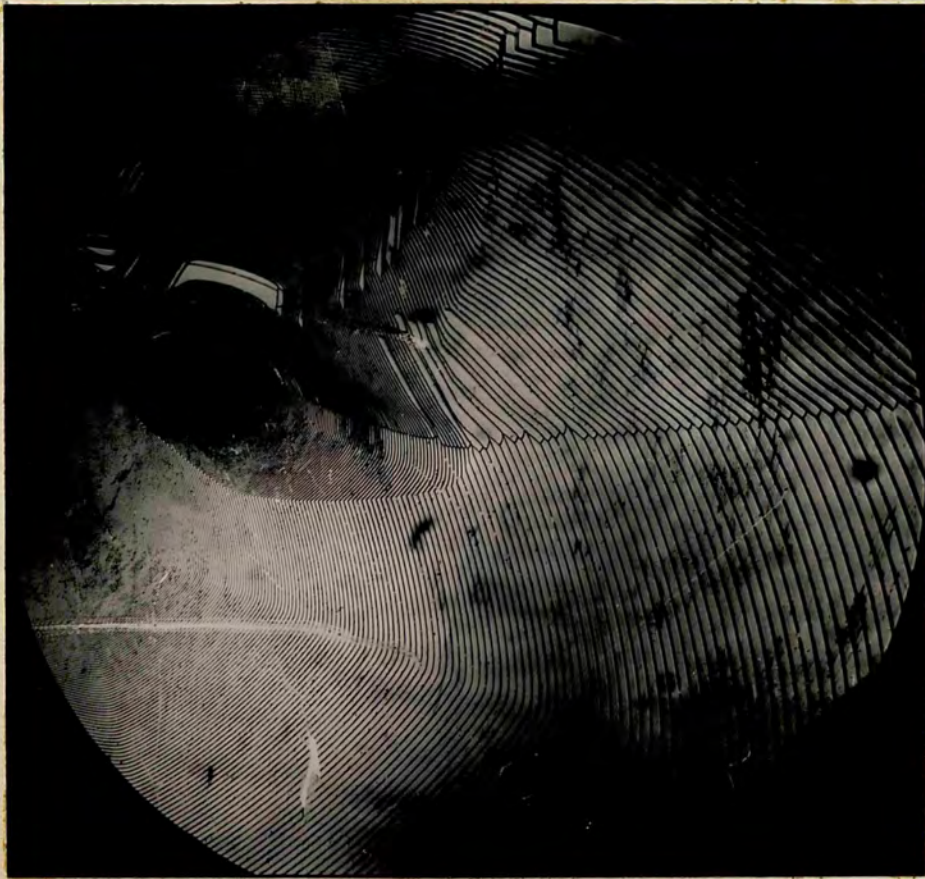
Fig 60.

X1000
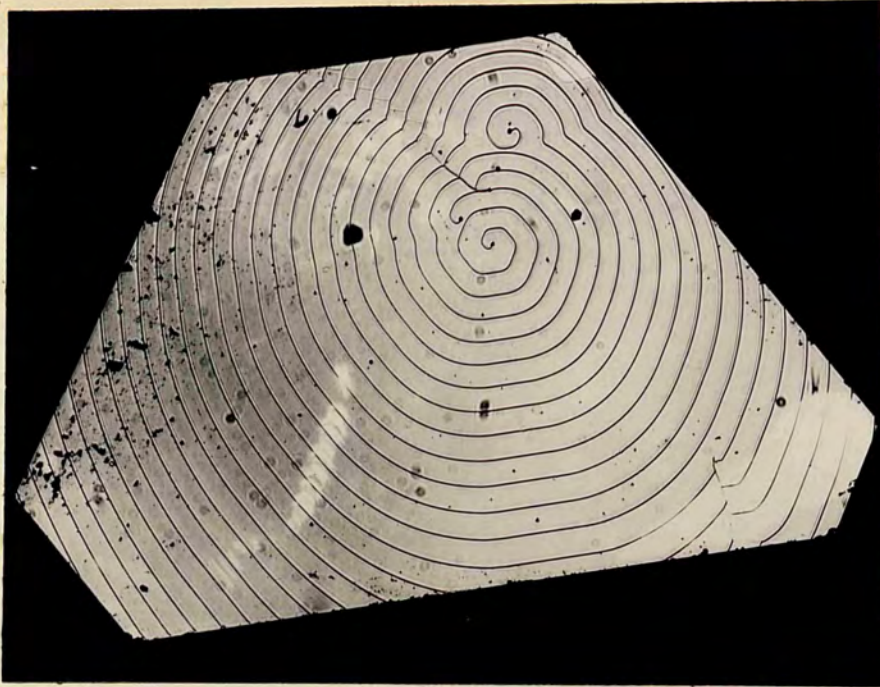
Fig 61.

X45

Fig 62.

X90

X90
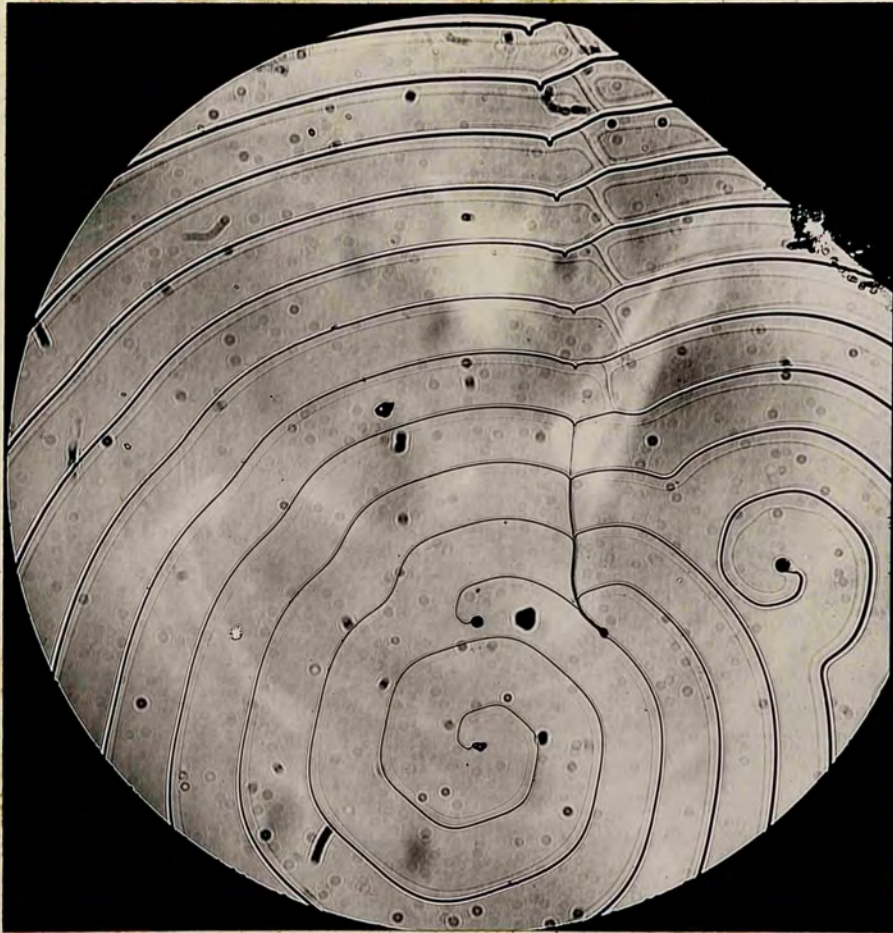
Fig 63.

X150

Fig 64. A group of dislocations arranged along
a line.

X90

Fig 65. Group of dislocations giving a repeat
pattern.

X90

Fig 66. Several groups of dislocations

interacting with one another

giving rise to a complex pattern.

X90

Fig 67. Two intersecting groups of

circular spirals.

41.
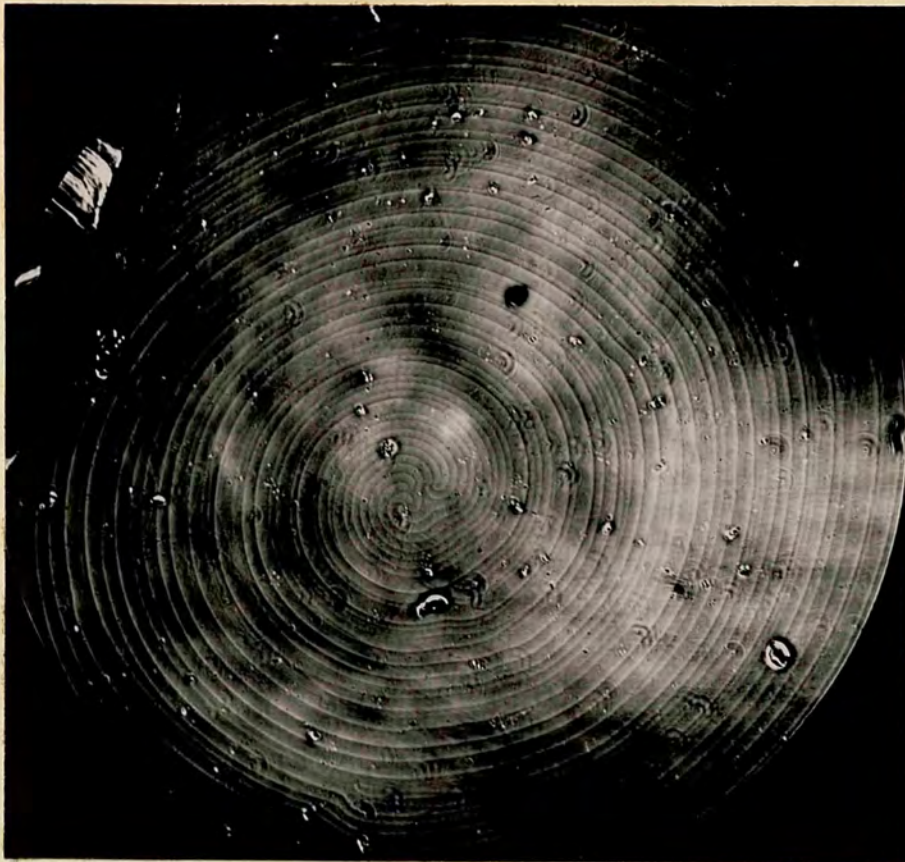
X90

Fig 68. A number of dislocations at the centre. The
growth steps bunch together away from the centre.
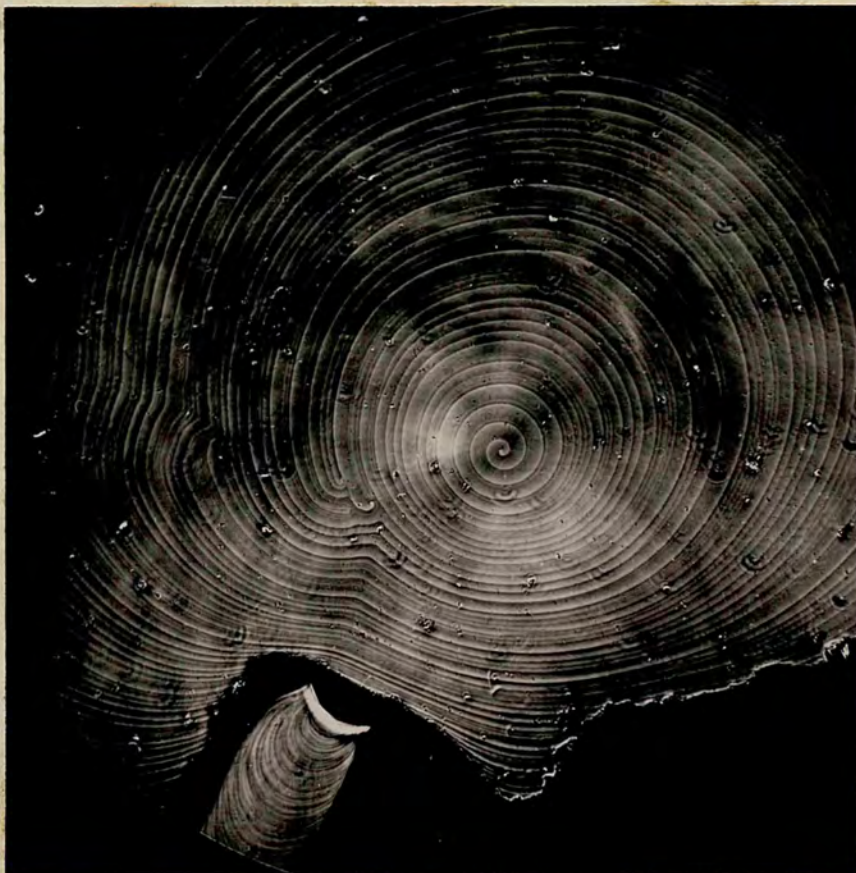
X90

Fig 69. Circular spirals with bunching of steps.

42.

SPIRALS ORIGINATING FROM DISLOCATIONS

OF MULTIPLE STRENGTH

AND

MULTIPLE DISLOCATIONS
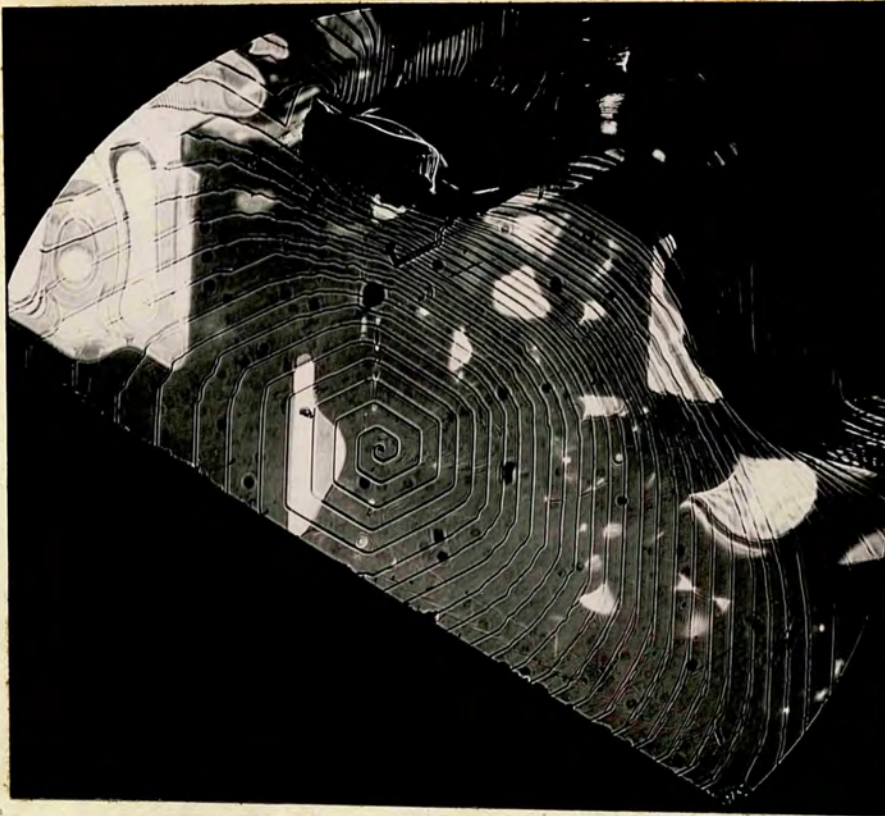
X45

Fig 70. Spiral originating from a dislocation
of multiple strength (bright field
illumination).
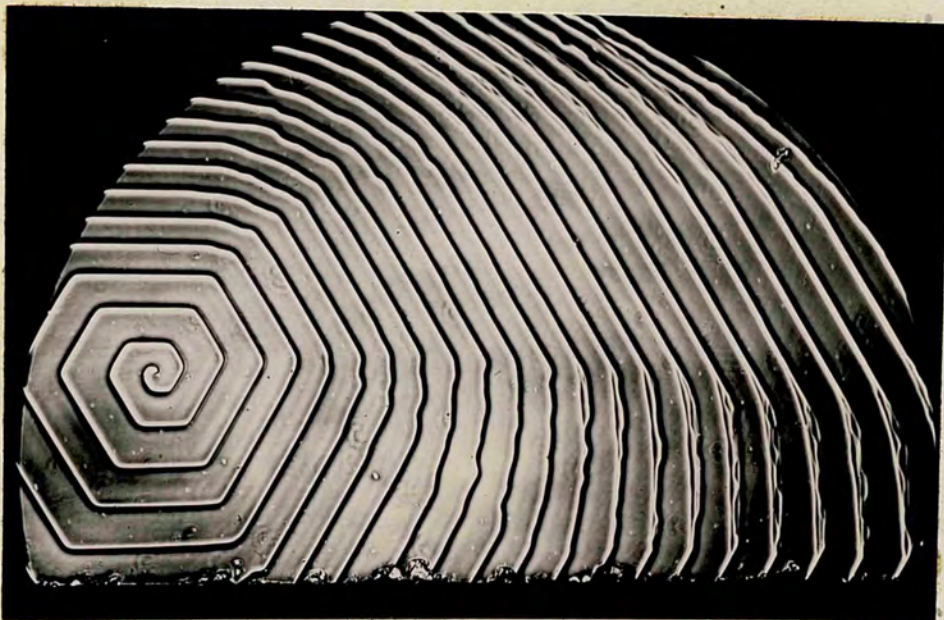
X90

Fig 71. Right half of fig 70 showing dissociation
of steps.

Fig 72. Enlargement of right half of fig. 71 showing preferential dissociation of steps in orientations at 60° to each other.

X150
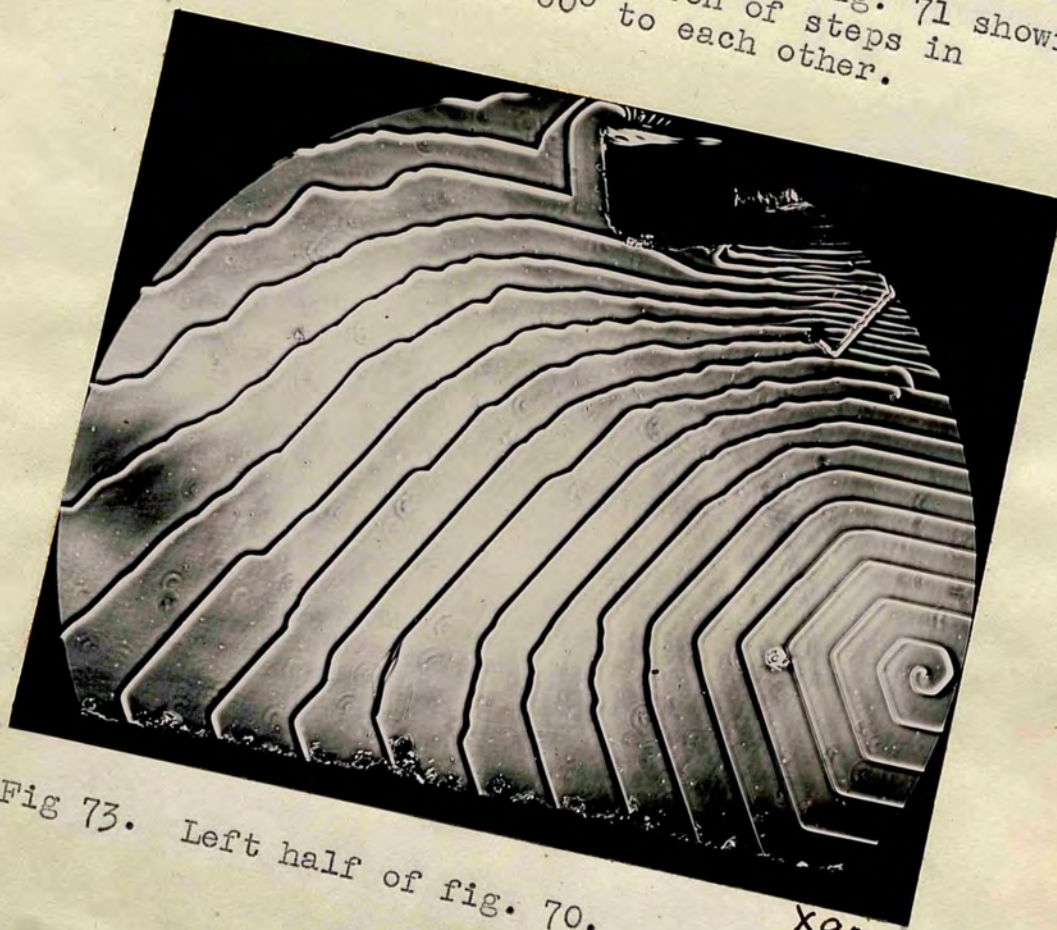
Fig 73. Left half of fig. 70.

X90

44.

X90

Fig 73A. Behaviour of steps further on the left of fig.73.
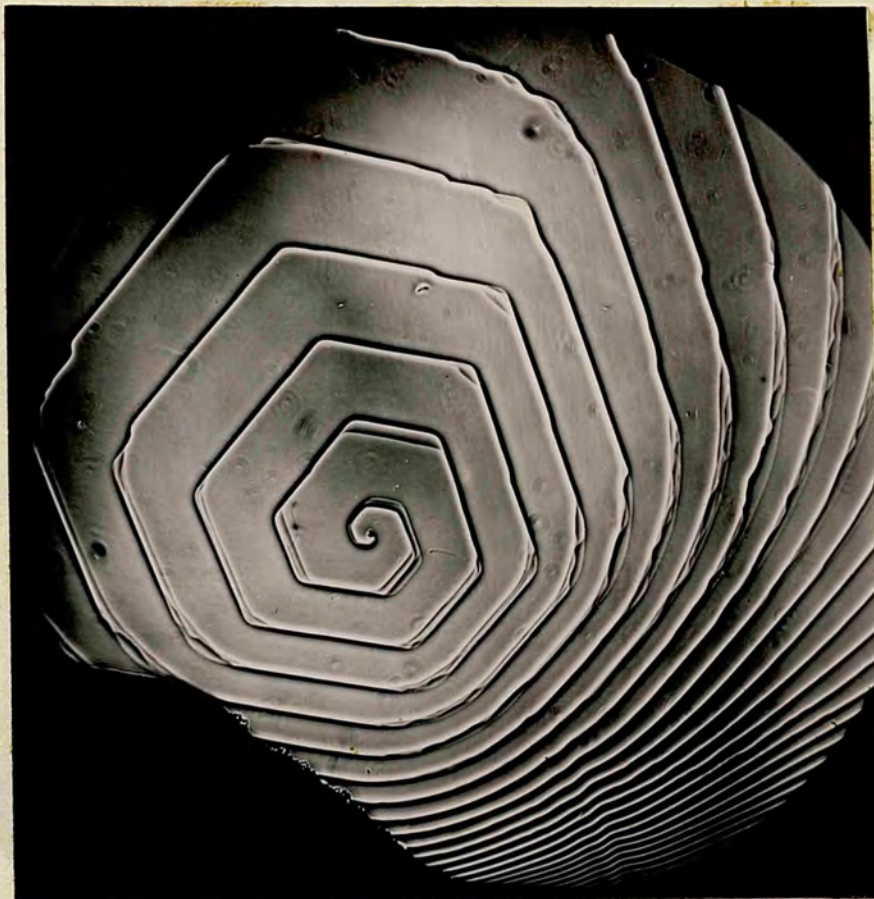
X90

Fig 74. Dissociation of steps on alternate edges of
hexagonal spiral.

45.
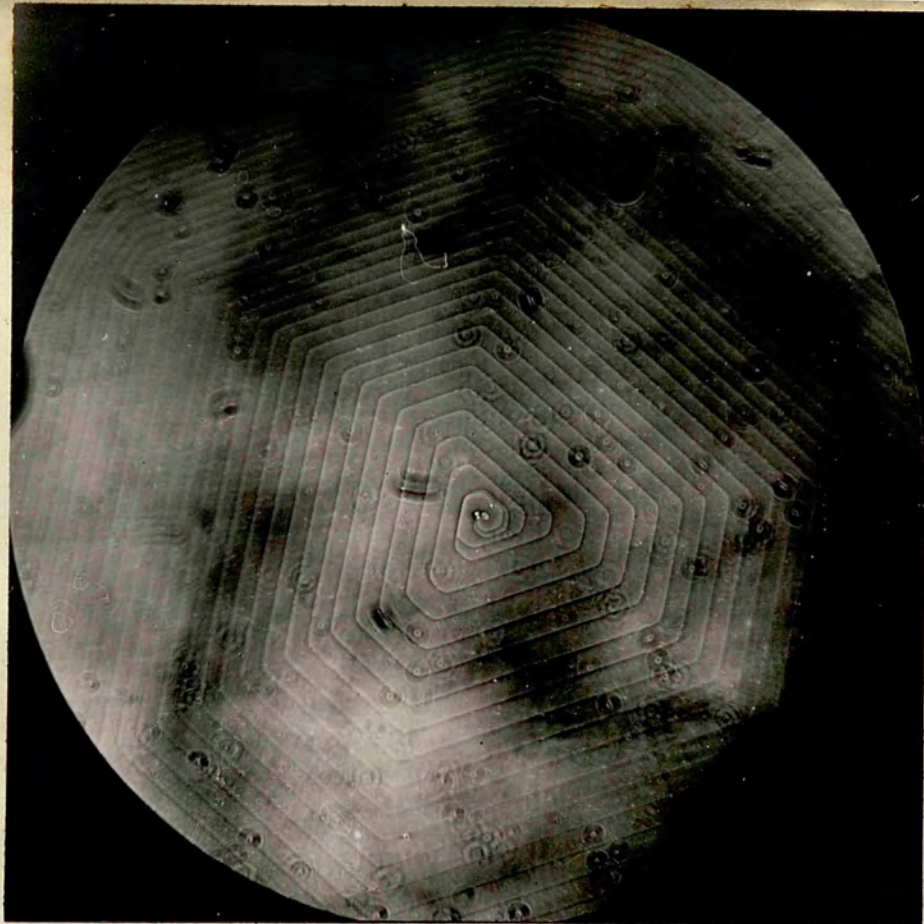
X150

Fig 75. A pair of spirals touching each other on one edge.

X90

Fig 76. A trigonal spiral with rounded corners.

46.

X90

Fig 77.   Showing part of fig. 78.

X90
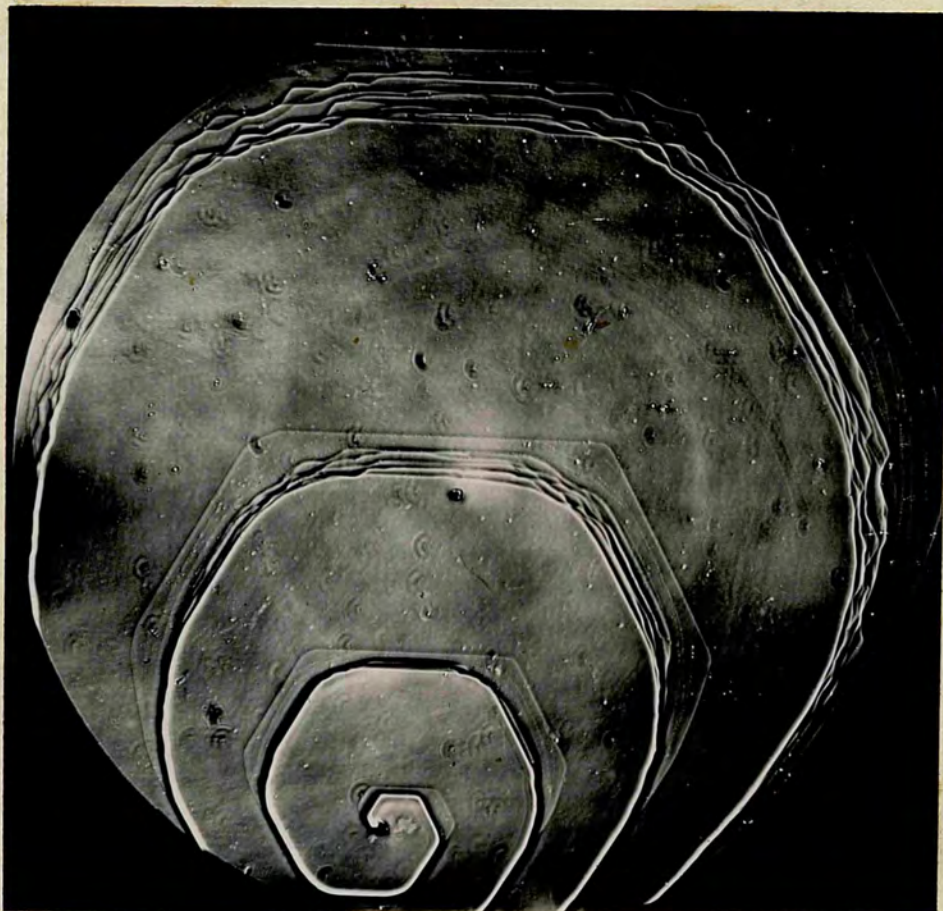
Fig 78. Multiple dislocations showing the straight
        edges in three orientations of the outer-
        most (or bottom) layers.

47.
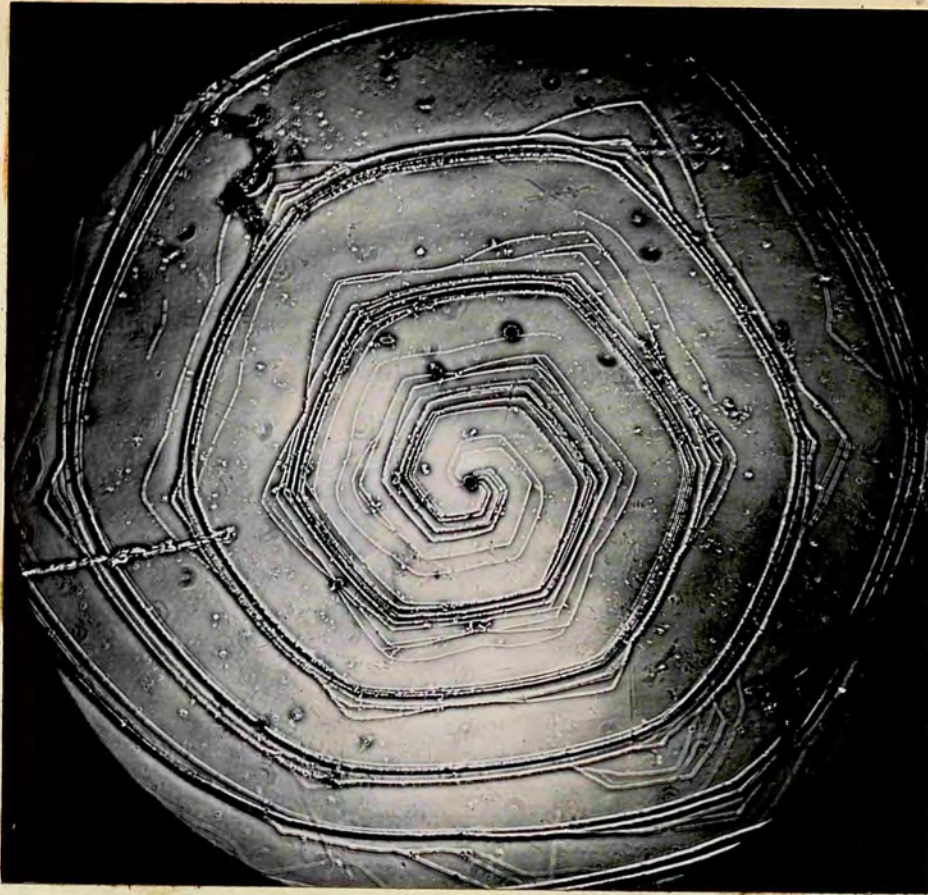
X150

Fig 79. Multiple dislocations with faster growth at corners.

X90

Fig 80. Multiple dislocations with straight edges of growth
steps.

INTERLACED   SPIRALS

Fig 81.

X90

Fig 82.

X90

Interlinking of four simple interlaced spirals; fig. 81
is the usual phase-contrast micrograph whereas fig. 82
had impurity smeared on it which gives this high visibility.

49.
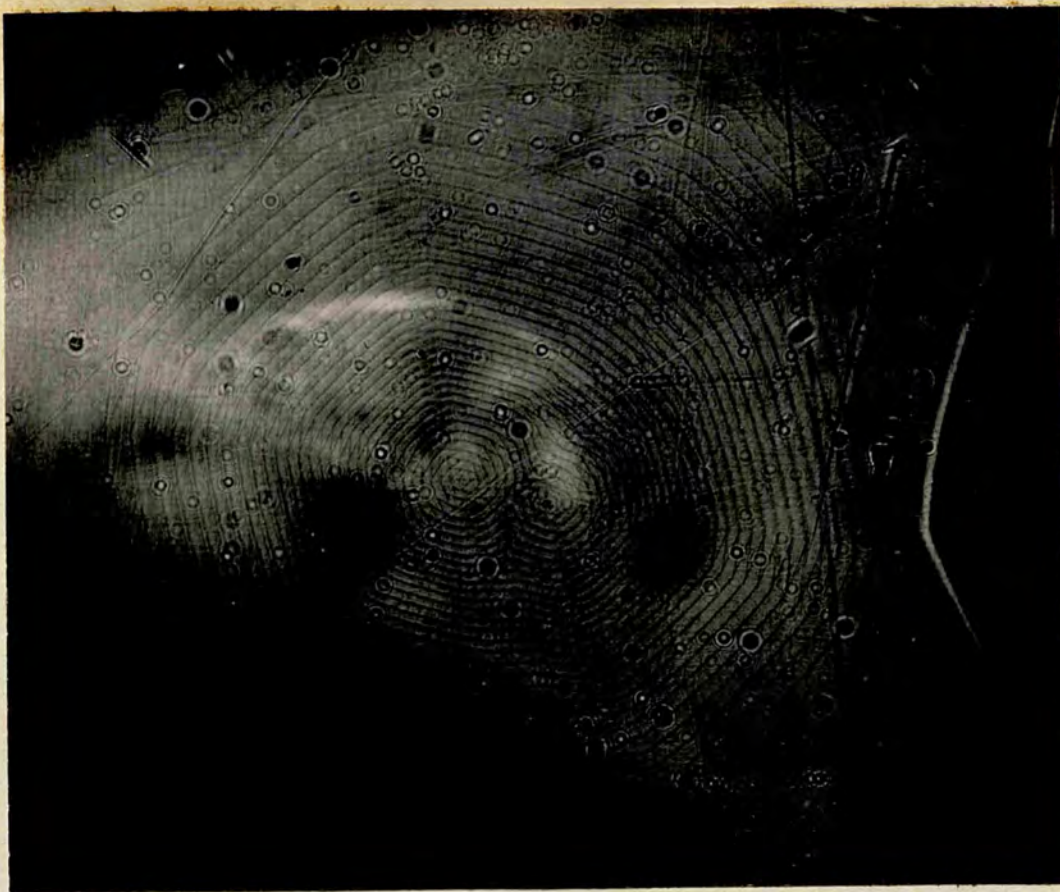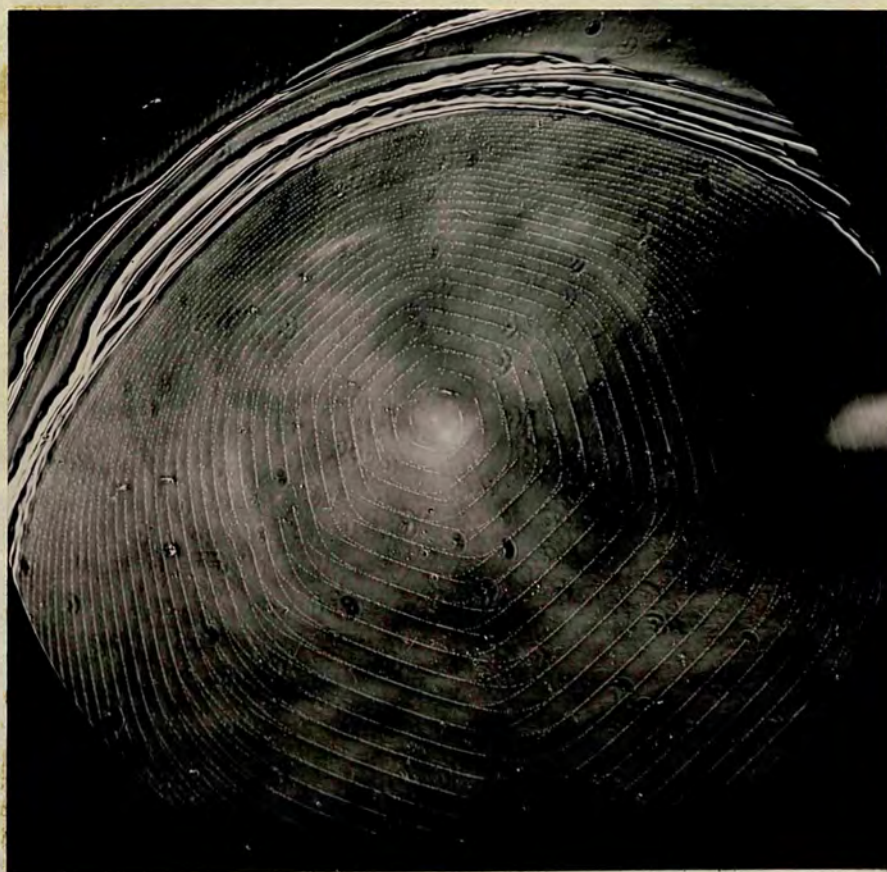
X90

Fig 84. Illustrating the phenomenon of domination for
interlaced spirals. The dominated dislocation
is towards the left of the centre and lies on
the 8th., edge from the first widely spaced turns.

X90

Fig 85. Illustrating several interlaced spirals, (bright
field illumination).

X90

Fig 86. The lower part of fig 85.

51.
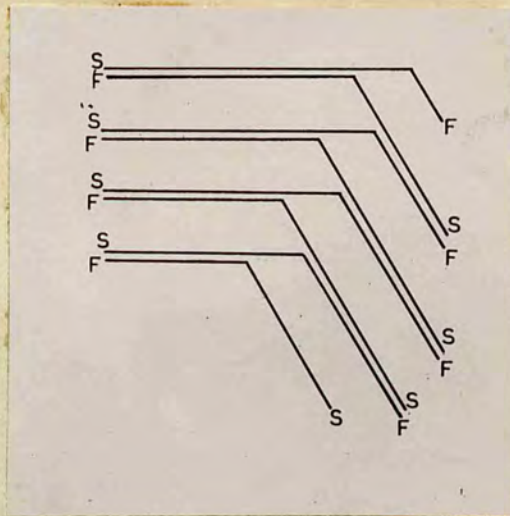
Fig 87. Schematic representation of the interlacing of edges. S represents the slowest F the fastest monolayer in the stack.

Fig 88.   Fig 89.

Double interlaced trigonal spirals.

Fig 90.

X90

A   B

Fig 91.

D   X90   C

An example of interlaced spiral with smooth
and rugged step lines on alternate edges.

53.
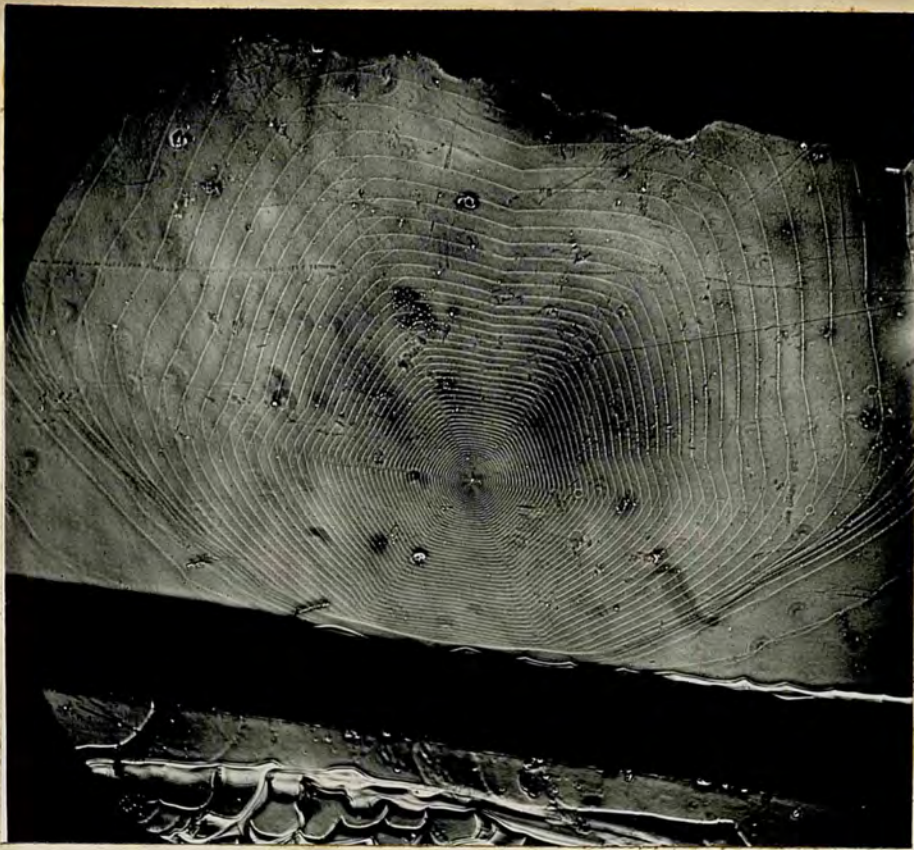
Fig 92.

X 90
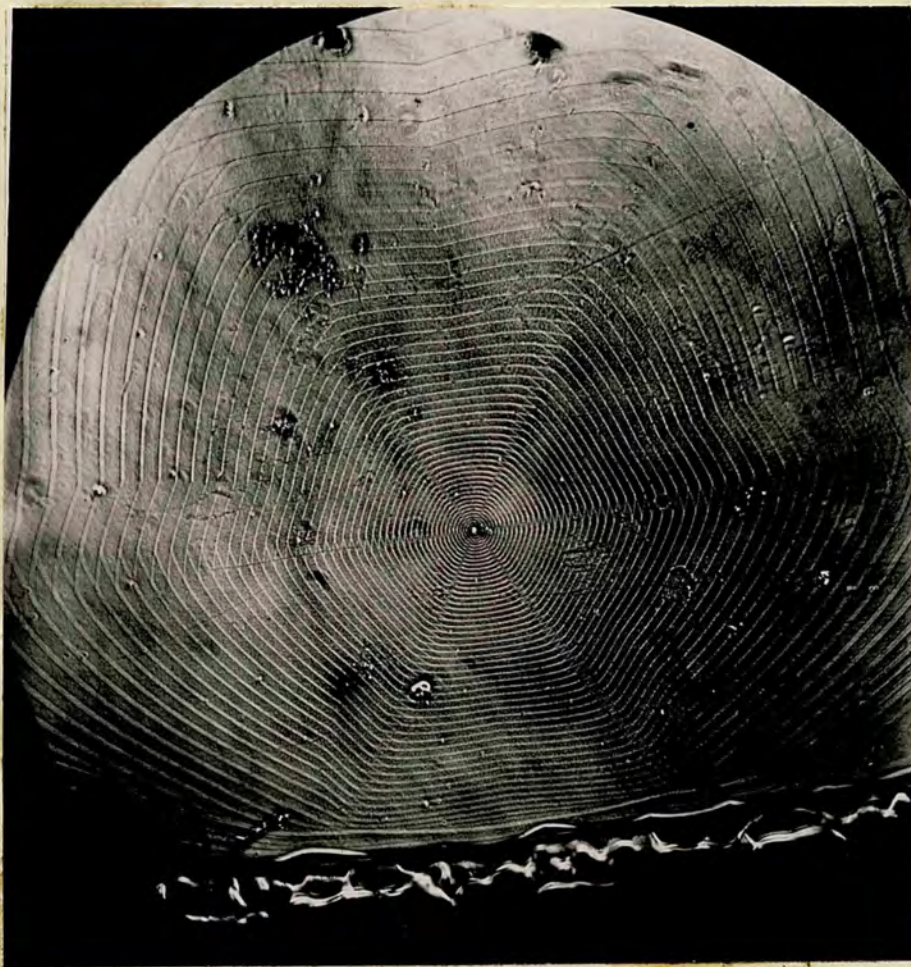
Fig 93.

X 150

An example of interlaced spiral with faster growth
at corners producing a cusp in the middle of the
straight edges.

54.
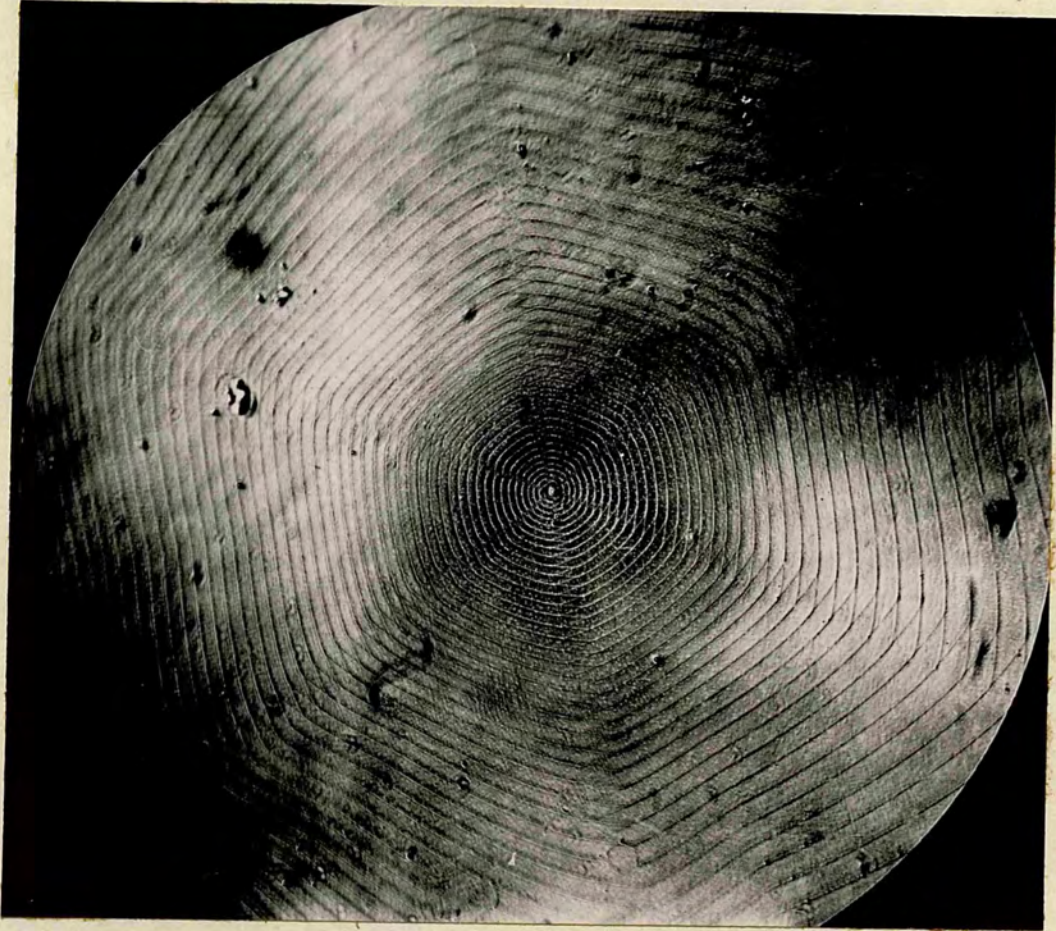
X 300

Fig 94. showing the centre of figs. 92 and 93. The
edges at the centre are seen to be convex.
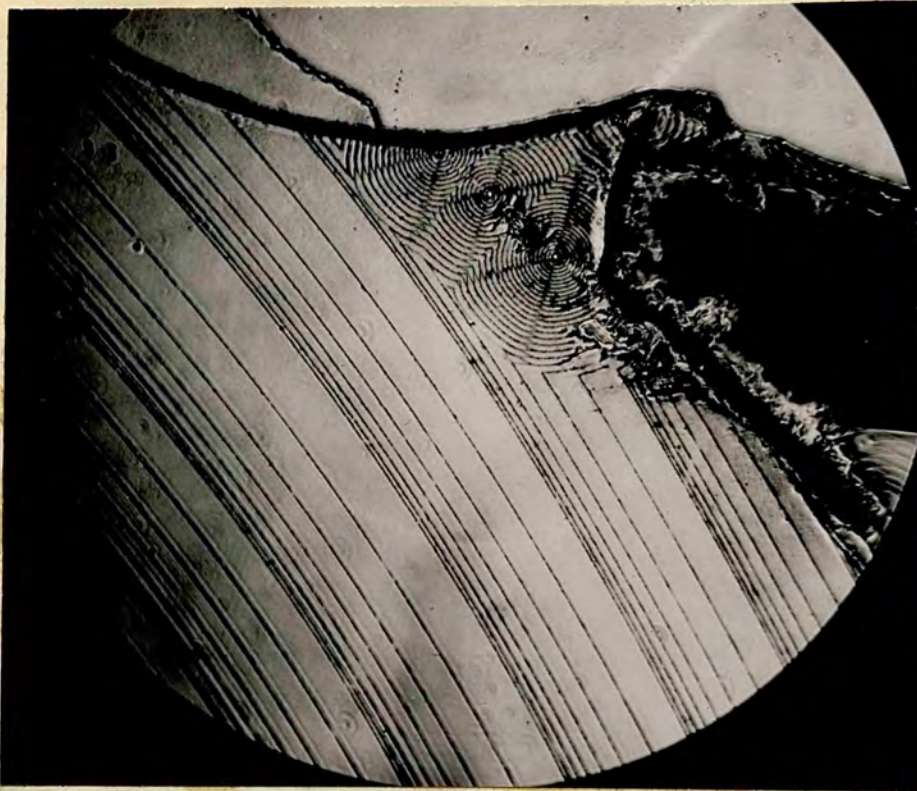
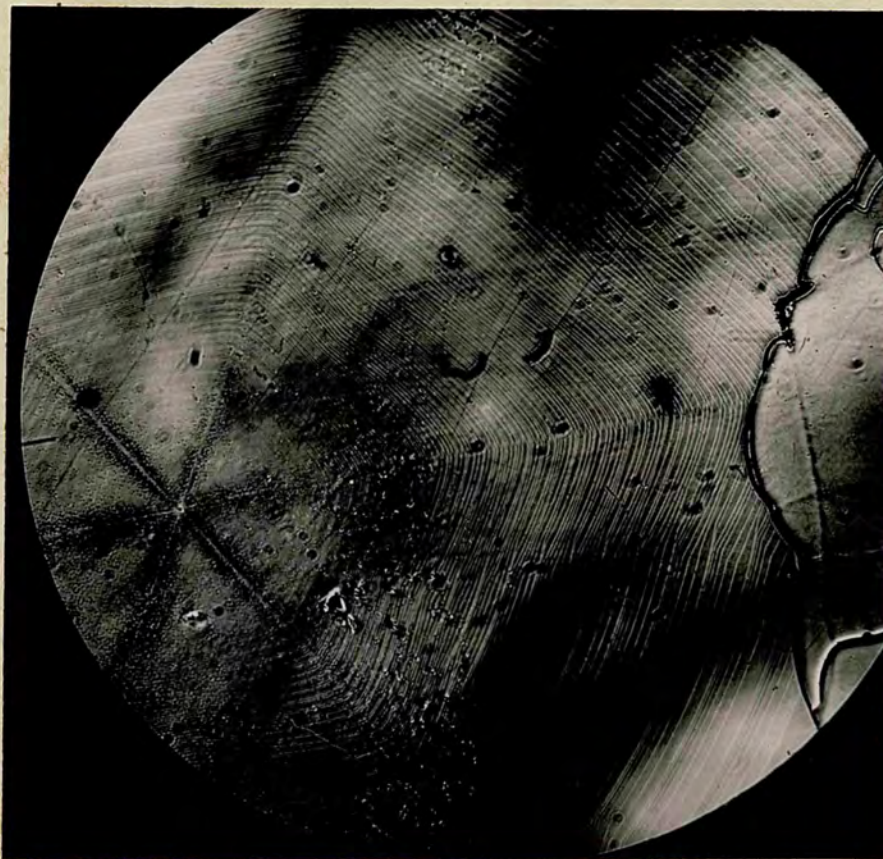Grouped   Interlaced Spirals.
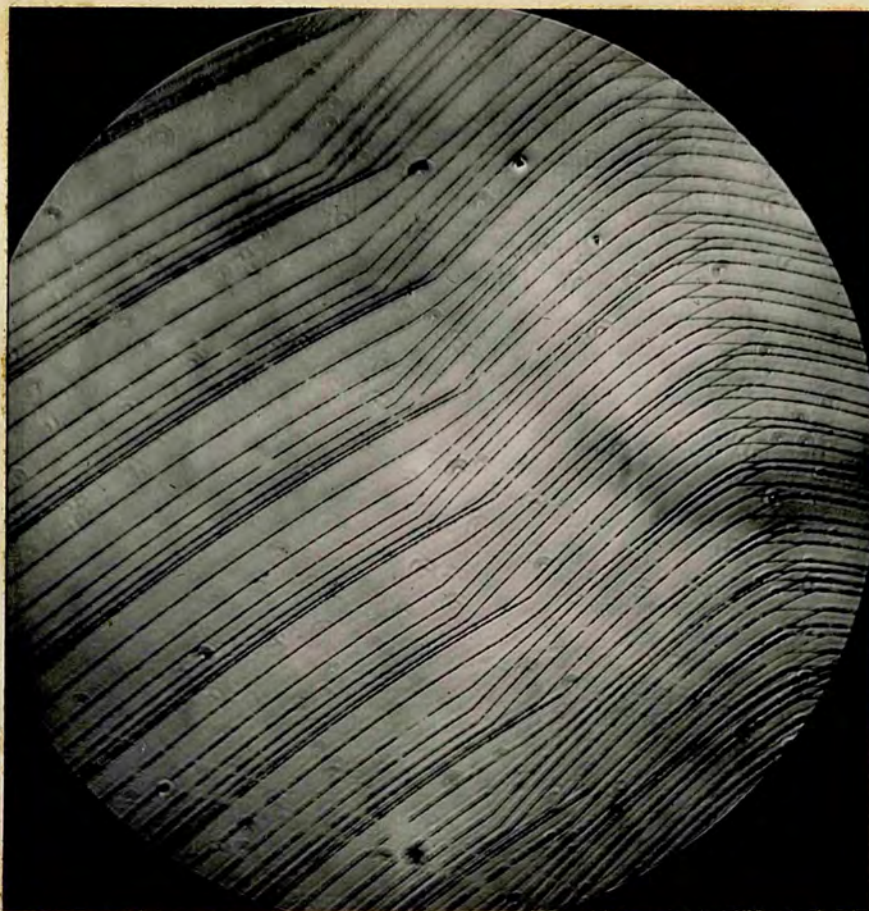
Fig 95.

X300
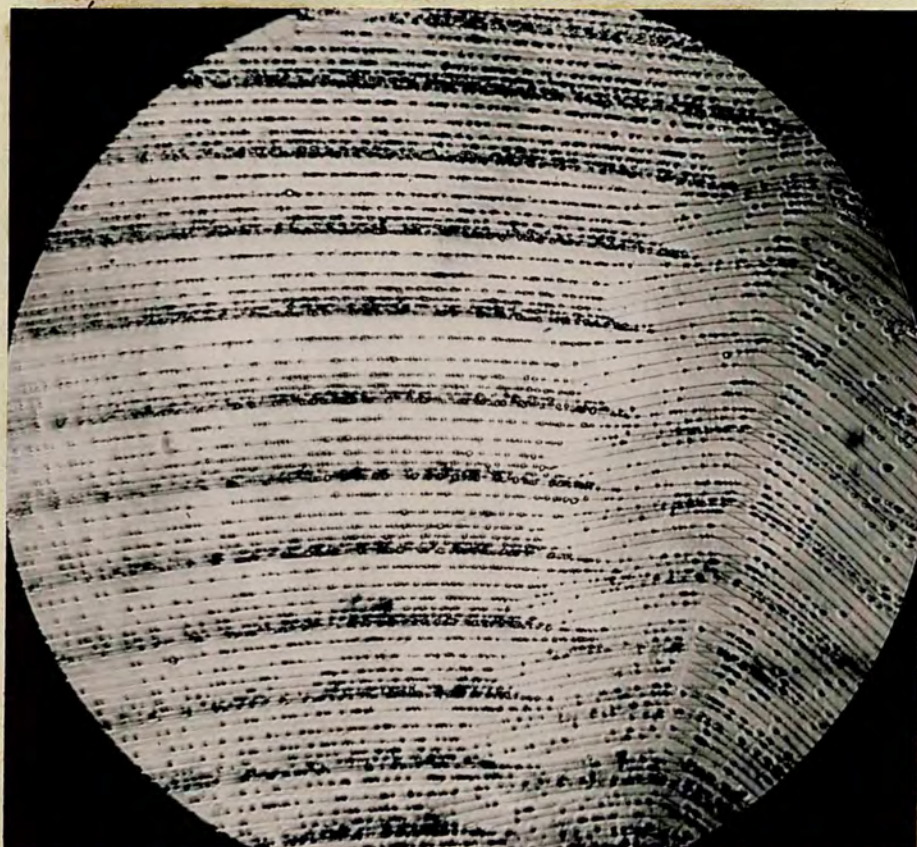
Fig 96.

X300

Grouping of seven steps together. Deposition of impurity
is seen on the step lines of fig.96, to lead to high visibility.

X300

Fig 97. Interaction of the advancing groups of seven

layers with three interlaced spirals.

X90

Fig 98. Showing the centre of the grouped spirals.

X150

Fig 99. Interlaced spiral with five steps grouping together.

X90

Fig 100. Interlaced spiral with varying number of steps grouping together.

58.

INTERFEROMETRIC STUDIES

X90

Fig 101. A double spiral observed on Si-C crystal type 33R.

X90

Fig 102. Fizeau fringes passing over the spiral steps of
fig 101. Fourth fringe from the top passes over
the centre of the spiral.
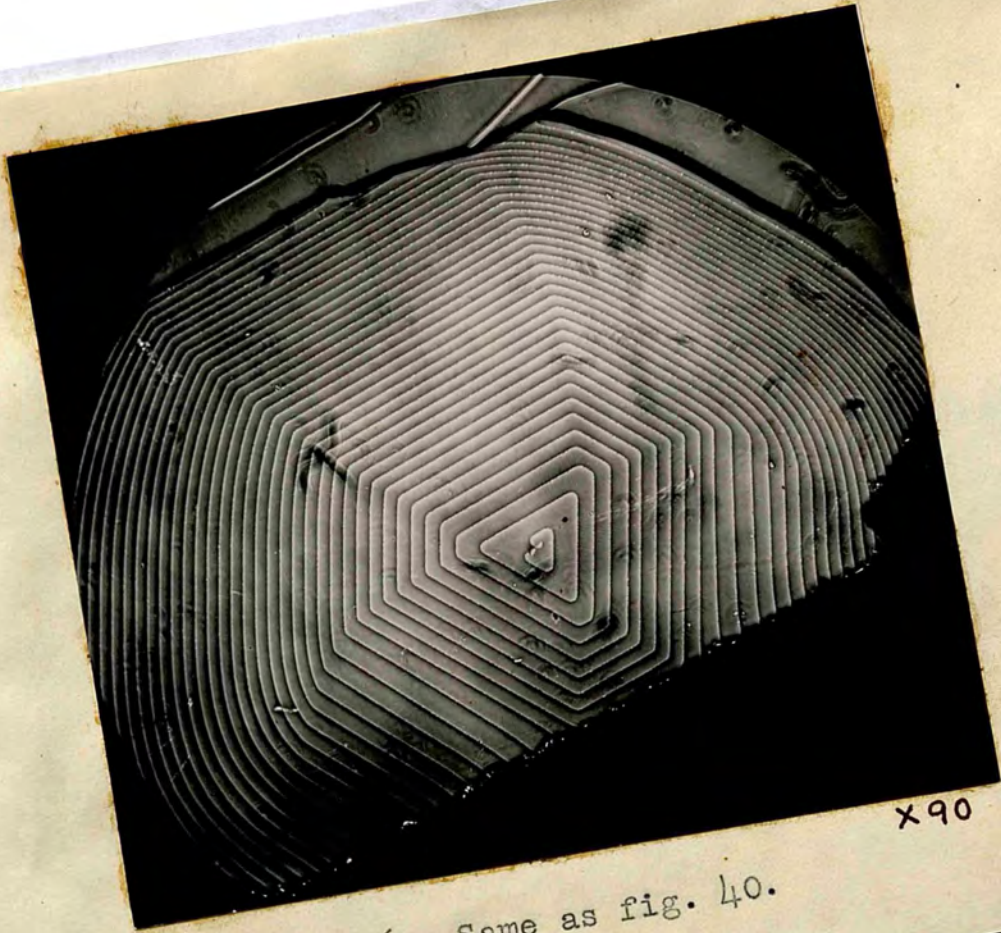
X90

Fig 103. showing superposition of figs.

101 and 102.
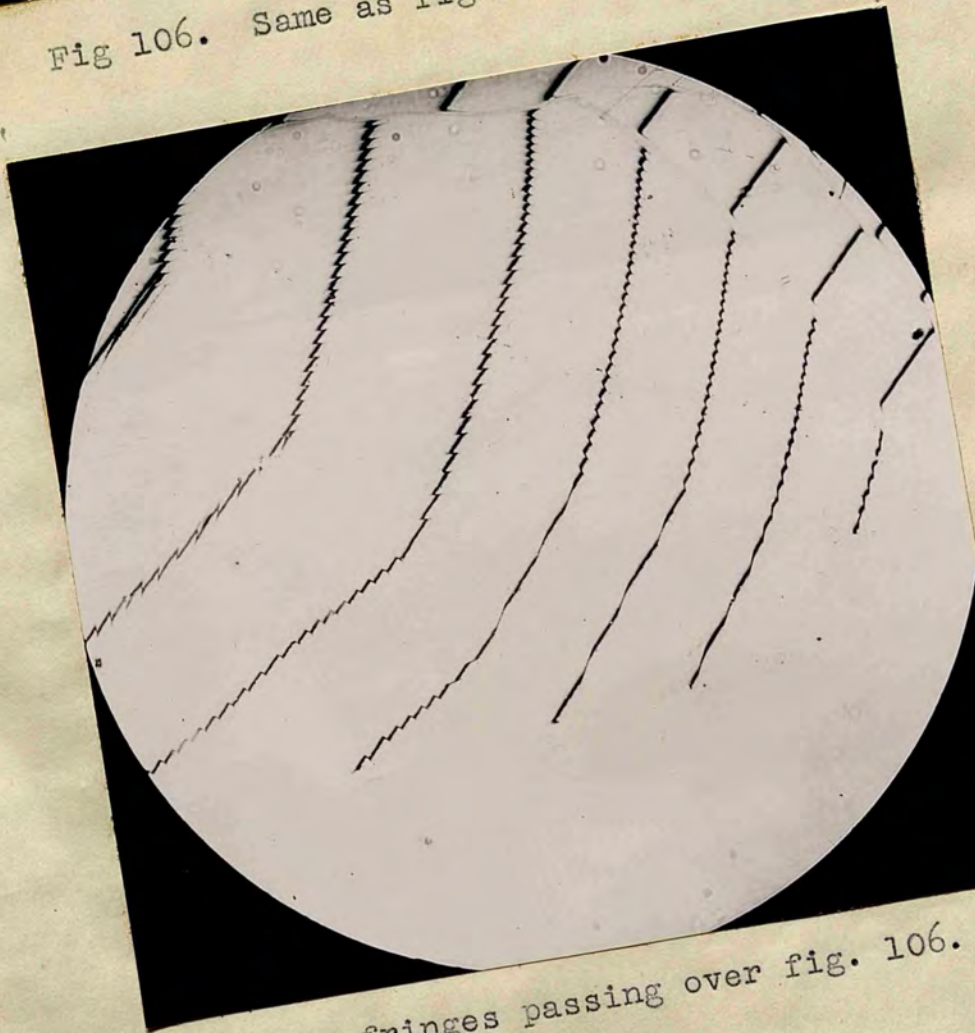
X 90

Fig 104. showing the centre of fig. 70.

X90

Fig 105. Fizeau fringes passing over fig. 70
          by using a lightly silvered glass flat.

X90

Fig 106. Same as fig. 40.

X90

Fig 107. Fizeau fringes passing over fig. 106.